

Russian Original Vol. 47, No. 6, December, 1979

June, 1980

SATEAZ 47(6) 971-1094 (1979)

SOVIET ATOMIC ENERGY

АТОМНАЯ ЭНЕРГИЯ
(ATOMNAYA ENERGIYA)

TRANSLATED FROM RUSSIAN

CONSULTANTS BUREAU, NEW YORK

SOVIET ATOMIC ENERGY

Soviet Atomic Energy is a cover-to-cover translation of *Atomnaya Énergiya*, a publication of the Academy of Sciences of the USSR.

An agreement with the Copyright Agency of the USSR (VAAP) makes available both advance copies of the Russian journal and original glossy photographs and artwork. This serves to decrease the necessary time lag between publication of the original and publication of the translation and helps to improve the quality of the latter. The translation began with the first issue of the Russian journal.

Consultants Bureau journals appear about six months after the publication of the original Russian issue. For bibliographic accuracy, the English issue published by Consultants Bureau carries the same number and date as the original Russian from which it was translated. For example, a Russian issue published in December will appear in a Consultants Bureau English translation about the following June, but the translation issue will carry the December date. When ordering any volume or particular issue of a Consultants Bureau journal, please specify the date and, where applicable, the volume and issue numbers of the original Russian. The material you will receive will be a translation of that Russian volume or issue.

Subscription (2 volumes per year)

Vols. 46 & 47: $147.50 per volume (6 Issues)
Vols. 48 & 49: $167.50 per volume (6 Issues)

Single Issue: $50
Single Article: $7.50

Prices somewhat higher outside the United States.

Soviet Atomic Energy is abstracted or indexed in *Chemical Abstracts, Chemical Titles, Pollution Abstracts, Science Research Abstracts, Parts A and B, Safety Science Abstracts Journal, Current Contents, Energy Research Abstracts,* and *Engineering Index.*

CONSULTANTS BUREAU, NEW YORK AND LONDON

c/b
227 West 17th Street
New York, New York 10011

Published monthly. Second-class postage paid at Jamaica, New York 11431.

SOVIET ATOMIC ENERGY

A translation of *Atomnaya Énergiya*
June, 1980

Volume 47, Number 6 December, 1979

CONTENTS

CONTENTS

(continued)

CONTENTS

(continued)

The Russian press date (podpisano k pechati) of this issue was 11/23/1979. Publication therefore did not occur prior to this date, but must be assumed to have taken place reasonably soon thereafter.

ARTICLES

STABILITY CALCULATION FOR LARGE PRESSURIZED-WATER REACTORS

V. I. Plyutinskii and P. A. Leppik

UDC 621.039.52.034.7.44:62-503

A pressurized-water reactor has the following forms of instability: neutron-physical (resonance), which is due to the strong feedback from the void coefficient of reactivity, hydraulic (between and within loops), and low-frequency, which is due to the pressure change in the reactor arising from unbalance between the production and use of heat. Many forms of instability have been discussed elsewhere [1-4]. Although the methods varied, the following general assumptions are used:

1) the point approximation is used for the reactor kinetics;
2) the neutron-physical and hydraulic instabilities are considered as independent, although it has been pointed out [5] that they interact.

The stability of a large reactor must be examined on models that incorporate the spatial kinetic effects, as well as the interaction between the hydrodynamic and neutron-physical processes. In particular, it becomes incorrect to assert [1] that the stability of the point model (the fundamental mode for the neutron flux) guarantees stability of the higher modes for a reactor with a negative void coefficient of reactivity.

Here we consider a method of calculating the stability that incorporates the interaction between the spatial hydraulic and neutron-physical effects. The following are the basic assumptions:

1) a linear approximation is used;
2) the pressure in the steam space and the temperature in the circulating water at the inlet to the core are taken as constant (low-frequency oscillations are neglected);
3) the monoenergetic diffusion approximation is used for the kinetics;
4) the reactivity is dependent only on the steam content (full temperature effects are neglected to simplify the expressions);
5) the heat production at point $\mathbf{r}$ in the fuel at the time τ is proportional to the neutron flux density $\Phi(\mathbf{r}, \tau)$;
6) the pressure differences in the coolant at any instant are the same for all the fuel cassettes;
7) the circulation loop outside the core is one-dimensional.

Assumptions 1 and 2 give us the Laplace transform for the neutron-flux density deviation $\Delta\Phi(\mathbf{r}, p)$ as

$$\Delta\Phi(\mathbf{r}, p) = \sum_{i=0}^{\infty} a_i(p) f_i(\mathbf{r}), \tag{1}$$

where f_i are orthonormalized functions (modes) that are solutions to

$$\operatorname{div}(D_0 \operatorname{grad} f_i) + \Sigma_0 (k_\infty^0 - 1) f_i + \mu_i \Sigma_0 k_\infty^0 f_i = 0 \tag{2}$$

subject to the boundary conditions

$$f_i(\mathbf{r}) + b(\mathbf{r}) \operatorname{grad} f_i(\mathbf{r}) \cdot \mathbf{n} = 0 \tag{3}$$

at the outer surface of the core ($\Phi_0 \equiv f_0$).

The coefficients in the expansion $a_i(p)$ are dependent on the changes in the reactor parameters and are found from

$$\operatorname{div}(\Delta D \operatorname{grad} \Phi_0) + \Delta\Sigma\Phi_0 [k_\infty^0 - 1 - k_\infty^0 W_\beta(p)] + \Delta k_\infty \Sigma_0 \Phi_0 [1 - W_\beta(p)] = \sum_{i=0}^{\infty} a_i(p) (p/v_0 + \Sigma_0 k_\infty^0 W_\beta(p) + \mu_i \Sigma_0 k_\infty^0) f_i. \tag{4}$$

The symbols in (1)-(4) are as follows: Σ is the macroscopic capture cross section; p is the variable in the Laplace transformation; $W_\beta(p) = p\sum_{m=1} \beta_m/(p+\lambda_m)$; $\mathbf{n}$ is the vector normal to the surface of the core; subscript 0 denotes values of the parameters corresponding to the unperturbed state; Δ represents deviations; and the other symbols are as in [6] (Section 1.1).

Translated from Atomnaya Énergiya, Vol. 47, No. 6, pp. 363-367, December, 1979. Original article submitted October 9, 1978; revision submitted June 18, 1979.

0038-531X/79/4706-0971 $07.50

In accordance with assumption 4, the deviations of the physical parameters in the perturbed reactor are dependent only on the steam content φ and can be put in the form

$$\left.\begin{aligned}\Delta D(\mathbf{r},\ \tau)&=\psi(\mathbf{r})\,\Delta\varphi(\mathbf{r},\ \tau)\\ \Delta k_\infty(\mathbf{r},\ \tau)&=\eta(\mathbf{r})\,\Delta\varphi(\mathbf{r},\ \tau)\\ \Delta\Sigma(\mathbf{r},\ \tau)&=\xi(\mathbf{r})\,\Delta\varphi(\mathbf{r},\ \tau)\end{aligned}\right\}, \tag{5}$$

where

$$\psi=\frac{\partial D(\mathbf{r})}{\partial\varphi(\mathbf{r})};\ \eta=\frac{\partial k_\infty(\mathbf{r})}{\partial\varphi(\mathbf{r})};\ \xi=\frac{\partial\Sigma(\mathbf{r})}{\partial\varphi(\mathbf{r})}. \tag{6}$$

It is possible to use a multiple-group approximation in employing (6) to incorporate the actual neutron spectrum at each point $\mathbf{r}$.

Therefore, the reactivity of the perturbed reactor can be determined by exact calculation of the spatial distribution of the steam content. For this purpose it is best to use numerical methods for determining the complex frequency response for the steam content and other necessary parameters along the channel [7, 8]. This method can be used for the complex frequency response corresponding to the transfer functions $W^k_{\varphi qij}(z, p)$ and $W_{\varphi qj}(z, p)$, which relate the change in the steam content at each section z in cassette j to the perturbations on mode i $[a_i(p)\,F_i(\mathbf{r})]$ and to the water flow rate at the inlet to the cassette $[\Delta g_j(p)]$; these transfer functions allow us to calculate the change in steam content:

$$\Delta\varphi(\mathbf{r},\ p)=\sum_{i=0}^{\infty}a_i(p)\,W^k_{\varphi ij}(z,\ p), \tag{7}$$

where $[W^k_{\varphi ij}=W^k_{\varphi qij}+W^k_{\varphi gj}(W^k_{gqij}+W^k_{gGj}W_{Gqi});\ W^k_{gqij}, W_{Gqi}]$ are transfer functions that relate respectively the change in flow rate at the inlet to a cassette and the change in total flow rate at the inlet to the core $[\Delta G(p)]$ with the perturbation on mode i, where W^k_{gGj} is a transfer function that relates the change $\Delta q_j(p)$ to the perturbation $\Delta G(p)$, and $j=j(\mathbf{r})$; $z=z(\mathbf{r})$.

The transfer functions for the perturbation in mode i are determined as the Laplace transforms of the changes in the corresponding parameters in response to changes in the heat production (Δq_{ij}) in the fuel rods in each cassette in accordance with the law

$$\Delta q_{ij}(z,\ \tau)=\frac{\bar q_{0j}(z)}{\bar f_{0j}(z)}\,\bar f_{ij}(z)\,\delta(\tau), \tag{8}$$

where $q_{0j}(z)$ is the heat production in the unperturbed reactor averaged over the cross section of the cassette, $\delta(\tau)$ is a Dirac δ function, $\bar f_{ij}(z)$ is the mean over the cross section of a cassette for mode i, and $f_{ij}(z)=f_i(\mathbf{r})$.

We substitute (7) and (5) into (4), multiply both parts by f_t, and integrate over the volume of the core. Then as the weighting factor $\Sigma_0 k^0_\infty$ applies to system $\{f_i\}$, which is orthonormalized, we get

$$\sum_{i=0}^{\infty}a_i(p)\,d_{ti}(p)-p\sum_{i=0}^{\infty}a_i(p)\,l^{ef}_{ti}=W^{-1}_{kt}(p)\,a_t(p), \tag{9}$$

where

$$d_{ti}=\int_V\Omega'_t(\mathbf{r},\ p)\,W^k_{\varphi ij}(z,\ p)\,dV+\int_S\Omega''(\mathbf{r},\ p)\,W_{\varphi ij}(z,\ p)\,dS; \tag{10}$$

$$\Omega'_t=-\psi\,\mathrm{grad}\,f_0\cdot\mathrm{grad}\,f_t+\xi f_0 f_t\,[k^0_\infty-1-k^0_\infty W_\beta(p)]+\eta\Sigma_0 f_0 f_t\,[1-W_\beta(p)];\quad \Omega''_t=\psi f_t\,\mathrm{grad}\,f_0\cdot\mathbf{n};$$

$W_{kt}=(pl^{ef}_{tt}+W_k+\mu_t)^{-1}$ is the transfer function for the kinetics for mode f_t and $l^{ef}_{ti}=\int_V(f_t f_i/v_0)\,dV$ is the effective neutron lifetime, $l^{ef}_{tt}\approx l^{ef}_{00}=l^{ef}$; $l^{ef}_{ti}\approx 0$ for $t\neq i$. The integration in the second term in (10) is over the external surface of the reactor S (it is frequently assumed that $\Omega''=0$ for large reactors).

We get the transfer functions that relate the change in reactor power to changes in water flow rate for the entire loop and for the individual channels. We split up the entire circulation loop into three parts: the core, the rising section, and the descending section (these are referred to by the superscripts co, ri, and de). We assign as the rising section the entire volume of the loop above the core with two-phase flow, while the descending section is all the part with a single-phase flow.

For simplicity we assume that the power deviation is described by mode i alone. Then the following is the change in the pressure drop $(\Delta P)^k_{ij}$ across channel j:

$$\Delta P_{ij}^{k}(p) = W_{Pqij}^{k}(p)\, a_i(p) + W_{Pgi}^{k}(p)\, \Delta g_{ij}(p), \tag{11}$$

where Δg_{ij} is the increment in the water flow rate at the inlet to the channel core by the change in mode i and W_{Pqij}^{k}, W_{Pqj}^{k} are transfer functions that relate the change in pressure drop across the channel to the perturbation of mode i and to the flow-rate change at the inlet to the channel respectively, whose complex frequency characteristics have already been derived [8].

With assumption 6 we get from (11) that

$$\Delta g_{ij}(p) = a_i(p)\, W_{gqij}^{k}(p) + W_{gGj}^{k}(p)\, \Delta G_i(p), \tag{12}$$

where

$$W_{gGj}^{k} = W_{PG}^{co}/W_{Pgj}^{k};$$
$$W_{gqij}^{k} = (W_{Pqi}^{co} - W_{Pqij}^{k})/W_{Pgi}^{k};$$
$$W_{PG}^{co} = [\sum_j (W_{Pgj}^{k})^{-1}]^{-1};$$
$$W_{Pqi}^{co} = W_{PG}^{co} \sum_j (W_{Pqij}^{k}/W_{Pgj}^{k});$$
$$\Delta G_i = \sum_j \Delta g_{ij}.$$

The increment in the water flow rate at the inlet to the core [$\Delta G_i(p)$] on perturbation in mode i can be put as

$$\Delta G_i(p) = -a_i(p)\, \frac{W_{Pqi}^{co}(p) + W_{Pqi}^{ri}(p)}{W_{PG}^{co}(p) + W_{PG}^{ri}(p) + W_{PG}^{de}(p)}, \tag{13}$$

where W_{Pqi}^{ri} is the transfer function that relates the change in pressure difference ΔP^{ri} to the perturbation on mode i (for $\Delta G = 0$), and W_{PG}^{ri} and W_{PG}^{de} are transfer functions that relate the changes ΔP^{ri} and ΔP^{de} to the perturbations ΔG.

The complex frequency characteristics of W_{PG}^{ri} and W_{Pqi}^{ri} are determined in accordance with assumption 7 by the method of [2, 9] with the complex frequency characteristics of [8] for the flow rates of water and steam at the exit from the cassette, while W_{PG}^{de} is determined from the equations of one-phase hydrodynamics.

Expressions have been derived for the quantities appearing in (9); we assume that in the stability analysis it is sufficient to restrict consideration to a finite number of modes. Then (9) can be put as the matrix equation

$$\mathbf{A} = \|W\| \cdot \mathbf{A}, \tag{14}$$

where A is a vector with components (a_0, a_1, a_2, .., a_S); $\|W\|$ is a square matrix of order s+1 having the elements

$$W_{ti}(p) = [d_{ti}(p) - pl_{ti}^{ef} c_{ti}]\, W_{kt}(p), \quad c_{ti} = \begin{cases} 0, & t = i; \\ 1, & t \neq i. \end{cases}$$

Equation (14) allows one to examine those forms of instability which interact; for example, poles in the right half plane for the transfer functions W_{ti} indicate interchannel instability (if there are zeroes in the right half-plane for W_{PG}^{co}), or general-loop instability (if there are zeros in the right half plane for the transfer function $W_{PG}^{co} + W_{PG}^{ri} + W_{PG}^{de}$). If we neglect the nondiagonal elements in $\|W\|$, analysis of (14) allows us to judge the stability of the individual modes without considering the coupling between them, e.g., the element $W_{00}(p)$ describes the kinetics in the point approximation. However, for a large pressurized reactor it is necessary to consider the mode interaction, as the examples below show.

Let $\nu_i(\omega)$ (i = 0, 1, ..., S) be the eigenvalues of $\|W\|$ for $p = j\omega$; it can be shown that if the transfer functions corresponding to the elements $\|W\|$ do not have poles in the right half plane (i.e., there is no hydraulic instability) then it is necessary and sufficient if the system of (14) is to be stable for the hodographs of all the vectors $\nu_i(\omega)$ not to enclose the point (1, j0) as ω goes from 0 to ∞ (by analogy with the Nyquist criterion for one-loop systems) [10]. Also, if the nondiagonal elements of $\|W\|$ are small, then the eigenvalues ν_i are close to the diagonal elements, and in the case of loss of stability we can talk of instability on the individual modes.

As the moduli of the elements of $\|W\|$ tend rapidly to zero as i and t increase, there will be little effect on the first eigenvalues (ν_0, ν_1, ν_2) if the dimensions of the matrix are more than three or four, while the higher eigenvalues are small in modulus. Therefore, we can increase the dimensions of the matrix step by step to estimate the number of modes that need be incorporated.

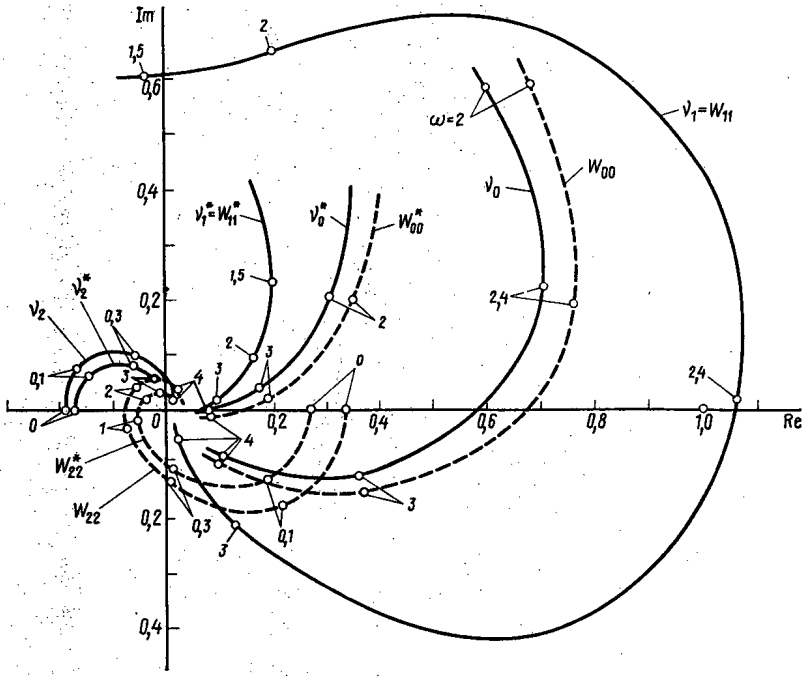

Fig. 1. Hodographs for the complex frequency characteristics of diagonal elements (broken line) and for the eigenvalues (solid line) of the $\|W\|$ matrix for N = 100%, Δi_u = 167 kJ/kg (the points show the values of the frequency ω is rad · sec^{-1}).

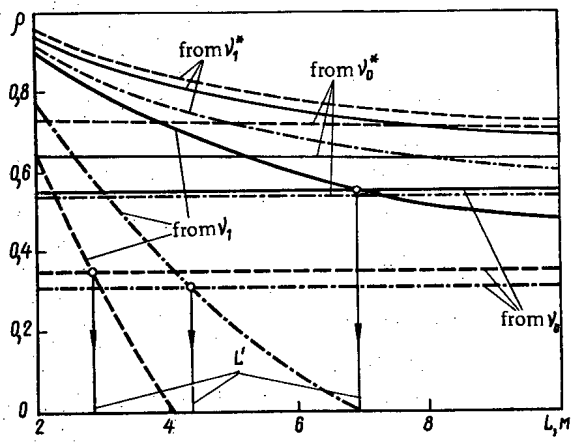

Fig. 2. Stability margin ρ as a function of diameter L: (——, ——) N = 100%, Δi_u = 115 kJ/kg; (---, ---) N = 100%, Δi_u = 167 kJ/kg; (-·-, -·-) N = 140%, Δi_u = 115 kJ/kg.

We give as an example the results from a simplified calculation on the stability of a reactor performed in this way; the reactor is considered as radially homogeneous (b = ∞ at the side surface of the core), while the asymmetry in the heat production over the height of the core is produced by manipulation of the lower and upper boundaries of the reactor (the nonuniformity factor $k_z = 1.5$); D_0, Σ_0, and k_∞^0 are taken as constant over the colume and the migration length $M_0 = \sqrt{D_0/\Sigma_0}$ is taken as 10 cm. The height of the core in all cases was 3 m, while the diameter of the core varied from 2 to 10 m, with the height of the rising part above the core 6.4 m and the pressure in the reactor 10 MPa.

We considered modes with various modes N and various degrees of underheating of the water at the inlet Δi_B^u; coefficient $\eta(z)$ was calculated on the basis of the actual distribution of the parameters over the height of the core as derived via two-group constants, while the coefficients $\xi(z)$ and $\psi(z)$ were taken as zero. The void effect on the reactivity varied from 0.03 to 0.07 under these conditions, while the steam content ε at the outlet varied over the range 0.5-0.7.

Figure 1 shows the hodographs for the complex frequency characteristics for the diagonal elements of $\|W\|$ corresponding to various modes (the subscripts 00, 11, and 22 refer to the fundamental, the first azimuthal mode, and the first axial mode, respectively), and it also shows the hodographs for the eigenvalues $\nu_i(\omega)$ (core diameter 4.3 m) for one of these states. To illustrate the effects of the circulation we also show the hodographs for W_{00}^*, ν_0^*, W_{22}^*, and ν_2^* calculated on the assumption of a constant total flow rate through the core, as well as the hodograph for ν_1^* calculated on the assumption of constant flow rate for the coolant in all channels in the core (in this model, any redistribution of the flow rate between the channels has no effect on ν_0 and ν_2, but a change in the total loop flow rate affects ν_1). The divergence of the hodographs for W_{00} and ν_0 resembles that for W_{22} and ν_2 and shows that the fundamental and first axial modes have substantial interaction (as a result, the stability of both modes is increased). The hodographs for W_{11} and ν_1 coincide, since $d_{10} = d_{12} = 0$ in this model. The effects of the circulation reduce the stability of all modes, which is very clearly seen for the azimuthal mode, which becomes unstable in this state.

The interchannel fluctuations in flow rate affect the stability in a large reactor, as is illustrated by Fig. 2 (the measure of the stability margin is the distance ρ of the corresponding hodograph from the point +1, j0). It has been assumed here that the hydraulic characteristics of the individual channels and of the loop and as a whole (i.e., W_{gqij}^{k} and W_{Gqi}^{ψ}) are independent of the diameter of the core. If the reactor has a core diameter exceeding some value L', the instability will set in earlier not on the fundamental but on the azimuthal mode. This L' decreases as the hydraulic stability of the channels against interchannel fluctuations falls.

CONCLUSIONS

The features of the thermophysical processes in large pressurized-water reactors require one to consider the spatial kinetics along with the equations of the circulation in the core channels and in the loop as a whole in discussing the stability. The loop circulation generally sometimes has a destabilizing effect on the fundamental mode. Therefore, a large reactor may give rise to loop hydroneutron instability, which is characterized by fluctuations in the circulation and the neutron flux. The first axial mode usually has a stabilizing effect on the fundamental mode.

In a large reactor, it is possible for there to be a special interchannel hydroneutron instability caused by the interaction between the interchannel hydraulic effects and the azimuthal mode in the neutron flux. A difference from a purely hydraulic instability is that this is dependent on the size of the core.

LITERATURE CITED

1. H. Hitchcock, Nuclear Reactor Stability [Russian translation], Gosatomizdat, Moscow (1963).
2. I. I. Morozov and V. A. Gerliga, Stability in Boiling Apparatus [in Russian], Atomizdat, Moscow (1969).
3. V. I. Gritskov et al., At. Energ., 25, No. 6, 514 (1968).
4. B. V. Kebadze and V. I. Plyutinskii, At. Energ., 31, No. 2, 89 (1971).
5. S. Zivy and F. Wright, in: Kinetics and Control for Nuclear Reactors (edited by P. A. Gavrilov) [Russian translation], Atomizdat, Moscow (1967), p. 187.
6. I. Ya. Emel'yanov, P. A. Gavrilov, and B. N. Seliverstov, Control and Safety in Nuclear Power Reactors [in Russian], Atomizdat, Moscow (1975).
7. and N. Ya. Khvostova, L. L. Fishgoit, At. Energ., 25, No. 6, 474 (1968).
8. G. A. Sankovskii, L. L. Fishgoit, and V. I. Plyutinskii, in: Nuclear Science and Technology, Series Nuclear Power Installation Dynamics [in Russian], Issue 2, Izd. TsNIIatominform (1977), p. 56.
9. V. M. Rushchinskii and V. I. Khvostova, in: Papers from the Central Complex Automation Research Institute [in Russian], Issue 16, Énergiya, Moscow (1967), p. 237.
10. A. Macfarlane and J. Belletrutti, Automatica, 9, No. 5, 575 (1973).

A THREE-PULSE REGULATOR FOR CONTROLLING THE COOLANT TEMPERATURE IN A FAST REACTOR UNDER EMERGENCY CONDITIONS

V. A. Afanas'ev, V. M. Gryazev,*
V. N. Efimov, V. I. Plyutinskii,
and A. N. Tyufyagin

UDC 658.52.011.56:621.311.25:621.039

A fast reactor produces considerable temperature rise in the coolant in the core; therefore, large thermal stresses can arise when the emergency protection gear operates, which represent a hazard for the constructional components. One of the ways of reducing the stresses is to control the coolant flow in such a way that the power-decay curve is similar to the coolant-flow decay. Then the coolant temperature at exit from the reactor will be approximately constant, so the thermal stresses will be minimal.

One of the commoner ways of powering the main circulation pump is that used in the BOR-60 (Fig. 1) [1, 2]. This includes the synchronous motor SM and the generator G, which supplies the dc motor DC. The speed of the main circulation pump MCP is controlled by including the variable resistor R_V in the exciting winding of the generator, which itself is controlled by the constant-speed motor CS. When the synchronous motor is switched out of the circuit, the kinetic energy is redistributed (by adjustment of the generator excitation), and this enables one to control the coolant flow law within fairly wide limits [2].

The BOR-60 has been used in an experiment in which a single-pulse temperature regulator was used to control the generator excitation when the emergency protection gear operates [2]. The signal to the regulator is derived from fast thermocouples at the exit from the fuel-rod assembly. Tests showed that it is possible to maintain the temperature quite accurately under these conditions. However, the fast thermocouples are not very reliable, so it was not possible to use them in the standard control system.

Here we consider the scope for controlling the temperature during emergency shutdown by means of signals from slow thermocouples at the exit. As there is considerable lag in the upper volume of the reactor and in the thermocouple, the control performance is improved by making use of pulses generated by the coolant flow and the neutron power level.

The purpose of the regulator of Fig. 1 is to maintain the coolant temperature at the exit at the level immediately before the emergency. Therefore, the basic control parameter is the temperature t_r recorded by the couple. The regulator should maintain the temperature at the value immediately before the emergency, and automatic adjustment of the temperature signal is provided for this purpose. The temperature-deviation signal is generated by a circuit consisting of the adder Σ_3, whose feedback circuit contains the integrator I_2.

In the normal state, the contact of the relay P is closed. When an unbalance signal appears at the output of Σ_3, the integrator output will vary until the unbalance signal from the adder vanishes, no matter what the absolute value of the temperature at the input. At the instant of the emergency, the contacts of relay P open and the output signal is

$$\Delta t = t_r - t_{r0},$$

where t_{r0} is the coolant temperature at the reactor outlet at the moment preceding the emergency and t_r is the current temperature.

This signal passes to the adder Σ_2 with the adjustment coefficient K_t, which is an adjustable parameter, and then to a relay component, which works with an integrating negative feedback circuit. The parameters K_{fb} and T_{fb} of the feedback circuit are also regulator-setting parameters. The relay controls the CS motor. The adder Σ_1 receives signals representing the power levels N and the flow rate G, where the power signal is supplied not directly but via the multiplier M, which multiplies the power signal by the signal from the integrator I_1. This is necessary in order to provide correspondence between the flow rate and power signals before the protection operates.

*Deceased.

Translated from Atomnaya Énergiya, Vol. 47, No. 6, pp. 367-370, December, 1979. Original article submitted May 15, 1978; revision submitted April 23, 1979.

0038-531X/79/4706-0976 $07.50

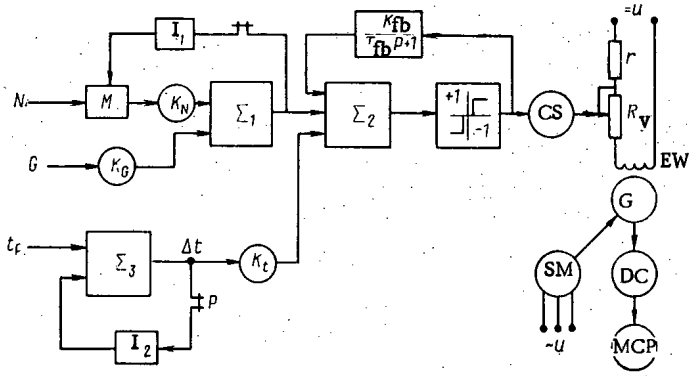

Fig. 1. Structural diagram of the temperature regulation system.

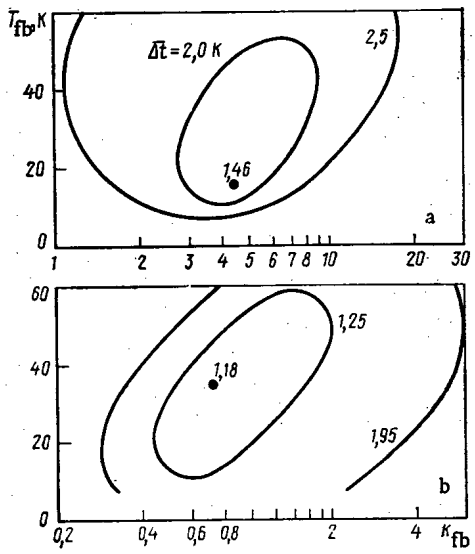

Fig. 2

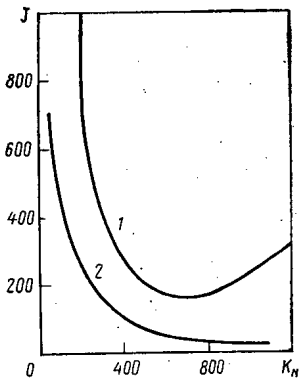

Fig. 3

Fig. 2. Lines of constant value for the rms temperature deviation for K_N of 1000 (a) and 600 (b).

Fig. 3. The K_N dependence of the minimum value of J for power levels of 60 (1) and 20 MW (2).

Calculations were performed for 60 and 20 MW in order to determine the optimum regulator settings. The mathematical description of the flow-rate control includes differential equations for the object, the drive, and the regulator.

Methods of defining the adjustable parameters for regulators in linearized automatic-control systems are not applicable in this case because of the substantial nonlinearity in the object, and also because the coefficients in the equations are explicit functions of time. Therefore, the optimum regulator settings are derived numerically by comparing various calculations made by computer. The optimality criterion is the minimum rms deviation of the temperature from the initial value during the pump deceleration time T_d (it is assumed that this time is the time needed for the flow rate to fall to 5% of the initial value).

The integral quadratic criterion J is defined by

$$J = \int_0^{T_d} (t_r - t_{r.0})^2 \, d\tau,$$

where $T_d = 80$ sec is the deceleration time and τ is time.

The static control accuracy is governed by K_t:

$$\Delta t = \Delta / K_t,$$

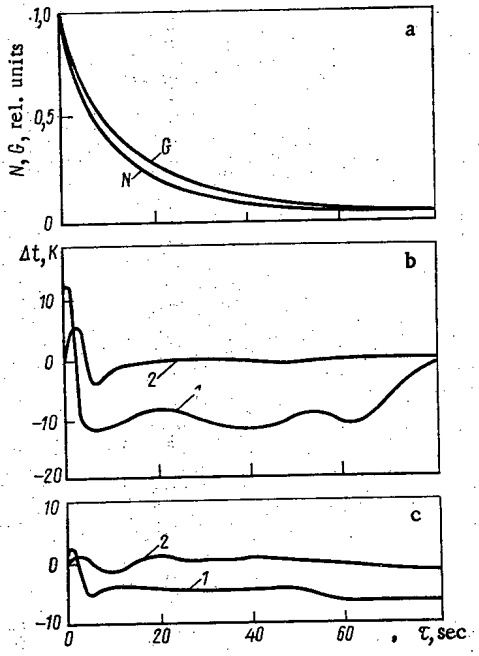

Fig. 4

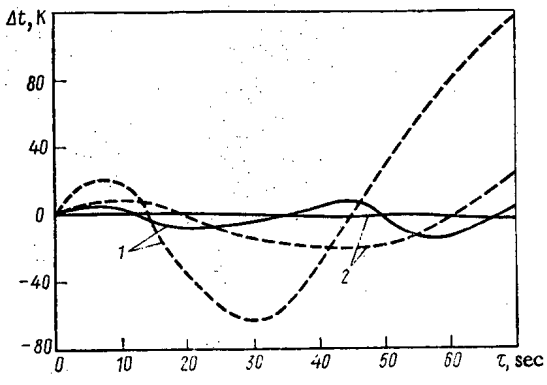

Fig. 5

Fig. 4. Calculated transient-response curves for the temperature-control system after operation of the emergency protection: a) curves for fall in power level and coolant flow; b, c) temperature curves for $Q_0 = 60$ and 20 MW, respectively; 1, 2) temperatures at the exit from the core and the reactor, respectively.

Fig. 5. Transient response with temperature control (solid line) and without control (broken line) in the experiment with operation of the emergency protection: 1, 2) temperatures at the exit from the core and reactor, respectively.

where Δ is the insensitive zone of the relay element. We assume $K_t = 1$, i.e., $\Delta t = 1°K$, and then this static accuracy can be obtained with standard temperature regulators. Any improvement on this would require special development, and calculations show that no change is desirable, since the static error of 1°K is much less than the dynamic error. The calculations were performed for various values of K_{fb}, T_{fb}, and K_N for a constant value of K_t ($K_t = 1$); in determining K_{fb} it was assumed that the voltage at the output of the relay elements was 1. Calculations on the transient response were performed for a nominal output of 60 MW, and Fig. 2 shows the lines of equal value for $\overline{\Delta t} = \sqrt{J/T_d}$.

Figure 3 shows the minimum value of J for the given K_N as a function of the latter for two different power levels. The minimum J for the nominal power is obtained with $K_N = 620$, which corresponds to the following optimum feedback adjustments: $K_{fb} = 0.8$, $T_{fb} = 35$ sec. Then $\Delta t = 1.18°K$.

Figures 2 and 3 show that slight changes in K_N do not produce substantial changes in $\overline{\Delta t}$, and these adjustments may be considered optimal for any initial reactor power. The transient response calculated for this optimal adjustment is shown in Fig. 4. Clearly, the excursions of the temperature at the exit from the core do not exceed 5-11°K, while those at the exit from the reactor are only 2-5°K.

This control system was tested with the BOR-60; the regulator was an instrument developed at the Central Complex Automation Research Institute from a standard RPIB regulator. The tests demonstrated the good performance in maintaining the exit temperature when the emergency protection gear operates, and they also served to refine the calculated adjustment figures. The initial parameters before the protection operated were as follows: reactor power 40 MW, coolant flow through reactor 900 m^3/h, $K_N = 600$, $T_{fb} = 40$ sec, $K_{fb} = 0.8$, $\Delta = 1.3°K$.

Figure 5 shows the transient response in the control system and the comparative curve when the protection operates without the regulator. The control performance is quite adequate, as is clear from the fact that the deviation in the temperature at the exit from the core is only 17°K, as against 5°K at the exit from the reactor, whereas the corresponding figures without the regulator were 115 and 25°K, respectively.

This method of shutting down the reactor is of high performance, which was demonstrated not only by the calculations but also by experiment, and it is recommended for use on fast power reactors, since it provides improved reliability and safety. However, the forms of equipment vary, as does the scope for controlling the circulation-pump speed, so the problem is best considered at the design stage if the appropriate flow-rate control range is to be provided, particularly from a source with an adequate kinetic-energy reserve. For example, a turbine generator might be employed.

LITERATURE CITED

1. O. D. Kazachkovskii et al., At. Energ., 34, No. 5, 341 (1973).
2. V. A. Afanas'ev et al., in: Nuclear Science and Engineering, Series Nuclear Power Plant Dynamics [in Russian], Issue 1(11), TsNIIatominform, Moscow (1977), p. 51.

SYNTHESIS OF AN UNSYMMETRICAL-ZONE CONTROL SYSTEM FOR REACTOR POWER DISTRIBUTION

I. Ya. Emel'yanov, L. N. Podlazov, A. N. Aleksakov, and V. M. Panin

UDC 621.039.562

A substantial problem is represented by the need to maintain given spatial energy distribution in a large nuclear reactor, on account of the tendency to spontaneous nonstationary deformation of the distribution [1]. This poses many problems for the designers of control systems for large reactors, and one of the most important of these is the optimum choice of the number and disposition of the control rods and transducers in automatic control system.

The traditional approach involving local control systems requires a number of local regulators equal to the number of unstable harmonics to be suppressed [2]. However, it has been shown [3, 4] that, in principle, it is possible to stabilize the neutron distribution with a smaller number of regulators.

The prospect for improving the stabilizing performance of an automatic control with fewer control elements has stimulated studies [5-7] in which various aspects of control for a one-dimensional reactor have been discussed, including unsymmetrical control systems. In particular, it has been shown [5] that one has to consider the control performance and stability in the synthesis of an unsymmetrical system, and that here the most promising systems involve a combination of the zone principle of automatic-control design with asymmetry. Here we consider the synthesis of an unsymmetrical-zone system for controlling the radial and azimuthal energy distributions.

Formulation. The neutron distribution is described by means of a linearized equation for the diffusion approximation in a cylindrical coordinate system on the assumption that only slow processes are involved, namely such that the delayed neutrons can be neglected. All changes in the quantities are assumed averaged over the axis with a weight proportional to the square of the neutron flux.

These assumptions give the equations for the dynamics of the reactor with a single power feedback as

$$\begin{cases} \Delta\varphi + \varkappa_0^2\varphi + (k_{fb} + k_c)\Phi_0 = 0; & (1) \\ \varphi|_{r=1} = 0; & (2) \\ \partial k_{fb}/\partial t = \alpha\varphi - k_{fb}, & (3) \end{cases}$$

where k_c describes the control action.

The time unit is the time-constant of the feedback; the steady-state neutron flux distribution Φ_0 satisfies

$$\Delta\Phi_0 + \varkappa_0^2\Phi_0 = 0 \quad (4)$$

with the boundary condition $\Phi_0|_{r=1} = 0$

$$\text{where } \varkappa_0^2 = \begin{cases} 0 & \text{for } r < R_1; \\ \text{const} > 0 & \text{for } R_1 < r \leqslant 1 \end{cases}$$

(here R_1 is the radius of the equalized energy distribution).

Translated from Atomnaya Énergiya, Vol. 47, No. 6, pp. 370-373, December, 1979. Original article submitted January 8, 1979.

0038-531X/79/4706-0979$07.50

The solution to (4) takes the form [6]

$$\Phi_0 = \begin{cases} 1 \text{ for } r < R_1; \\ A\left[J_0(\varkappa_0 r)\, Y_0(\varkappa_0) - Y_0(\varkappa_0 r)\, J_0(\varkappa_0)\right] \\ \text{for } R_1 \leqslant r \leqslant 1, \end{cases}$$

where $A = [J_0(\varkappa_0 R_1)\, Y_0(\varkappa_0) - Y(\varkappa_0 R_1) J_0(\varkappa_0)]^{-1}$.

We consider the case where the automatic control is based on regulators working in proportional (static) mode and write the equation for k_c as

$$k_c = -\sum_{i=1}^{M} A_i \delta(r - r_i,\ \theta - \theta_i) \sum_{j=1}^{N_i} \varphi|_{\substack{r=r_{ij} \\ \theta=\theta_{ij}}}, \tag{5}$$

where M is the number of control rods, $A_i > 0$ is the transfer coefficient for rod i, r_i and θ_i are the coordinates of rod i, N_i is the number of transducers corresponding to rod i, r_{ij}, θ_{ij} are the coordinates of transducer j corresponding to rod i, and $\delta(r, \theta)$ is a two-dimensional δ function.

After Laplace transformation we write (1) and (2) on the basis of (3) and (5) as

$$\begin{cases} \Delta\bar{\varphi} + \varkappa_0^2 \bar{\varphi} + \dfrac{\alpha\Phi_0}{s+1}\bar{\varphi} - \\ -\Phi_0 \sum_{i=1}^{M} A_i \delta(r - r_i,\ \theta - \theta_i) \sum_{j=1}^{N_i} \bar{\varphi}|_{\substack{r=r_{ij} \\ \theta=\theta_{ij}}} = 0; \end{cases} \tag{6}$$

$$\bar{\varphi}|_{r=1} = 0, \tag{7}$$

where $L[\varphi(t, r, \theta)] = \bar{\varphi}(s, r, \theta)$.

We can use Galerkin's method [8] to solve the boundary-value problem of (6) and (7) approximately: we rewrite (6) as $F[\bar{\varphi}(s, r, \theta)] = 0$, where F is a linear operator.

Approximation n to the solution is the function

$$\bar{\varphi}_n(s,\ r,\ \theta) = \sum_{i=0}^{n-1} b_i(s)\, \psi_i(r,\ \theta),$$

where $\psi_i(r, \theta)$, $i = 0, 1, 2, \ldots$, are the eigenfunctions for the self-conjugate boundary-value problem

$$\begin{cases} \Delta\psi = -\lambda\psi; \\ \psi|_{r=1} = 0. \end{cases}$$

The coefficients b_k ($k = 0, 1, 2, \ldots$) are determined from the condition for orthogonality of $F(\bar{\varphi}_n)$ to the functions ψ_k in the region $\Omega = (0 \leqslant r \leqslant 1,\ 0 \leqslant \theta \leqslant 2\pi)$:

$$\int_0^{2\pi} \int_0^1 F(\bar{\varphi}_n)\, \psi_k\, r dr d\theta = 0,\ k = 0,\ 1,\ 2,\ \ldots,\ n-1. \tag{8}$$

Equations (8) constitute a linear homogeneous algebraic system for the coefficient b_i:

$$\sum_{i=0}^{n-1} B_{ki} b_i = 0,\ k = 0, 1, 2,\ \ldots,\ n-1,$$

where

$$B_{ki} = \int_0^{2\pi} \int_0^1 F(\psi_i)\, \psi_k r\, dr\, d\theta.$$

We equate the determinant of this system to zero to get an approximate characteristic equation:

$$|B_{ki}| = 0. \tag{9}$$

Numerical analysis shows that acceptable accuracy is obtained in determining the roots of the characteristic equation for (1)-(3) by incorporating 17 terms in the expansion of the neutron flux in terms of the spatial harmonics, i.e., for $\max k = \max i = 16$ in (9). Study of the roots of (9) can provide reasonably complete information on the general effects of the control-system parameters on the stability of the steady state in the reactor.

The optimization involves a choice of optimality criterion; here we have used the following scheme for defining the optimum location of the means of measurement and control. We seek to define a location such that the function J defined by

$$J = \max_i Re(s_i), \quad i = 1, 2, \ldots, n,$$

is minimized, where S_i are the roots of (9). We use the local-variation method with a computer [9] to define min J. Then we examine the performance in the transient response in the system with this disposition. The basic performance criteria in this case are the transient decay time and the error in maintaining the mean power. If the control performance satisfies the requirements, it is assumed that the control system is optimal, but otherwise it is necessary to increase the number of regulators.

Three Regulators. We assume that one rod corresponds to one transducer. It is known [2] that an automatic control with three local regulators can stabilize a reactor unstable on not more than three harmonics without the control system.

It has been shown [4-7] that the stabilizing features of an automatic control for a one-dimensional reactor are substantially dependent on the mutual disposition of the transducers and rods. One therefore naturally supposes that a similar feature occurs in the present control system. We assume that each local zone containing the rods and transducers has central symmetry, and then the adjustable parameters are the coordinates r_1 and θ_1 of the rod and those r_{11} and θ_{11} of the transducer. For example, we consider a reactor in which the radius of the equalized energy distribution $R_1 = 0.7$, and we further assume $A_i = 30$, $i = 1, 2, 3$, and $\alpha = 20$. A reactor with this α is unstable on five harmonics without the control system. We examine how the roots of (9) vary with r_1, r_{11}, θ_1, θ_{11}. On account of the symmetry, the independent parameters are r_1, r_{11}, $\theta_{11} - \theta_1$.

The initial disposition is the following local control system:

$$r_1 = r_{11} = 0{,}6; \quad \theta_{11} - \theta_1 = 0. \tag{10}$$

The solution to (9) with these parameters is three roots each with a positive real part. The azimuthal distribution of the transducers and rods, i.e., variation of $\theta_{11} - \theta_1$, produces a stabilizing effect, and for $0.8 \leq \theta_{11} - \theta_1 \leq 1.25$ the automatic control system with three control rods stabilizes this reactor that otherwise is unstable on five harmonics.

The local-variation method allows us to minimize J; Fig. 1 illustrates the sequence. The azimuthal paths of the transducers and rods are nominal, since the independent parameter is the difference of the azimuthal angles $\theta_{11} - \theta_1$. The final point in the search corresponds to an unsymmetrical zone control system with parameters $r_1 \approx 0.4$; $r_{11} \approx 0.9$; $\theta_{11} - \theta_1 \approx 0.8$.

Stability in a control system is an important characteristic but not the only one; from the practical viewpoint, it is also necessary to consider the transient response and the precision in maintenance of the mean power during control. This system was checked for performance by comparison with the local control system of (10). First we examine the stabilizing effects of the various forms of mutual disposition of the rods and transducers. For this we consider again a reactor unstable on five harmonics ($\alpha = 20$). We assume $A_i = 30$, $i = 1, 2, 3$, and introduce a feedback perturbation of the form

$$\Delta K_{fb} = \sum_{i=0}^{n-1} \psi_i(r, 0). \tag{11}$$

The behavior of the amplitudes of the harmonics is closely demonstrated by the amplitude of the zeroth harmonic. In the case of the local system of (10), we find that b_0 increases exponentially (curve 1 in Fig. 2), because this system does not control the instability on the five harmonics. The unsymmetrical zone system

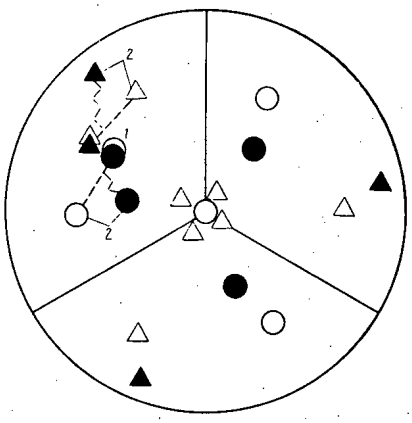

Fig. 1. Definition of the optimal location for measuring and control devices by the local-variation method: ● and Δ, three regulators; ○ and Δ, four regulators; ● and ○, rods; Δ and Δ, sensors; 1 and 2, initial and final points in search, respectively.

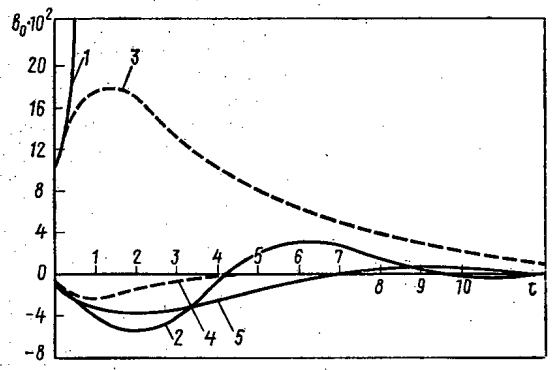

Fig. 2. Variations in amplitude of fundamental for $\alpha = 20$ (——) and $\alpha = 6$ (- - -); 1 and 3) local control system with three regulators; 2 and 4) zone-asymmetric system with three regulators; 5) zone-asymmetric system with four regulators.

does stabilize this instability. The amplitude changes then take the form of damped oscillations (curve 2 in Fig. 2). It is of interest to consider the behavior of the zeroth-harmonic amplitude when the control system of (10) stabilized an unstable reactor ($\alpha = 6$). Figure 2 shows that the maximum deviation and the transient-response time for this unsymmetrical control are substantially smaller than those for the local system.

It is important that the control should maintain the total reactor power with a given accuracy. In the present case, contributions to the total power come only from the radial harmonics:

$$\int_0^{2\pi}\int_0^1 \varphi r\, dr d\theta = 2\pi\left(b_0\int_0^1 \psi_0 r\, dr + b_5\int_0^1 \psi_5 r\, dr + b_{14}\int_0^1 \psi_{14} r\, dr + \ldots\right).$$

The behavior of the total power for the case of Fig. 2 is close to that of b_0, i.e., the unsymmetric system maintains the total power with much better accuracy. The analysis shows that the transient response with the unsymmetrical system optimized to min J is far better than that of the local system of (10).

Four Regulators. As in the previous case we assume that one rod corresponds to one transducer. If the rods and transducers are uniformly distributed in azimuth, there is no unsymmetrical control system that can stabilize the second azimuthal harmonic of the form

$$R_{02}\cos 2\theta \quad \text{or} \quad R_{02}\sin 2\theta. \tag{12}$$

It is impossible to stabilize this harmonic because, in principle, any combination of the harmonics of (12) is possible, and among these there is always one such that the deviation of the parameters at the points of disposition of the transducers will be zero. On the other hand, the above unsymmetrical control system with three regulators does stabilize the azimuthal harmonic of (12), i.e., three regulators uniformly disposed in azimuth in the core provide better stabilization than do four regulators under the same conditions. One naturally therefore disposes the four regulators in such a way that one is at the center and the other are uniformly placed in the core. A local control system using this principle does not stabilize a reactor that in unstable without a control system on more than three harmonics. If we introduce asymmetry into the peripheral control and measurements components, we get a system that can stabilize six unstable harmonics. The local-variation method gives us the search sequence (Fig. 1). In this case the central rod is coupled to four transducers. As we have seen above, the variations in θ_{11} and θ_1 are nominal. The final point has coordinates $r_1 \approx 0.65$; $r_{11} \approx 0.7$; $\theta_{11} - \theta_1 \approx 1.1$; $r_{2i} \approx 0$, where r_{2i} is the radial coordinate of a transducer coupled to the central rod.

Curve 3 of Fig. 2 shows the change in the amplitude of the zeroth harmonic for $\alpha = 20$, $A_i = 30$, $i = 1, 2, 3, 4$ in the perturbation of (11); the transient response is in no way inferior to that shown in curve 2 of Fig. 2. The deviation in the amplitude of the zeroth harmonic maximum in modulus is less for the system with four regulators than that for three. The following feature is also implied by this study: if an unsymmetrical system is to be constructed with a rod at the center of the core, it is recommended that an odd number of regulators should be arranged at the periphery. Although in this study we considered one transducer per rod, all the qualitative results apply for a larger number of transducers coupled to a rod, and so does the method of defining the optimum structure.

Conclusions. An automatic control has been synthesized for a two-dimensional reactor by a combination of the zoning and asymmetry principles, in which the reactor is split up into zones with spatial dispersal of the

means of measurement and control in each zone, which improves the control characteristics. Complete utilization of all the favorable features of such a system requires optimization of the mutual disposition of the transducers and rods in the zone.

This method of defining the optimum configuration by computer provides satisfactory working performance in the control system not only as regards stabilization but also as regards transient response.

The unsymmetrical-zone automatic control with three regulators constructed in this way can stabilize a reactor unstable without a control system on five harmonics. There is also satisfactory transient-response performance as regards control time and stabilization of the total power.

If an unsymmetrical control system with a central rod is being designed, it is desirable to place an odd number of rods at the periphery, which considerably improves the stabilizing performance of the control system.

This approach can also be used in synthesizing control systems for the energy distribution in the volume of the reactor.

LITERATURE CITED

1. I. Ya. Emel'yanov, P. A. Gavrilov, and B. N. Seliverstov, Control and Safety in Nuclear Power Reactors [in Russian], Atomizdat, Moscow (1975).
2. A. Hitchcock, Nuclear Reactor Stability [Russian translation], Gosatomizdat, Moscow (1963).
3. D. Wiberg, Nucl. Sci. Eng., 27, 600 (1967).
4. I. S. Postnikov and E. F. Sabaev, At. Energ., 26, No. 1, 56 (1969).
5. I. Ya. Emel'yanov et al., At. Energ., 46, No. 2, 82 (1979).
6. A. M. Afanas'ev and B. Z. Torlin, in: Nuclear Science and Technology, Series Dynamics of Nuclear Power Systems [in Russian], Issue 1(7), Izd. TsNIIatominform, Moscow (1975), p. 65.
7. A. M. Afanas'ev and B. Z. Torlin, At. Energ., 43, No. 4, 243 (1977).
8. V. D. Goryachenko, The Methods of Researching the Stability of Nuclear Reactors [in Russian], Atomizdat, Moscow (1977).
9. G. Sea, Optimization: Theory and Algorithms [Russian translation], Mir, Moscow (1973).

OPTIMIZATION OF PLASMA PARAMETERS IN A HYBRID REACTOR-TOKAMAK

A. S. Kukushkin and V. I. Pistunovich

UDC 621.039.6

In recent years numerous calculations have been made of the parameters of a thermonuclear reactor-tokamak [1, 2] which mainly involve a parametric analysis of systems rather than closed models of a reactor. The current lack of a reliable model for computing the plasma parameters is due to ignorance of the behavior of plasmas in reactor regimes. However, available information makes it possible to derive several important conclusions about the optimum values of the plasma parameters in a reactor.

In this paper we present data on the optimum dimensions of a reactor and on its operating regime using simple energy and particle balance equations for the tokamak plasma and employing numerical calculations made with the aid of the extended plateau model for the ion thermal conductivity [3, 4]. The effect of bumpiness in the toroidal magnetic field on the plasma energy balance is also examined.

Optimum Plasma Dimensions for a Hybrid Reactor-Tokamak. We shall consider as an example a tokamak with a circular plasma cross section of radius a, a blanket of thickness d_b, toroidal magnetic field coils of thickness d_c, and a divertor layer d_d. The thickness d_b is determined from the conditions for protecting the magnetic system from neutron and secondary radiation. In most designs for hybrid reactors, $d_b \sim 1.4$ m [5] and depends very weakly on the power and size of the device. Thus, the minimum radius a is determined purely by

Translated from Atomnaya Énergiya, Vol. 47, No. 6, pp. 374-377, December, 1979. Original article submitted February 14, 1979.

0038-531X/79/4706-0983$07.50

economic considerations: for $a < d_b$ the toroidal magnetic field will be used inefficiently and the economic viability of the system is reduced. We therefore obtain $a \geq d_b \approx 1.4$ m.

The aspect ratio $A = R/a$, where R is the major radius of the plasma, can be determined from the condition on the duration of the current in the plasma due to the change in the magnetic flux passing through the central part of the torus which is free of magnets, $\Delta\Phi = 2\pi R_0^2 B_0$ (V·sec). The factor 2 means that magnetic reversal of the inductor is used and $R_0 = R - a - d_d - d_b - d_c - d_i$ (where d_i and B_0 are the thickness of the inductor winding and its magnetic field, respectively). When $a = 1.4$ m we have $A = R/a \geq 4$. The upper bound on A is the maximum allowable plasma pressure:

$$p = 2nT \leqslant \gamma \frac{B_z^2}{q^2 A}, \tag{1}$$

where n and T are the density and temperature of the plasma; γ is a coefficient in units of $8\pi[\beta_\theta = (R/a)\gamma]$; q is the stability (safety) factor of the plasma colume; B_z is the magnetic field on the axis of the torus. When a is varied from 1 to 5 m, A changes from 5 to 3.

For the next calculations we write the energy balance equation for a plasma of volume V:

$$\frac{3nT}{\tau_E} V = P_0 + \varphi S E_\alpha - P_{\text{rad}}. \tag{2}$$

Here τ_E is the energy lifetime in the plasma; P_0 is the power delivered to the plasma; φ is the flux of thermonuclear neutrons per cm^2; S is the surface area of the reactor chamber; $E_\alpha = 3.52$ MeV; P_{rad} is the power loss due to radiation.

Substituting Eq. (1) in Eq. (2) and using the fact that $\tau_E = a^2 \tau_0$, we obtain

$$\varphi = \frac{3}{4} \gamma \frac{B_z^2}{q^2 A a \tau_0 E_\alpha} - \frac{P_0 - P_{\text{rad}}}{S E_\alpha}. \tag{3}$$

We define the power gain coefficient of the plasma, Q, as the ratio of the thermonuclear power to the input power:

$$Q = \varphi S (E_{\text{th}}/P_0), \tag{4}$$

where $E_{\text{th}} = 17.6$ MeV.

It is clear from Eqs. (3) and (4) that the basic plasma characteristics φ and Q of a hybrid reactor at which the maximum allowable plasma pressure (1) is obtained are fairly simply related to the plasma size. Thus, for all other conditions the same, φ decreases as a is increased, while Q remains constant in systems with $P_0 = \text{const}$. Only under conditions close to ignition of a thermonuclear reaction does Q increase due to a reduction in P_0. This result was obtained previously in [1]. For hybrid reactors $Q \lesssim 5$ and is practically independent of a.

Therefore, to obtain maximum neutron loading on the wall, a hybrid reactor must have a minimum size a; very good plasma confinement is not required since φ decreases as τ_0 increases. There is, however, a minimum value of the confinement parameter $n\tau_0$, below which a fairly large injection power is required to reach thermonuclear temperatures and φ decreases due to the growth in P_0.

The above discussion and the numerical calculations [3, 4] of the plasma energy balance in a hybrid reactor using the extended plateau model lead to the conclusion that the optimum size a must be chosen on the basis of economic indices for the reactor as a whole; that is, $a \approx d_b \approx 1.4$ m. At the present time there is sufficient basis to hope that thermal conduction processes in a reactor plasma will not require a significant enlargement of the minor radius.

Effect of Longitudinal Bumpiness in the Magnetic Field on Transport Phenomena in a Tokamak. One-dimensional calculations of energy and particle transport in tokamaks are based on averaging the transport coefficients over the magnetic surfaces. The customary neoclassical and classical coefficients are calculated assuming that the system has azimuthal symmetry (for example, [6, 7]). In that case the inhomogeneity of the magnetic field on the magnetic surface along a major circumference of the torus is neglected.

In fact, the toroidal magnetic field is created by a set of coils and is naturally inhomogeneous along the magnetic axis. This inhomogeneity (bumpiness) causes additional trapping of part of the ions in the plasma. The ions that are trapped in the bumps do not "feel" the rotational transform of the magnetic field and escape to the chamber walls due to toroidal drift. Collisions knock particles out of this state and inhibit their escape; thus, the contribution to the transport coefficients due to capture of particles in the magnetic field bumps is

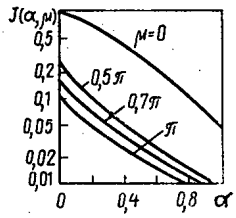

Fig. 1. The effective reduction in the transport coefficients corresponding to the field bumpiness when the toroidal inhomogeneity is superimposed.

reduced as the collision frequency is increased. Diffusion and thermal conductivity coefficients of this form were apparently first derived by Connor, Hastie, and Taylor [9]:

$$D = 4.34\,\delta^{3/2}\nu_{ei}^{-1}\left(\frac{cT_e}{eBR}\right)^2;$$
$$\chi_i = 46.5\,\delta^{3/2}\nu_{ii}^{-1}\left(\frac{cT_i}{eBR}\right)^2, \tag{5}$$

where $\nu_{ii} = \frac{4}{3}\frac{\sqrt{2\pi}\,ne^4\ln\Lambda}{\sqrt{m_i}T_i^{3/2}}$ is the collision frequency (here all units are taken in the cgs system; T_i and T_e are the ion and electron temperatures; m_i is the ion mass; e is the electron charge; c is the speed of light; n is the plasma density; and, ln Λ is the Coulomb logarithm); δ is the amplitude of the bumpiness in the magnetic field; and, ν_{ei} is the electron–ion collision frequency.

Two effects which reduce the effective depth of the field bumpiness and thus reduce the transport coefficients (5) were pointed out in [8, 10-12]. The first, examined by Stringer [11], consists of a reduction in the effective depth of the bumpiness when the toroidal inhomogeneity of the field is superimposed. In [8, 10, 12] a reduction in the transport coefficients due to nonparallelism of the longitudinal field coils was also taken into account.

Since the transport caused by the bumpiness in the field depends strongly on the value of δ, which falls toward the center of the plasma column, it is important to know the behavior of δ(r) at the edge of the column. The final expression for the transport coefficient is

$$\chi_i = 4.7\cdot 10^{17}\,\delta(r)^{3/2}\frac{T_i^{7/2}}{B^2R^2n}J(\alpha),\ \text{cm}^2/\text{sec} \tag{6}$$

(here and in the following T is measured in eV, B in kG, R in cm, and n in cm^{-3}) by analogy with Eq. (5), in which δ must be replaced by δ(r) and the factor $J(\alpha, \mu)$ must be included, where

$$J(\alpha,\ \mu) = \frac{1}{\pi}\int_0^{2\pi} f^{3/2}(\hat{\alpha},\ \theta)\exp\left(-\frac{3}{2}\frac{\mu\theta^2}{\pi}\right)\sin^2\theta\,d\theta, \tag{7}$$

where $\hat{\alpha} = \hat{\alpha}(r,\ 0) = \varepsilon\ \exp\ (\mu\theta^2/\pi)/qN\delta(r) \equiv \alpha\ \exp\,(\mu\theta^2/\pi)$; θ is the angle; N is the number of windings around the minor circumference of the torus; and, $\varepsilon = r/R$. The value of μ is determined from calculations of the magnetic field for a given device. The function $J(\alpha, \mu)$ [12] is plotted in Fig. 1. It is clear that the effective reduction in the depth of the bumpiness upon averaging over the magnetic surface may cause a reduction in the transport coefficients by more than an order of magnitude. In our calculations δ(r) was given by the expression

$$\delta(r) = \delta\frac{I_1(0.7\,Nr/R)}{I_1(0.7\,Na/R)},$$

where I_1 is the modified Bessel function, N = 16, and μ = 2.4. This form of δ(r) was chosen by analogy with the calculations for the T-10 tokamak [13] (which has circular coils). The thermal conductivity χ_i^r corresponding to the bumpiness of the field is added to the coefficient χ_i^{pl} for the extended plateau model [3, 4] to yield

$$\chi_i = \frac{1}{\xi}\chi_i^{pl} + \chi_i^r,\ \chi_i^{pl} = 7.3\cdot 10^4 qT_i^{3/2}/RB^2. \tag{8}$$

Here ξ is the "optimism coefficient" of the model (the diffusion of the plasma was not examined and the plasma density was assumed to be distributed parabolically). Naturally, in the central region of the column $\chi_i^r \ll \frac{1}{\xi}\chi_i^{pl}$,

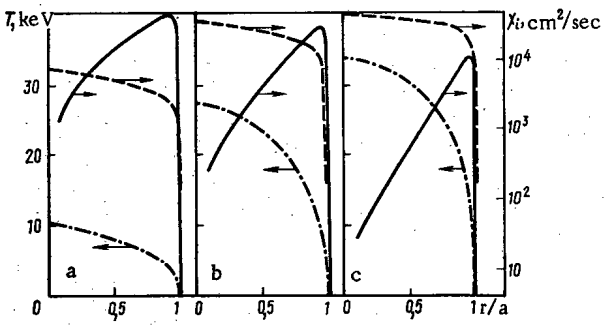

Fig. 2

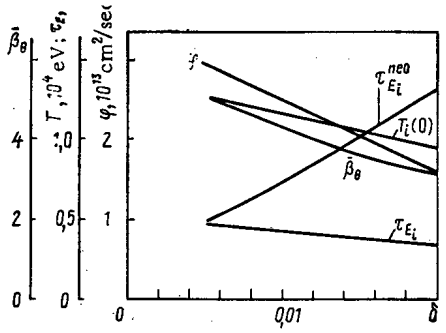

Fig. 3

Fig. 2. The radial distribution of the transport coefficients χ_i^r (—), χ_i^{pl} (– – –) and of the temperature T_i (—·—) for $\xi = 10$ and $\delta = 0.05$ (a); 0.01 (b); 0.005 (c).

Fig. 3. The variation in the neutron flux φ to the wall of a reactor, in the energy lifetime τ_{E_i}, and in the "neoclassical" lifetime $\tau_{E_i}^{neo}$ (without bumpiness of the field) for $R = 4$ m, $a = 1$ m, $B_0 = 6$ T, $\xi = 5$, $P_0 = 60$ MW, $E_0 = 400$ keV [$T_i(0)$ is the ion temperature at the center of the plasma column].

while at the edge they are comparable and the bumpiness may cause a significant deterioration in the plasma parameters. Figure 2 shows the radial distributions of the ion thermal conductivity due to the bumpiness of the field, χ_i^r (6), and in the extended plateau model, χ_i^{pl} (8). It is clear that for $\xi = 10$ the change in the amplitude δ of the bumpiness from 5% to 0.5% causes a qualitative change in the nature of energy release to the wall of the reactor. If in the first case the losses are controlled by the bumpiness of the field, then for $\delta = 0.5\%$ the bumpiness practically has no effect on the energy balance of the plasma.

Figure 3 shows the dependence on δ of the energy lifetime of the plasma and of the neutron wall loading in a reactor with $R = 4$ m, $a = 1$ m, $B_0 = 6$ T, and a plasma current $I = 2.5$ MA, while Fig. 4 shows the same dependence on ξ. It is clear that in the case of large ξ ($\xi \geq 5$) for $\delta \geq 0.01$ (i.e., a bumpiness of depth $\geq 2\%$ at the outer edge of the plasma column) the energy lifetime and, therefore, the economic viability of the reactor, are determined by the bumpiness in the field.

Figure 5 shows the dependence of the energy lifetime of the ions τ_{E_i} on the ion temperature at the axis of the plasma column when the bumpiness of the toroidal field is taken into account ($\delta = 0.01$) and when it is neglected for various values of the parameter ξ. It is clear that in all cases of practical interest ($\xi \geq 2$) the amplitude of the bumpiness $\delta = 0.01$ has a significant effect on the behavior of the plasma. Thus, in designing a reactor-tokamak the bumpiness of the toroidal field must evidently be no larger than ± 1% in order that the plasma confinement time should be sufficiently large.

Extended Plateau Model for Designing a Reactor-Tokamak. In [3, 4] the authors have used the so-called extended plateau model for the ion thermal conductivity [Eq. (8)]. Compared to the other models for the plasma part of a reactor-tokamak, the extended plateau model is the most pessimistic. However, a number of important results have been obtained with its aid.

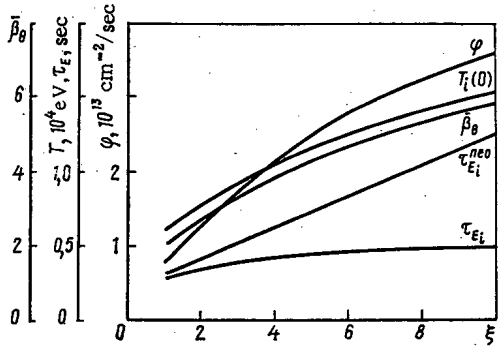

Fig. 4. The dependence of the neutron flux φ, $\tau_{E_i}^{neo}$, and τ_{E_i} on the "optimism coefficient."

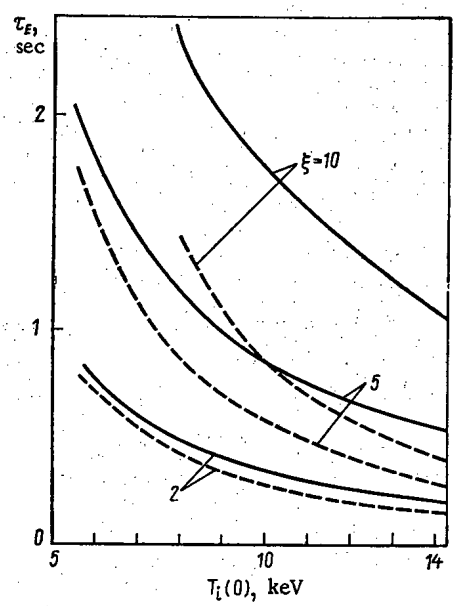

Fig. 5. The dependence of the ion energy lifetime of the plasma τ_{E_i} on the ion temperature at the center of the plasma column taking the bumpiness into account (– – –) and neglecting it (———) for various values of ξ when $\delta = 0.01$.

It seems that for determining the parameters of a practical reactor (thermonuclear neutron flux at the first wall of $\varphi \approx 5 \cdot 10^{13}$ neutrons/(cm^2 · sec), $Q \approx 4$) an "optimism coefficient" of $\xi \approx 3$ is sufficient. It follows from this that in the case of the best plasma confinement it is possible to obtain larger values of Q by reducing the injection power. However, for a given plasma pressure the neutron flux to the first wall will not increase. Thus it appears that at present the most important problem for the reactor-tokamak is to obtain the maximum possible values of $\beta_\theta^{max} = (2nT/B_0^2)\, 8\pi$, where B_0 is the magnetic field produced by the discharge current. In our calculations it was assumed that $\beta_\theta^{max} \approx (R/a)\,\gamma$, where γ is the elongation of the transverse plasma cross section. In this case the value of β along the toroidal field is $\beta \approx a\gamma/Rq^2$ and equals a few percent. Calculations show that for $\beta_\theta < (R/a)\,\gamma$ it is difficult to construct a hybrid reactor-tokamak of practical interest since then $\varphi < 5 \cdot 10^{13}$ neutrons/(cm^2 · sec) and $Q < 4$.

Another important result of our calculations is that prolonged operation of a reactor (about 900 sec) is impossible without intense pump-out of helium ions and fuel. Otherwise the thermal and neutron loading on the system structure will occur in pulses with a time constant of 20-30 sec. Whether a reactor can operate for a long time (about 10 years) in a short pulse (about 50 sec with a pause $\leq$5 sec) regime is difficult to answer today; however, an increase in the number of working pulses by an order of magnitude may change the situation qualitatively by placing insoluble technical problems in the way.

Conclusions. The basic results may be summarized as follows:

There is an optimum plasma size for a hybrid reactor-tokamak which is apparently determined by the thicknesses of the blanket, magnetic coils, etc., and, therefore, by the economic indices for the system as a whole.

Further progress in the development of a reactor-tokamak depends to a great extent on the achievement of the maximum pressures at which the plasma remains stable.

A hybrid reactor-tokamak presupposes the existence of powerful devices (for example, a divertor) for efficient removal of helium and fuel ions from the reactor volume and for protecting the plasma from impurities.

In designing a reactor-tokamak it is necessary to ensure that the bumpiness in the toroidal magnetic field not exceed ± 1%.

LITERATURE CITED

1. D. Jassby, Nucl. Fusion, 17, No. 2, 309 (1977).
2. E. Bertolini et al., No. 5, 955 (1977).

3. A. S. Kukushkin and V. I. Pistunovich, in: Proceedings of the Second Soviet–American Seminar on Fusion–Fission [in Russian], Atomizdat, Moscow (1978), p. 123.
4. V. A. Abramov, A. S. Kukushkin, and V. I. Pistunovich, Talks at the All-Union Conference on Engineering Problems of Thermonuclear Reactors [in Russian], Vol. II, Izd. NIIEFA, Leningrad (1977), p. 178.
5. E. P. Velikhov et al., ibid., Vol. I, p. 5.
6. A. A. Galeev and R. Z. Sagdeev, in: Problems of Plasma Theory [in Russian], Vol. 7, Atomizdat, Moscow (1973), p. 205.
7. F. Hinton and R. Hazeltine, Rev. Mod. Phys., 48, 239 (1976).
8. J. Davidson, Nucl. Fusion, 16, 731 (1976).
9. J. Connor et al., in: Proceedings of Conference on Plasma Physics and Controlled Nuclear Fusion Research, Vol. I, IAEA, Vienna (1972), p. 15.
10. K. Tsang, Nucl. Fusion, 17, 557 (1977).
11. T. Stringer, ibid., 12, 689 (1972).
12. Yu. N. Dnestrovskii, D. P. Kostomarov, and S. E. Lysenko, Yad. Sintez, 15, 1185 (1975).
13. Yu. N. Dnestrovskii and S. E. Lysenko, Preprint IAE-2566, Moscow (1975).

SIMULATION OF NUCLEAR-FUEL SOLVENT-EXTRACTION REPROCESSING

7. SEPARATION OF MACROSCOPIC AMOUNTS OF PLUTONIUM AND URANIUM BY DISPLACEMENT REEXTRACTION OF PLUTONIUM IN REPROCESSING FAST-REACTOR FUEL (SECTION 1)

É. V. Renard and M. Ya. Zel'venskii

UDC 621.039.59.001.57

Formulation. The fuel in the core of a fast reactor produces a great deal of heat, which leads to special design features in the fuel assemblies, and this leads to complexity in fuel-rod exchange in the central zone, so the best approach to fuel reprocessing may be joint processing at the desheathing and dissolution stage applied to fuel from the end shield and the core [1, 2].

The purpose of reprocessing fast-reactor fuel is to produce mixed uranium–plutonium fuel for reloading, which requires partial or complete separation of the uranium and plutonium with the object of ultimately producing a uranium–plutonium mixture with the ratio required for fabricating core fuel pins (for example, U : Pu = 3 : 1). Several methods can be used to separate the uranium and plutonium: chemical or electrochemical reduction of the plutonium, reextraction of Pu(IV) in weakly acid solution, reextraction of Pu(IV) by the use of complexing agents, and displacement reextraction of Pu(IV) by saturating the extract with the readily extracted U(VI) [1]. The latter method appears extremely promising [3] because it does not involve the use of salts and is rapid. The only reagent used is the uranium produced in the scheme as the reextracted solution.

Here we examine displacement reextraction applied to the reprocessing of fast-reactor fuel. It is necessary to establish the scope for producing the uranium (the uranium extract) adequately free from plutonium and the plutonium (plutonium reextract) with the appropriate amount of uranium (or less), which means that it is necessary to establish the working parameters in this separation. A study is performed by simulation on a model with the algorithm of [4].

Calculations and Discussion. We examined the process in a multistage system with two inputs (Fig. 1). The calculations were based on a program that describes the dynamics of the process, and the calculations were carried through to the exit from the stage in the steady state (99% in each component). The main results from the simulation are the concentrations of uranium and plutonium in the outgoing water reextract X_U^{out} and X_{Pu}^{out}, for which we calculate the ratio $[U/Pu]_x = X_U^{out}/X_{Pu}^{out}$, together with the concentrations of uranium and plutonium in the outgoing extract Y_U^{out} and Y_{Pu}^{out}, from which we determine the coefficient for elimination of plutonium from uranium $K = Y_{Pu}^0 Y_U^{out}/Y_U^0 Y_{Pu}^{out}$, as well as the extraction of plutonium into the reextract $\Gamma = (1 -$

Translated from Atomnaya Énergiya, Vol. 47, No. 6, pp. 377-381, December, 1979. Original article submitted March 26, 1979.

0038-531X/79/4706-0988$07.50

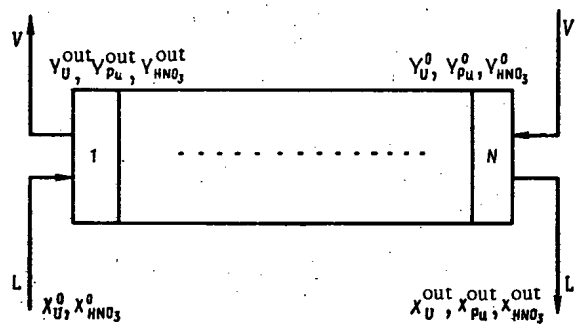

Fig. 1. Scheme for displacement reextraction apparatus; symbols for flows and concentrations (1...N are the numbers of the stages).

$Y_{Pu}^{out}/Y_{Pu}^0) \cdot 100\%$ and the content of plutonium in the uranium $S = (Y_{Pu}^{out}/Y_U^{out}) \cdot 10^9$ μg Pu/kg U. The assumulation of plutonium within the system was determined as the ratio of the maximum plutonium concentration in aqueous phase to the concentration in the outgoing reextract ($M = X_{Pu}^{max}/X_{Pu}^{out}$). We varied the working parameters that influence the separation performance: the concentrations of uranium and nitric acid in the reextraction agent X_U^0, $X_{HNO_3}^0$, the number of stages N, the water phase flow L or the ratio of the flows (the flow of the initial organic solution V^0 was taken as 1 in all the states), and the composition of the initial organic solution for saturation of the 30% TBP with respect to the sum of the metal with a constant ratio $Y_U^0 : Y_{Pu}^0 = 10 : 1$.

We consider the effects of each parameter on the process characteristics.

Effects of Reextractant Acidity. The calculations were performed for the following conditions: N = 10 and 15; $X_U^0 = 80$ and 100 g/liter; L = 0.5 (n = V/L = 2.0); $Y_U^0 = 70$ g/liter; $Y_{Pu}^0 = 7$ g/liter; $Y_{HNO_3}^0 = 0.24$ M; the nitric acid concentrations in the input reextractant were 0.1, 0.3, 0.5, and 1.0 M. Figure 2 shows the results (the situation of the initial organic solution was 64% in the sum of the metals and L/V = 0.5).

When the acidity is low, one can get hydrolysis and polymerization of the Pu(IV), so $X_{HNO_3}^0 = 0.1$ M is not appropriate from this viewpoint, although low acidity favors fuller reextraction of the plutonium. On the other hand, excessively high acidity (1 M and above) does not provide proper reextraction of the plutonium and leads to the formation of a plutonium peak (for example, $X_{HNO_3}^0 = 4$ M, M = 8.0). Figure 2 shows that increasing the acidity improves the $[U/Pu]_X$ ratio, but at the same time it adversely affects the purification of the uranium extract from plutonium. An applicable acidity is 0.3 M (one should then have $N \geq 15$, $X_U^0 \geq 100$ g/liter, n = 2.0).

Effects of U(VI) Concentration on the Reextractant. This relationship was derived by calculation for an 18-stage extractor with $X_{HNO_3}^0 = 0.3$ M, L = 0.5 and with either 64% saturation of the initial organic solution in the sum of the metals ($Y_U^0 = 70$ g/liter, $Y_{Pu}^0 = 7$ g/liter, $Y_{HNO_3}^0 = 0.24$ M) or 82.5% saturation ($Y_U^0 = 90$ g/liter, $Y_{Pu}^0 = 9$ g/liter, $Y_{HNO_3}^0 = 0.17$ M). The values of X_U^0 were 80, 85, 90, 95, and 100 g/liter, which corresponds to typical U(VI) level in hot weak-acid reextraction from 30% TBP solution. Figure 3a shows S and $[U/Pu]_X$ for the 64 and 82.5% saturation levels (numbers on curves). Clearly, 64% saturation produces satisfactory* purification of the uranium extract from plutonium when X_U^0 is reduced from 100 to 85 g/liter, but already at $X_U^0 =$ 80 g/liter we get considerable retention of the plutonium in the extract. The ratio $[U/Pu]_X$ varies only slightly as X_U^0 is varied, and it remains at the level 2.9-3.1,† which is acceptable. At 82.5% saturation, the U(VI) concentration in the reextract is roughly double, while the content of plutonium in the reextract is increased by about a factor 1.3, which very adversely affects the $[U/Pu]_X$ ratio, which rises to about 4.5. The composition of the uranium extract is then largely unaltered, and the uranium remains reasonably free from plutonium. Therefore, a U(VI) concentration in the reextractant in the range 85-100 g/liter is acceptable.

Effects of Number of Stages. This was examined for $X_U^0 = 90$ g/liter; $X_{HNO_3}^0 = 0.3$ M; n = 2.0; $Y_U^0 = 70$ g/liter; $Y_{Pu}^0 = 7$ g/liter and $Y_{HNO_3}^0 = 0.24$ M; the numbers of stages were taken as 10, 15, 18, 20, and 25, i.e., within the range usually employed for a single reprocessing cycle for nuclear power stations. Figure 3b shows the results.

*We have taken as an acceptable level of plutonium in uranium S = 100 μg Pu/kg U.

†It is desirable to produce a U–Pu product with a proportion of plutonium exceeding the maximum necessary for making the fuel for the core with any enrichment, since the U–Pu mixture can be adjusted to the exact ratio at the solution+solution level by the use of depleted uranium. Here we have assumed that an acceptable value is $[U/Pu]_X \leq 3$.

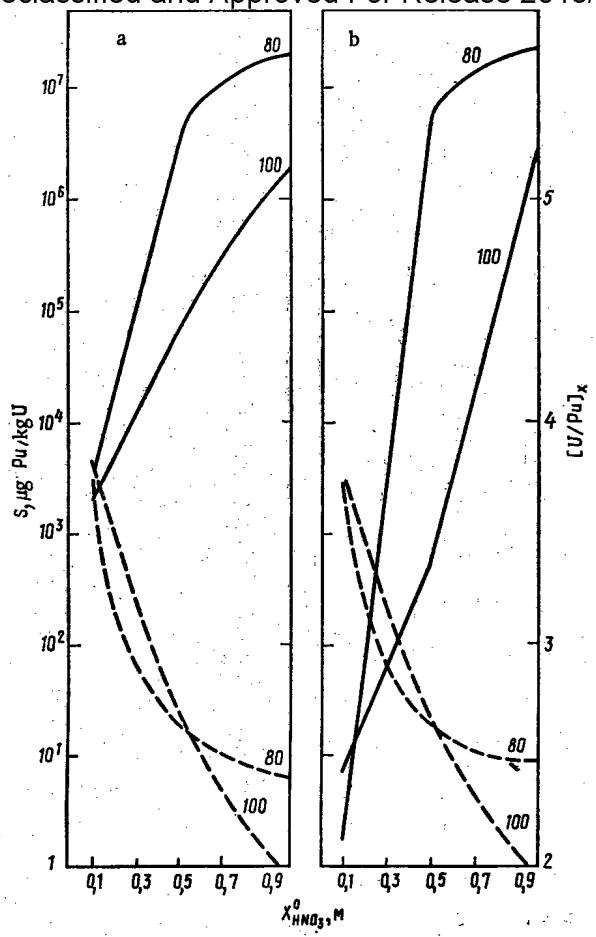

Fig. 2

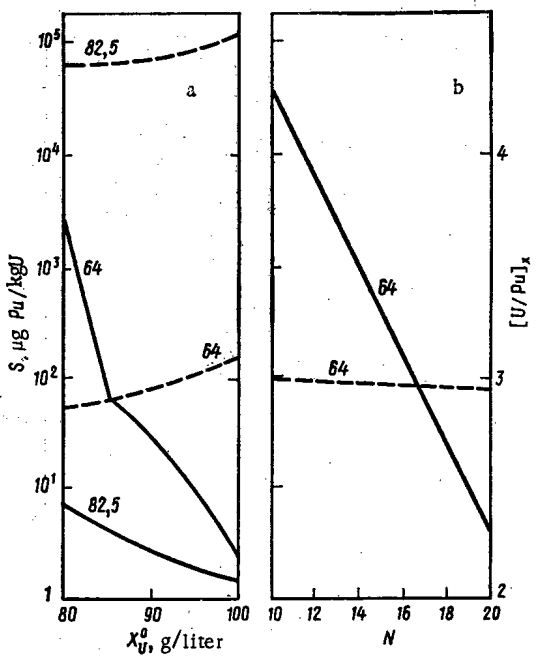

Fig. 3

Fig. 2. Content of the plutonium in uranium (solid line) and $[U/Pu]_X$ ratio (broken line) as functions of the acidity of the reextractant for an extractor with: a) 10; b) 15 stages (the numbers on the curves are X^0_U in g/liter).

Fig. 3. Plutonium content of the uranium (solid line) and $[U/Pu]_X$ ratio (broken line) as functions of: a) uranium concentration in the extractant for N = 18, L/V = 0.5 $X^0_{HNO_3}$ = 0.3 M; b) number of stages in extractor for X^0_U = 90 g/liter; $X^0_{HNO_3}$ = 0.3, and L/V = 0.5.

It is clear that increasing the number of stages has virtually no effect on $[U/Pu]_X$, but it does substantially improve the elimination of plutonium from the uranium. In our case, each stage improves the purification by about a factor 2.5, i.e., the plutonium content of the uranium at the output from a N-stage unit with 64% saturation of the initial solution is $\sim 5 \cdot 10^4 / 2.5^{(N-10)}$ μg Pu/kg U. Clearly, an 18-stage extractor under these conditions provides not only the required $[U/Pu]_X$, which is largely independent of N, but also satisfactory purification of the uranium (S < 100 μg Pu/kg U); 15 stages is inadequate for reliable elimination of the plutonium from the uranium under these conditions. More than 18-20 stages may be undesirable, since this increases not only the capital costs but also the amount of plutonium held up in the system, which is disadvantageous for emergencies.

Effects of Flow Ratio. The flow of the aqueous phase is the most readily controlled parameter, and it is therefore very important to know how the separation is affected by the flow ratio. Figure 4 shows calculations for displacement reextraction of plutonium from the organic solution with 64% saturation (Y^0_U = 70 g/liter; Y^0_{Pu} = 7 g/liter and $Y^0_{HNO_3}$ = 0.24 M) for a water reextractant having $X^0_{HNO_3}$ = 0.3 M and X^0_U = 80-100 g/liter in an extractor with 15-20 stages for L of 0.4 and 0.5. Clearly, the process parameters are unsatisfactory for L = 0.4, and then neither increasing the number of stages (from 15 to 20) nor increasing the U(VI) concentration in the reextractant (from 80 to 100 g/liter) has any appreciable effect ($[U/Pu]_X$ = 2.62 and S = $1.8 \cdot 10^7$ μg Pu/kg U). However, with L = 0.5 the same change in the process parameters does produce a substantial improvement: an increase in N from 15 to 20 does not alter $[U/Pu]_X$ but reduces the plutonium level in the reextract from 3800 to 540 μg Pu/kg U (with X^0_U = 80 g/liter) or even from 425 to 5 μg Pu/kg U (with X^0_U = 90 g/liter); with N = 18, an

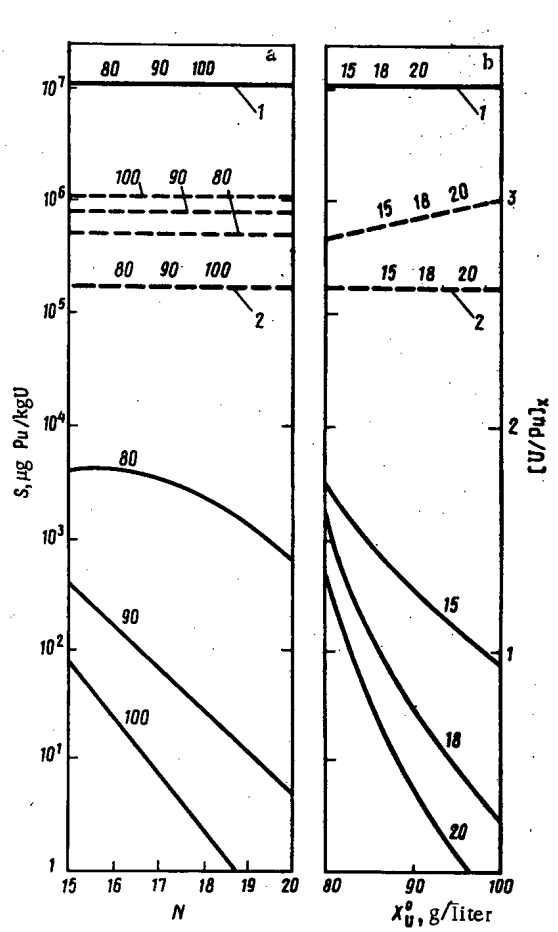

Fig. 4

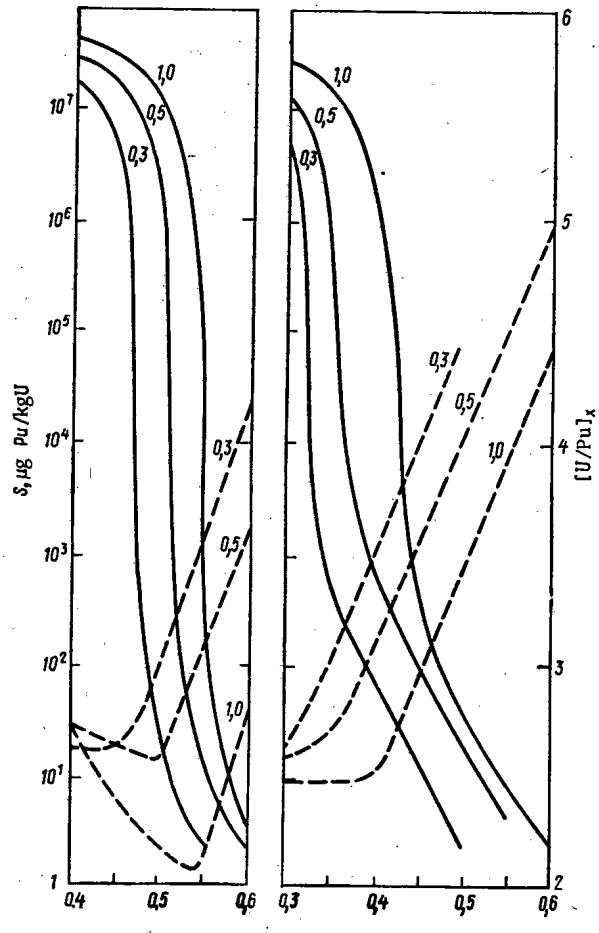

Fig. 5

Fig. 4. Plutonium content of uranium (solid line) and $[U/Pu]_X$ ratio (broken line) as functions of: a) number of stages in extractor (the numbers on the curves are the uranium concentrations in the reextractant); b) uranium concentration in the reextractant (numbers on the curves are the number of stages in the extractor) for L/V of 0.4 (lines 1 and 2) and 0.5.

Fig. 5. Plutonium content of uranium (solid line) and $[U/Pu]_X$ ratio (broken line) in relation to flow of reextractant for saturation levels in the sum of the metals in the initial organic solution of: a) 64%; b) 82.5%.

increase in X^0_U from 80 to 100 g/liter increases $[U/Pu]_X$ slightly (from 2.86 to 3.1) but greatly reduces the amount of plutonium in the uranium (from 2700 to 2.5 μg Pu/kg U). The same picture is observed for N = 15 and 20.

Therefore, the most readily controlled parameter (the flow of aqueous phase) is also a major control parameter; this was confirmed by calculations on an 18-stage system with $X^0_U = 90$ g/liter and $X^0_{HNO_3} = 0.3$, 0.5, and 1.0 M (numbers on the curves) for other saturation levels in the initial organic solution (77 and 99 g/liter for the sum of the metals) and variable values for the aqueous flow (Fig. 5).

An increase in the flow of the reextractant results in a certain rise in $[U/Pu]_X$ but a sharp fall in the level of plutonium in the outgoing extract. The uranium content of the outgoing organic flow (i.e., the saturation of the extract) is almost unaltered. The uranium concentration in the reextract increases with the water flow, while the plutonium concentration passes through a small peak and falls, and the plutonium peak within the apparatus completely vanishes (i.e., the nuclear hazard of the process is reduced as well as the possibility of formation of a second organic phase).

Here we must note that the $S - L$ and $[U/Pu]_X - L$ curves are steep; at 64% saturation with $X^0_{HNO_3} = 0.3$ M we can attain $[U/Pu]_X \leq 3$ only provided that $L \leq 0.5$; for $S \leq 100$ μg Pu/kg U we must have $L \geq 0.485$. Both conditions can be met together if $0.485 \leq L \leq 0.5$, which is clearly a very narrow range for the permissible flow fluctuation, and would be difficult to implement on a large scale. Figure 5 shows that for any given choice of the initial parameters (i.e., the concentrations of the components in the flows of organic and aqueous solutions) there is one value for the flow ratio that results in the required characteristics in the outgoing flows.

Conclusions. These data have been obtained from simulating displacement reextraction in a system with two inputs (system for reprocessing a fast-reactor fuel), and they show that it is possible to obtain a uranium extract with not more than 100 μg Pu/kg U in a countercurrent system with 18 stages to provide partial separation of the uranium and plutonium by reprocessing of an organic solution containing U + Pu (10 : 1) with 64% saturation in the sum of the metals to produce reextract containing plutonium with U : Pu ≤ 3 and over 99.99% extraction of the uranium; this requires 90 g/liter of uranium in the reextractant and the parameters n = 2.06-2.00 ($X^0_{HNO_3}$ = 0.3 M); n = 1.82-1.87 ($X^0_{HNO_3}$ = 0.5 M); n = 1.61-1.78 ($X^0_{HNO_3}$ = 1.0 M).

Full data obtained from the simulation are to be found in [5], from which one can extract the parameters of the working state of the extractor and other data on the separation of uranium and plutonium, e.g., for other specifications for the plutonium level in the uranium. The next part of the present study will be concerned with engineering solutions that can extend the range of conditions that provide the appropriate output parameters within specified ranges and thereby improve the reliability in operating the process in the optimal region.

LITERATURE CITED

1. É. V. Renard, Radiokhimiya, 18, No. 4, 560 (1976).
2. V. B. Shevchenko, I. E. Nakhutin, and É. V. Renard, Paper at the IAEA Conference on Fast-Reactor Fuel Reprocessing, Leningrad, May 17-21, 1976 [in Russian].
3. A. M. Rozen and M. Ya. Zel'venskii, At. Energ., 41, No. 2, 91 (1976).
4. A. M. Rozen and M. Ya. Zel'venskii, Radiokhimiya, 18, No. 4, 572 (1976).
5. É. V. Renard, M. Ya. Zel'venskii, and V. E. Vereshchagin, in: Proceedings of the Fourth COMECON Symposium on Researches in Irradiated Fuel Reprocessing [in Russian], Vol. 2, Izd. ChKAE, Prague (1977), p. 132.

LINEAR COEFFICIENT OF THERMAL EXPANSION OF GRAPHITIC MATERIALS

P. A. Platonov, O. K. Chugunov, V. I. Karpukhin, V. N. Kuznetsov, S. I. Alekseev, and V. P. Golovin

UDC 536.41:620.179.15

Thermal Expansion of Graphite. A characteristic feature of formed graphitic materials is the large difference between the expansion of the crystal lattice and the macroscopic thermal expansion which results from the considerable porosity of these materials. The thermal expansion of reactor graphite is also anisotropic and strongly temperature dependent. The anisotropy of the coefficient of thermal expansion (CTE) arises as a result of the corresponding orientation of anisotropic granules (particles) of the raw materials (coke) which develops during the forming process (extrusion or molding). The degree of this anisotropy depends on the properties of the raw material, the size grading of the mixture, the type and amount of added binder, the number of successive impregnations, the method of forming, etc. (Tables 1 and 2).

When the graphitization temperature is increased from 1000 to 2000°C, the CTE of reactor graphite increases somewhat, but decreases rather sharply when the temperature is increased further (Fig. 1). This characteristic dependence of the CTE on processing temperature is observed for all domestic and imported reactor graphite. The observed regularity in the change of the CTE of graphite can be accounted for only by the change in the magnitude of the CTE of the crystallites themselves in the heat-treatment process, or a change of oriented microporosity.

Table 3 shows that the CTE of pyrographite does not change appreciably when the processing temperature is increased from 2100 to 3200°C. Consequently, the largest effect on the CTE of reactor graphite comes from its microporosity, or more accurately the technological cracks formed in it (Mrozowski cracks between the crystallites parallel to the basal planes [8]) which partially compensate the expansion of the crystallites along a hexagonal axis and thus diminish the total CTE of graphite (cf. Fig. 1).

Translated from Atomnaya Énergiya, Vol. 47, No. 6, pp. 382-386, December, 1979. Original article submitted October 23, 1978; revision submitted April 9, 1979.

0038-531X/79/4706-0992 $07.50

TABLE 1. Structural Parameters and Anisotropy of Thermal Expansion of Various Grades of Reactor Graphite

Grade of graphite	Perfection of structure			Dimensions of crystal		Anisotropy	
	degree of graphitization γ	disorder coefficient of layers, P	degree of graphitization J_{112}/J_{110}	L_c, Å	L_a, Å	$(J_{002})_\perp/(J_{002})_\parallel$	$(\alpha_\perp/\alpha_\parallel)_{400°C}$
GMZ (Lot 120)	0,81	0,36	0,38	210—230	1000	1,26	1,27
RBM-KP	0,79	0,39	0,58	190—230	710—730	1,05	1,26
RBM-K	0,76	0,42	0,63	210—230	570—640	1,23	1,29
VPG	0,71	0,48	0,57	190—230	400—730	1,18	1,27
PGG	0,69	0,50	0,33	190—210	860—920	0,99	0,94

Note: $\gamma = (3.44 - \bar{d})/(3.44 - 3.354)$; $\bar{d}$, mean interlayer spacing, related to the disorder coefficient of the layers by the expression $\bar{d} = 3.44 - 0.86(I - P) - 0.064(I - P)$; $J_{112,110,002}$ are the intensities of the corresponding x-ray lines.

TABLE 2. CTE of Various Grades of Reactor Graphite

Grade of graphite	$\alpha \cdot 10^{-6}$, deg^{-1}														
	20°C			200°C			400°C			600°C			800°C		
	$\alpha_\parallel$	$\alpha_\perp$	α_v	$\alpha_\parallel$	$\alpha_\perp$	α_v	$\alpha_\parallel$	$\alpha_\perp$	α_v	$\alpha_\parallel$	$\alpha_\perp$	α_v	$\alpha_\parallel$	$\alpha_\perp$	α_v
GMZ	3,9	5,1	14,1	4,6	5,9	16,4	5,1	6,5	18,1	5,3	6,8	18,9	5,9	6,9	19,4
KPG	6,1	5,7	17,5	6,8	6,4	19,6	7,2	6,9	21	7,6	7,2	22	7,9	7,5	22,9
RBM-K	2,8	4,4	11,6	3,8	5,2	14,1	4,4	5,7	15,8	4,8	6,0	16,8	5,1	6,1	17,3
RBM-KP	3,5	4,6	12,7	4,5	5,7	15,9	4,8	6,1	17,3	5,3	6,5	18,3	5,4	6,7	18,8
VPG	3,4	5,0	13,6	4,3	5,6	15,5	4,8	6,1	17	5,1	6,3	17,7	5,3	6,4	18,1

TABLE 3. Dependence of CTE of Pyrographite on Thermomechanical Processing

Processing temperature of pytographite, °C	$\alpha \cdot 10^{-6}$, deg^{-1}											
	200°C			400°C			600°C			800°C		
	α_a	α_c	α_v	α_a	α_c	α_v	α_a	α_c	α_v	α_a	α_c	α_v
2100	0	25	25	0,6	25	26,2	1,2	27	29,4	1,5	27	30
2400	—0,5	29	28	—0,1	29	28,8	0,6	30	31,2	0,6	30	31,2
2800	—0,7	28	26,6	0	30	30	0,6	31	32,2	1,0	31	33
3200	—0,5	27,3	26,3	0	28	28	0,5	28	29	0,95	31	32,9
Single crystal	—0,85	27,9	26,2	0	28,3	28,3	0,7	28,8	30,2	0,95	29,3	31,2

The character of the change of the CTE of graphite as a function of the processing temperature (and a comparison of the changes of the CTE with changes in other properties in Fig. 1) once again confirms the conclusion that the formation of a three-dimensional structure of graphite in the graphitization process begins only at a temperature between 2000 and 2100°C.

The temperature dependence of the CTE of graphite blocks of the RBM-K reactor is shown in Fig. 2a. Research showed that the CTE of all grades of graphite increases rapidly up to a temperature of ~100°C, and then its rate of change decreases sharply. This temperature dependence of the CTE is characteristic of practically all domestic and imported reactor graphite.

Calculation of Thermal Strains of Reactor Graphite Using a Single-Phase Model. The development of representations of the relation of microscopic and macroscopic thermal expansion of graphitic materials [7, 10] led to the creation of a semiempirical model of the thermal expansion of polycrystalline graphite in which the difference between the values of the thermal expansion of the lattice and a graphite monolith is explained by the presence of a special kind of porosity ("nonremovable porosity" in Mrozowski's terminology) arising in the cooling of graphite from the graphitization temperature (2300-3000°C) to room temperature, and amounting to ~8 vol. %.

In this model thermal expansion along the principal directions of a graphite block ($\alpha_\parallel$ and $\alpha_\perp$) is related to the CTE of its crystal lattice (α_a and α_c) by textural parameters which indicate the degree of preferential orientation of the individual crystallites:

$$\alpha_\parallel = A\alpha_c + (1 - A)\alpha_a; \quad (1)$$

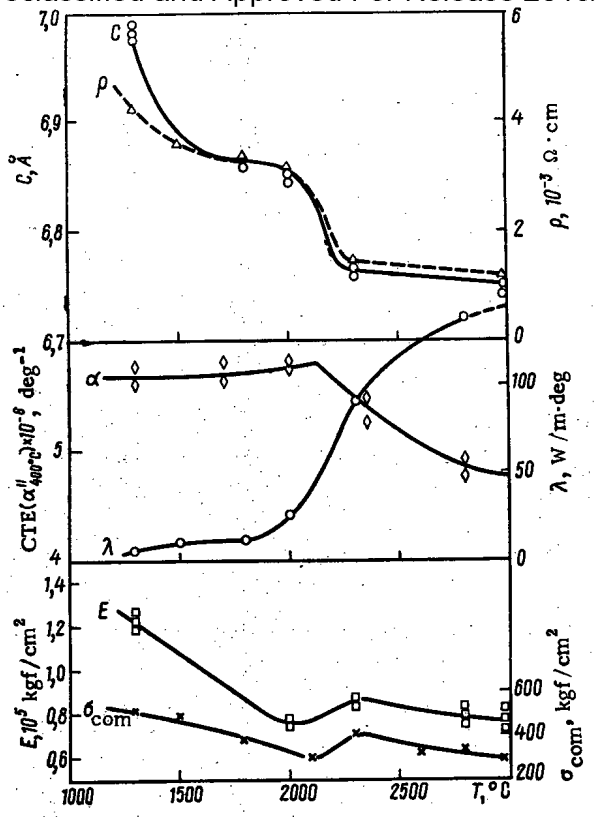

Fig. 1

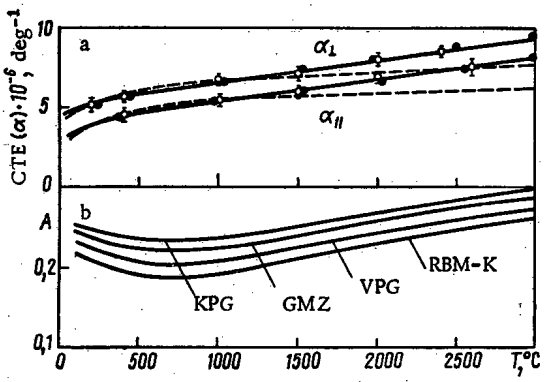

Fig. 2

Fig. 1. Effect of processing temperature on structure and physical properties of reactor graphite. Symbols on curves mark experimental points.

Fig. 2. a) Temperature dependence of linear CTE ($\alpha_{\parallel}$ and $\alpha_{\perp}$) of RBM-K reactor graphite and b) corresponding variations of textural parameter A for various grades of graphite: ----) CTE calculated with constant A and B; ●) CTE calculated with A and B depending on temperature of measurement.

$$\alpha_{\perp} = B\alpha_c + (1-B)\,\alpha_a, \tag{2}$$

where A and B are dimensionless parameters.

In general these parameters are determined from Eqs. (1) and (2). However, at a temperature of 400° C the coefficient α_a is zero, and the expressions are considerably simplified. In this case

$$A = \left(\frac{\alpha_{\parallel}}{\alpha_c}\right)_{400^\circ\mathrm{C}} \text{and} \; B = \left(\frac{\alpha_{\perp}}{\alpha_c}\right)_{400^\circ\mathrm{C}}. \tag{3, 4}$$

Thus, by measuring the CTE of reactor graphite in two directions ($\alpha_{\parallel}$ and $\alpha_{\perp}$) at 400°C, and knowing α_c for a single crystal of graphite, the parameters A and B can be determined for any grade of graphite. Then, knowing the values of these parameters, the thermal strain of graphitic products at any temperature can be calculated from the following equations:

$$\left(\frac{1}{l}\frac{\Delta l}{\Delta T}\right)_{\parallel} = A\left(\frac{1}{L_c}\frac{\Delta L_c}{\Delta T}\right) + (1-A)\left(\frac{1}{L_a}\frac{\Delta L_a}{\Delta T}\right); \tag{5}$$

$$\left(\frac{1}{l}\frac{\Delta l}{\Delta T}\right)_{\perp} = B\left(\frac{1}{L_c}\frac{\Delta L_c}{\Delta T}\right) + (1-B)\left(\frac{1}{L_a}\frac{\Delta L_a}{\Delta T}\right), \tag{6}$$

where $\left(\frac{1}{l}\frac{\Delta l}{\Delta T}\right)_{\parallel}$ and $\left(\frac{1}{l}\frac{\Delta l}{\Delta T}\right)_{\perp}$ are the thermal strains per unit change of temperature of polycrystalline reactor graphite in directions parallel and perpendicular to the axis of formation of the product; $(1/L_c)(\Delta L_c/\Delta T)$ and $(1/L_a)(\Delta L_a/\Delta T)$ are the thermal strains of a single crystal of graphite along hexagonal axes c and a, respectively.

The parameters A and B were determined for various grades of reactor graphite under the assumption that the CTE of a single graphite crystal (α_a) is zero at 400°C, and $\alpha_c = 28.3 \cdot 10^{-6}\ \mathrm{deg}^{-1}$. The results obtained are listed in Table 4.

TABLE 4. Textural Parameters A and B for Various Grades of Reactor Graphite

Grade of graphite	A	B
GMZ	0,180	0,230
RBM-K	0,156	0,201
RBM-KP	0,177	0,220
VPG	0,170	0,215
KPG	0,254	0,244
PGA	0,084	0,160

TABLE 5. Values of the Correction Δ(T)*

T, °C	Δ (T)	T, °C	Δ (E)
100	+0,012	900	−0,008
200	+0,005	1000	−0,007
300	+0,001	1100	−0,004
400	−0,003	1200	±0
500	−0,007	1300	+0,003
600	−0,009	1400	+0,007
700	−0,010	1500	+0,012
800	−0,009		

*For T > 1500°C the correction Δ = 0.016 for each 500°C.

Using the parameters found, the thermal strains for various grades of reactor graphite were calculated on a BÉSM-6 computer, using a special program. Up to 1000-1500°C the experimental and calculated values agree satisfactorily (Fig. 2a). At higher temperatures, however, the difference between the experimental and calculated values becomes larger, with the calculated values being smaller than the experimental for samples both parallel and perpendicular to the cut.

To bring the calculated data into accord with the experimental it is formally necessary to increase the values of the parameters A and B. An increase of A and B with the temperature of measurement also corresponds to the physical nature of the thermal expansion of polycrystalline graphite, since for large thermal strains of individual crystallites the Mrozowski cracks close, and this must lead to an increase in the contribution of α_c to the total expansion of graphite and thus to the increase of parameters A and B.

A comparison of experimental and calculated data determined the temperature dependence of the parameters A and B for various materials. Figure 2b shows the variation of A for RBM-K, GMZ, VPG, and KPG graphite. Similar variations were found for parameter B.

Since the temperature dependence of A and B is practically the same for all grades of graphite investigated, including raw coke graphite, it is assumed that this behavior will be common to all materials.

In this case the temperature dependence of the parameters A and B will be expressed by the relations:

$$A = A_0 + \Delta(T); \quad (7)$$

$$B = B_0 + \Delta(T), \quad (8)$$

where A_0 and B_0 are the values of the parameters calculated from Eqs. (3) and (4), and Δ(T) is a correction which depends on temperature (Table 5).

Thus, the true values of α can be calculated in the 100-3000°C range. A comparison of calculations with experiments showed satisfactory agreement (Fig. 3a).

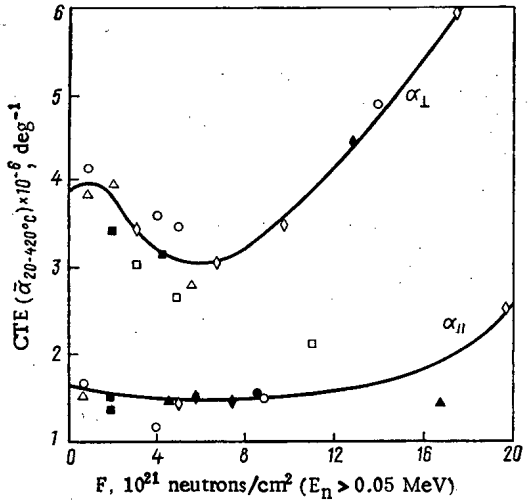

Fig. 3. Effect of irradiation on CTE of CSF reactor graphite [5] at the following irradiation temperatures: ○) 400-450; ▲) 500-550; ●) 550-650; ◆) 650-750; ◇) 800; △) 900; □) 950-1000; ■) 1200°C.

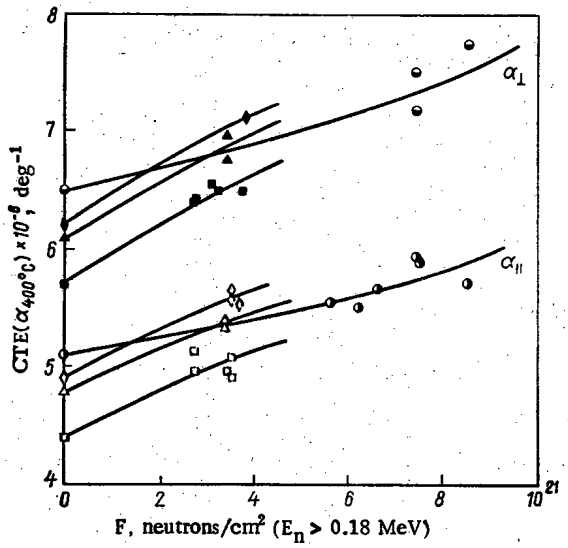

Fig. 4

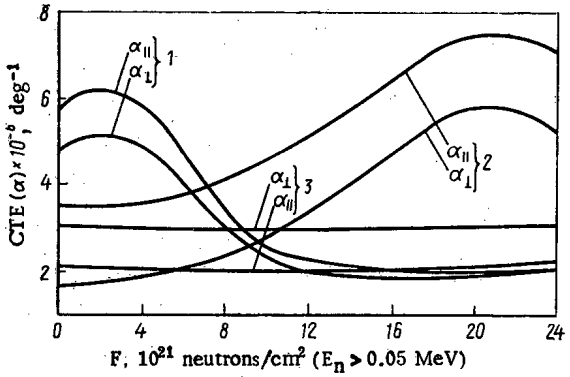

Fig. 5

Fig. 4. Effect of irradiation on CTE of various grades of domestic reactor graphite: ◑, ◒) $\alpha_\parallel$ and $\alpha_\perp$ of standard GMZ reactor graphite; □, ■) RBM-K; ◇, ◆) RBM-KP; △, ▲) VPG.

Fig. 5. Variations of CTE of graphites of various structures under high-temperatue irradiation [6]: 1) gilsographite (T_{irr} = 950-1300°C); 2) molded needle-coke graphite (T_{irr} = 1200°C); 3) impregnated needle-coke graphite (T_{irr} = 950-1200°C).

It should be noted that the laws obtained are the analog of the temperature corrections for finding averages of CTE of reactor graphite over a temperature interval [2].

The fact that the variation of A and B with the thermal strain of graphite is smooth rather than stepwise indicates the gradual closing of technological cracks over a wide temperature range. Moreover, the calculations and experiments show that the complete closing of Mrozowski cracks begins only at 2500-3000°C when the volume CTE of reactor graphite α_v becomes approximately equal to the volume CTE of a single crystal.

In conclusion it should be emphasized that attempts have been made to calculate thermal strains of reactor graphite in other ways by introducing special accommodation coefficients taking account of the closing of Mrozowski cracks during heating of the material [1, 7]. However, calculations with this model did not give any significant advantage over the Simmons thermodynamic model.

Change of CTE of Graphite under Reactor Radiation. An investigation of the effect of irradiation on the CTE of individual crystallites (single crystals of graphite or pyrographite) showed that substantial changes in the CTE occur only under low-temperature irradiation (T_{irr} < 250°C); in this case the coefficient α_c is approximately halved, while α_a increases and becomes positive. For a neutron fluence of ~ (1-2) · 10^{21} neutrons/cm^2 the CTE of these materials is hardly changed.

When the irradiation temperature is increased, the CTE of single crystals is hardly changed, and the perfection of the original structure of the material (for pyrographite) has essentially no effect on the character of the change in the CTE of these materials under either high- or low-temperature irradiation.

The change of the CTE of polycrystalline reactor graphite under irradiation is considerably complicated by the fact that the macrostructure of the material (relative orientation of individual crystallites, total volume and distribution of pores, etc.) has a substantial effect. Technological factors (type of raw material, kind of filler, method of forming, etc.) also have an effect. Since the factors enumerated frequently do not have a unique effect, only the most general laws can be formulated for the change of the CTE of various grades of reactor graphite under irradiation (Figs. 3-5).

The experimental data show that under low-temperature irradiation (T_{irr} < 250°C) the CTE of most grades of graphite first increases somewhat, and then decreases to the initial value and even lower.

Under high-temperature irradiation the changes of the CTE of various grades of graphite are substantially different in both absolute magnitude and sign. The most general conclusion seems to be that graphites with a low initial α show an increase in the CTE when irradiated, while high-density isotropic materials with a large α show a decrease.

The causes of this phenomenon have not been explained theoretically. Clearly, while under low-temperature irradiation radiation defects (small interstitial clusters of atoms and vacancies) play a decisive role in the change of the CTE, strongly distorting the graphite lattice [9] and causing a change in the character of its thermal expansion, under high-temperature irradiation characterized by enhanced distortion of individual crystallites without substantial distortion of the crystal lattice itself, the macrostructure of the material (porosity), its strength and ability to withstand large deformations of individual crystallites without violating the integrity of the material begin to play a decisive role.

LITERATURE CITED

1. Yu. S. Virgil'ev and I. P. Kalyagina, At. Energ., 31, 497 (1971).
2. S. E. Vyatkin et al., Nuclear Graphite [in Russian], Atomizdat, Moscow (1967).
3. A. I. Lutkov et al., Neorg. Mater., 8, 1409 (1972).
4. P. A. Platonov et al., Preprint IAÉ-2247, Moscow (1972).
5. J. Cox and J. Helm, Carbon, 7, 319 (1969).
6. G. Engle and W. Eatherly, High Temperature-High Pressure, 4, 119 (1972).
7. I. Mason and R. Knibbs, J. Nucl. Energy, Parts A and B, 18, 311 (1964).
8. S. Mrozowski, in: Proceedings of the First and Second Conference on Carbon, Pergamon, Oxford (1956), p. 31.
9. P. A. Platonov et al., Rad. Effects, 25, 105 (1975).
10. J. Simmons, Radiation Damage in Graphite, Pergamon, Oxford (1965).

TRANSPORT OF THERMAL NEUTRONS FROM A PULSED SOURCE IN AN INHOMOGENEOUS MODERATOR WITH A LARGE CAVITY

Zh. M. Dzhilkibaev and M. V. Kazarnovskii

UDC 539.125.52:621.039.51.12

A theoretical analysis of the transport of thermal neutrons from a pulsed source in a homogeneous moderator containing a large cavity whose characteristic dimension is much larger than the neutron mean free path in the moderator showed that although the asymptotic damping law of the neutron current is far from exponential in such a system, under certain conditions, e.g., for weak absorption, there is a rather long period after the neutron pulse when the damping of the neutron current in the moderator and at its boundary with the cavity is close to exponential. By measuring the corresponding effective damping factor it is possible to determine the neutron albedo at this boundary averaged over the angles of entrance and exit. In practice, however, inhomogeneous sytems, in particular layered systems, are of special interest (a reactor channel, a borehole for geophysical measurements, etc.). The present paper is devoted to a theoretical analysis of the unsteady transport of neutrons in such systems.

Statement of the Problem and General Formalism. We consider a cavity surrounded by an inhomogeneous moderator within which a pulsed neutron source is located. We assume that the transport of thermal neutrons in the moderator is satisfactorily described by the diffusion approximation, and that the neutron spectrum in the moderator is Maxwellian with a temperature T equal to that of the moderator (the inhomogeneities of the moderator distort the neutron distribution slightly at distances of the order of a mean free path). Then the neutron density $\varphi(\mathbf{r}, t)$ at point $\mathbf{r}$ at time t satisfies the equation*

$$\partial\varphi/\partial t = \nabla (D \nabla \varphi) - \alpha\varphi; \tag{1}$$

$$\varphi(\mathbf{R}, t) = 0; \tag{2}$$

$$-D(\mathbf{r}_0)\varphi'(\mathbf{r}_0, t) \equiv -D(\mathbf{r}_0)\mathbf{v}(\mathbf{r}_0) \nabla \varphi(\mathbf{r}, t)|_{\mathbf{r}=\mathbf{r}_0} = J^+(\mathbf{r}_0, t) - J^-(\mathbf{r}_0, t); \tag{3}$$

*A condition analogous to (3) is given in [1] for the exact kinetic equation.

Translated from Atomnaya Énergiya, Vol. 47, No. 6, pp. 386-389, December, 1979. Original article submitted April 3, 1978; revision submitted May 3, 1979.

0038-531X/79/4706-0997$07.50

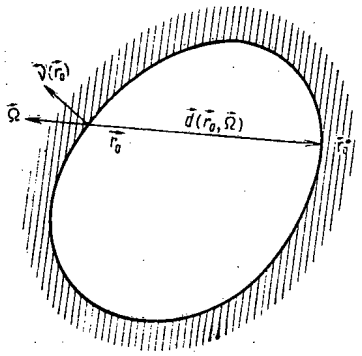

Fig. 1. Schematic diagram of vectors in Eqs. (7).

$$D(\mathbf{r}) = \left\langle \frac{1}{3} \frac{v}{\Sigma_{tr}(\mathbf{r}, v)} \right\rangle_T; \quad \alpha(\mathbf{r}) = \langle v \Sigma_c(\mathbf{r}, v) \rangle_T. \tag{4}$$

Here $D(\mathbf{r})$ and $\alpha(\mathbf{r})$ are respectively the diffusion coefficient and the rate of absorption of thermal neutrons; $\Sigma_{tr}(\mathbf{r}, v)$ is the macroscopic transport cross section; $\Sigma_c(\mathbf{r}, v)$ is the macroscopic cross section for the absorption of neutrons of velocity v at point $\mathbf{r}$; the symbol $\langle \ldots \rangle_T$ denotes an average over the Maxwellian spectrum; $\mathbf{R}$ is the radius vector to points on the outer extrapolated boundary of the moderator; $\mathbf{r}_0$ is the radius vector to the surface of the cavity; $\boldsymbol{\nu}(\mathbf{r}_0)$ is a unit vector along the outward normal to this surface at point $\mathbf{r}_0$; $J^+(\mathbf{r}_0, t)$ and $J^-(\mathbf{r}_0, t)$ are respectively the neutron current densities at the surface of the cavity at point $\mathbf{r}_0$ at time t from the cavity into the moderator and vice versa, i.e.,

$$J^+(\mathbf{r}_0, t) = -\frac{1}{4\pi} \int\limits_{\mu<0} \mu \, d\Omega \left\{ \langle \varphi(\mathbf{r}_0^*, t^*) v \rangle_T - \left\langle \frac{v}{\Sigma_{tr}(\mathbf{r}_0^*, v)} \varphi'(\mathbf{r}_0^*, t^*) \right\rangle_T \mu^* \right\} + J_s^+(\mathbf{r}_0, t); \tag{5}$$

$$J^-(\mathbf{r}_0, t) = \frac{1}{4} \varphi(\mathbf{r}_0, t) \langle v \rangle_T + \frac{1}{2} D(\mathbf{r}_0) \varphi'(\mathbf{r}_0, t), \tag{6}$$

where (Fig. 1) Ω is a unit vector along the direction of motion of a neutron:

$$\begin{aligned} &\mu = \Omega \boldsymbol{\nu}(\mathbf{r}_0); \quad \mu^* = -\Omega \boldsymbol{\nu}(\mathbf{r}_0^*); \\ &t^* = t - d(\mathbf{r}_0, \Omega)/v; \quad \mathbf{r}_0^* = \mathbf{r}_0 + \mathbf{d}(\mathbf{r}_0, \Omega); \end{aligned} \tag{7}$$

$J_S^+(\mathbf{r}_0, t)$ is the neutron current density in the moderator at point $\mathbf{r}_0$ at time t emitted directly by the source.

We take the Laplace transforms of Eqs. (1)-(7) with respect to t and denote the transform of a function by a tilde. Then, taking account of the fact that

$$\int\limits_0^\infty dt e^{-\lambda t} \varphi(\mathbf{r}_0^*, t^*) \equiv \int\limits_0^\infty dt e^{-\lambda t} \varphi\left[\mathbf{r}_0^*, t - \frac{d(\mathbf{r}_0, \Omega)}{v}\right] = \exp\left[-\lambda \frac{d(\mathbf{r}_0, \Omega)}{v}\right] \tilde{\varphi}(\mathbf{r}_0^*, \lambda) \tag{8}$$

we obtain after some simple calculations:

$$\nabla(D \nabla \tilde{\varphi}) = (\lambda + \alpha) \tilde{\varphi}; \quad \tilde{\varphi}(\mathbf{R}, \lambda) = 0; \tag{9}$$

$$\frac{1}{4} \langle v \rangle_T \tilde{\varphi}(\mathbf{r}_0, \lambda) - \frac{1}{2} D(\mathbf{r}_0) \tilde{\varphi}'(\mathbf{r}_0, \lambda) + \frac{1}{4\pi} \int\limits_{\mu<0} \mu \, d\Omega \left\{ \left\langle v \exp\left[-\lambda \frac{d(\mathbf{r}_0, \Omega)}{v}\right] \right\rangle_T \tilde{\varphi}(\mathbf{r}_0^*, \lambda) - \right. \tag{10}$$

$$\left. - \mu^* \left\langle \frac{v}{\Sigma_{tr}(\mathbf{r}_0^*, v)} \exp\left[-\lambda \frac{d(\mathbf{r}_0, \Omega)}{v}\right] \right\rangle_T \tilde{\varphi}'(\mathbf{r}_0^*, \lambda) \right\} = \tilde{J}_s^+(\mathbf{r}_0, \lambda);$$

$$J^-(\mathbf{r}_0, t) = \frac{1}{2\pi i} \int\limits_{\sigma - i\infty}^{\sigma + i\infty} d\lambda e^{\lambda t} \tilde{J}_s^+(\mathbf{r}_0, \lambda) \left[\frac{1}{k(\mathbf{r}_0, \lambda)} - f(\mathbf{r}_0, \lambda)\right]^{-1}; \tag{11}$$

$$k(\mathbf{r}_0, \lambda) = \frac{1 - \varepsilon(\mathbf{r}_0, \lambda)}{1 + \varepsilon(\mathbf{r}_0, \lambda)}; \quad \varepsilon(\mathbf{r}_0, \lambda) = -\frac{2D(\mathbf{r}_0) \tilde{\varphi}'(\mathbf{r}_0, \lambda)}{\langle v \rangle_T \tilde{\varphi}(\mathbf{r}_0, \lambda)}; \tag{12}$$

$$f(\mathbf{r}_0, \lambda) = -\frac{1}{\pi} \int\limits_{\mu<0} \mu \, d\Omega \frac{\tilde{\varphi}(\mathbf{r}_0^*, \lambda)}{\tilde{\varphi}(\mathbf{r}_0, \lambda)} \frac{1}{\langle v \rangle_T} \left\langle v \exp\left[-\frac{\lambda}{v} d(\mathbf{r}_0, \Omega)\right] \right\rangle_T [1 + \delta(\mathbf{r}_0, \Omega, \lambda)];$$

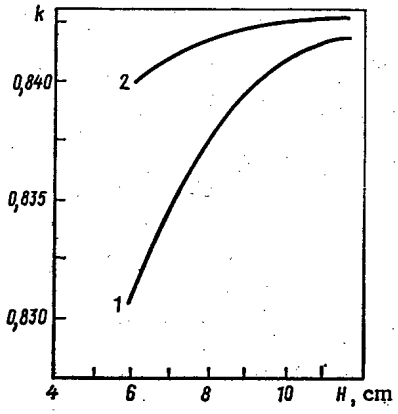

Fig. 2. Albedo as a function of thickness of first layer for 1) single-layer and 2) two-layer systems.

$$\delta(\mathbf{r}_0,\ \Omega,\ \lambda)=\frac{\varepsilon(\mathbf{r}_0,\ \lambda)}{1-\varepsilon(\mathbf{r}_0,\ \lambda)}\left\{1+\frac{\mu^*}{2}\frac{\varepsilon(\mathbf{r}_0^*,\ \lambda)}{\varepsilon(\mathbf{r}_0,\ \lambda)}\frac{\frac{1}{D(\mathbf{r}_0^*)}\left\langle\frac{v}{\Sigma_{tr}(\mathbf{r}_0^*,\ v)}\exp\left[-\frac{\lambda}{v}d(\mathbf{r}_0,\ \Omega)\right]\right\rangle_T}{\frac{1}{\langle v\rangle_T}\left\langle v\exp\left[-\frac{\lambda}{v}d(\mathbf{r}_0,\ \Omega)\right]\right\rangle_T}\right\}. \tag{13}$$

Analysis of Results. As in the special cases treated earlier, $k(\mathbf{r}_0, \lambda)$ is the ratio of the neutron current densities from the moderator into the cavity, and from the cavity into the moderator at point $\mathbf{r}_0$ under the condition that over a long period of time these current densities are proportional to exp (λt). The quantity f as a function of λ has an essential singularity at $\lambda = 0$ which contributes to a nonexponential asymptotic decrease of J^- with time. However, as in the cases treated earlier, under certain conditions, e.g., for $\varepsilon \ll 1$, there is a rather extended time interval during which integral (11) is determined mainly by a range of values of λ close to the negative root $-\lambda_0$ of the equation

$$1/k(\mathbf{r}_0,\ \lambda)=\mathrm{Re}\,[f(\mathbf{r}_0,\ \lambda)], \tag{14}$$

which has the smallest absolute value. Accordingly, in this time interval in the first approximation $J^+ \sim \exp(-\lambda_0 t)$. The neutron current density over the whole volume of the moderator will also be damped according to a law which is nearly exponential with an effective damping constant λ_0. Therefore, knowing $f(\mathbf{r}_0, \lambda)$ and having measured λ_0 it is possible to determine $k(\mathbf{r}_0, -\lambda_0)$. In general, however, the calculation of $f(\mathbf{r}_0, \lambda)$ is complicated. It is considerably simplified when because of the symmetry of the problem $\tilde{\varphi}(\mathbf{r}_0, \lambda)$ and $\tilde{\varphi}'(\mathbf{r}_0, \lambda)$, and consequently d, ε, $D(\mathbf{r}_0) \equiv D_0$, $\Sigma_{tr}(\mathbf{r}_0, v) \equiv \Sigma_0(v)$, and f are independent of $\mathbf{r}_0$, and $\mu^* = \mu$. Then f can be conveniently written in the form

$$f(\lambda)=-\frac{1}{\pi}\int\limits_{\mu<0}\mu\,d\Omega\,\frac{1}{\langle v\rangle_T}\left\langle v\exp\left[-\frac{\lambda}{v}d(\Omega)\right]\right\rangle_T+\delta f(\lambda); \tag{15}$$

$$\delta f(\lambda)=-\frac{1}{\pi}\frac{\varepsilon(\lambda)}{1-\varepsilon(\lambda)}\int\limits_{\mu<0}\mu\,d\Omega\left\{\frac{1}{\langle v\rangle_T}\left\langle v\exp\left[-\frac{\lambda}{v}d(\Omega)\right]\right\rangle_T+\frac{\mu}{2D_0}\left\langle\frac{v}{\Sigma_0(v)}\exp\left[-\frac{\lambda}{v}d(\Omega)\right]\right\rangle_T\right\}. \tag{16}$$

It is easy to confirm that for weak absorption ($\varepsilon \ll 1$) $\delta f(\lambda)$ is negligibly small ($\sim \varepsilon^2$). This was shown in [2] for the special case of a spherical cavity in a homogeneous moderator. Thus, in the first approximation $f(\lambda)$ depends only on the moderator temperature and the shape and size of the cavity. In particular,* for a spherical cavity [2] of radius r_s and a cylindrical cavity [3] of radius r_c

$$\mathrm{Re}\,[f]=1-\frac{\sqrt{\pi}}{3}x_s+\frac{1}{4}x_s^2-\frac{\sqrt{\pi}}{15}x_s^3+\frac{1}{36}x_s^4(1{,}384\ldots-\ln|x_s|)-\ldots; \tag{17}$$

*For plane geometry the corresponding series converges very slowly [4] and its analysis is hardly practical.

$$\mathrm{Re}\,[f] = 1 - \frac{\sqrt{\pi}}{2} x_c + \frac{1}{6} x_c^2 - \frac{\sqrt{\pi}}{8} x_c^3 (\ln|x_c| + 0.262\ldots) + \ldots; \tag{18}$$

$$x_{c,s} = 2r_{c,s}\lambda_0/v_T;\ v_T = \sqrt{2kT/m} = \sqrt{\pi}\langle v\rangle_T/2, \tag{19}$$

where these equations are applicable for both homogeneous moderators and moderators whose properties depend on the radius (e.g., layered moderators). By using these equations with the experimental value of λ_0 it is possible to determine $k(-\lambda_0)$.

Although Eqs. (17) and (18) were derived in the diffusion approximation, it can be shown that the nondiffusion corrections are due mainly to the anisotropy of the neutron current from the moderator into the cavity and are small.

Calculation of Albedo for Layered Systems. We consider the calculation of k for the practically important case of layered systems with spherical and cylindrical symmetries, and just as before, we use the diffusion approximation. According to (12)

$$k(\lambda) = \left[1 - \frac{2D_0}{\langle v\rangle_T}\Phi(R_0, \lambda)\right] \Big/ \left[1 + \frac{2D_0}{\langle v\rangle_T}\Phi(R_0, \lambda)\right]; \tag{20}$$

$$\Phi(r, \lambda) = -(\partial/\partial r)\ln\tilde{\varphi}(r, \lambda),$$

where R_0 is the radius of the cavity. For a system consisting of n layers of homogeneous moderator, $\Phi(R_0, \lambda)$ can be found by solving Eq. (9) in each of the layers and imposing standard boundary conditions (continuity of $D(r)\Phi(r, \lambda)$ at the boundaries between layers). In particular, for a two-layer spherical system

$$\Phi_s(R_0, \lambda) = \frac{1}{R_0} + \frac{1}{L_0}\frac{1+\beta_s \exp\left(-2\frac{R_1-R_0}{L_0}\right)}{1-\beta_s \exp\left(-2\frac{R_1-R_0}{L_1}\right)};$$

$$\beta_s = \frac{\frac{1}{R_1}\left(\frac{D_1}{D_0}-1\right) - \frac{1}{L_0} + \frac{D_1}{D_0}\frac{1}{L_1}\operatorname{cth}\frac{R-R_1}{L_1}}{\frac{1}{R_1}\left(\frac{D_1}{D_0}-1\right) + \frac{1}{L_1} + \frac{D_1}{D_0}\frac{1}{L_1}\operatorname{cth}\frac{R-R_1}{L_1}}, \tag{21}$$

for a two-layer cylindrical system

$$\Phi_c(R_0, \lambda) = \frac{1}{L_0}\frac{K_1(R_0/L_0) - \beta_c I_1(R_0/L_0)}{K_0(R_0/L_0) - \beta_c I_0(R_0/L_0)};$$

$$\beta_c = \frac{K_1(R_1/L_0) - \gamma_c K_0(R_1/L_0)}{I_1(R_1/L_0) + \gamma_c I_0(R_1/L_0)};$$

$$\gamma_c = \frac{L_0 D_1}{D_0 L_1}\frac{K_1(R_1/L_1) I_0(R/L_1) + K_0(R/L_1) I_1(R_1/L_1)}{K_0(R_1/L_1) I_0(R/L_1) - K_0(R/L_1) I_0(R_1/L_1)}, \tag{22}$$

where D_0, D_1 and L_0, L_1 are respectively the diffusion coefficients and diffusion lengths in the inner and outer layers, and R_1 is the radius of the boundary between layers.

As an example Fig. 2 shows graphically the albedo for a spherical system as a function of the thickness ($H = R_1 - R_0$) of the first layer of light water. The second layer (of infinite thickness) is light water poisoned with boron of density $\rho_B = 2.6$ mg/cm^3.

LITERATURE CITED

1. K. D. Ilieva, Candidate's Dissertation, P. N. Lebedev Institute of Physics, Academy of Sciences, Moscow (1973).
2. K. D. Ilieva and M. V. Kazarnovskii, At. Energ., 39, 186 (1975).
3. Zh. M. Dzhilkibaev and M. V. Kazarnovskii, At. Energ., 42, 139 (1977).
4. K. D. Ilieva and M. V. Kazarnovskii, [1], p. 347.
5. K. D. Ilieva and M. V. Kazarnovskii, Kr. Soobshch. po Fiz., No. 3, 19 (1973); At. Energ., 35, 346 (1973).

MASS SPECTROMETRIC METHOD OF ISOTOPIC ANALYSIS OF XENON FORMED IN NUCLEAR FISSION

Yu. A. Shukolyukov, Ya. S. Kapusta, and A. B. Verkhovskii

UDC 539.173.8

The nuclides $^{129-136}Xe$ are formed in the fission of any nuclei by neutrons or charged particles. Isotopic analysis of xenon may be of interest for both nuclear physics research and the solution of certain applied problems of nuclear engineering. In the present article we describe a procedure developed for the mass spectrometric investigation of xenon with a maximum sensitivity of detection of $\sim 10^{-14}$ cm^3 ($\sim 10^5$ atoms) of individual nuclides. We used a reconstructed MI-1201 mass spectrometer, an analog-to-digital converter, and a universal Nairi-2 computer.

Extraction of Xenon from Solids. In order to separate xenon from materials of various compositions it is necessary to produce a sufficiently high temperature in a closed volume with vacuum purity and a low xenon background. A vacuum furnace (Fig. 1) is recommended for the complete separation of xenon from practically any solid containing fissile nuclei. The heating element and shell of screens were located in a vacuum of 10^{-5} mm Hg; the samples being investigated were first degassed at 10^{-7} mm Hg and 200°C for 5-10 h and then placed in the working volume of the furnace – a molybdenum tube. The tube was first pumped out at 1900-2000°C for 2-5 h to ensure the removal of chemically active gases (hydrogen, nitrogen, carbon dioxide, organic compounds) and xenon from the walls. The completeness of the outgassing of the tube was checked with the mass spectrometer by running dummy tests. After careful outgassing of the tube the background of atmospheric ^{136}Xe did not exceed $\sim 10^{-14}$ cm^3 ($\sim 10^5$ atoms).

In extracting fission product xenon from solids it is sufficient to maintain the necessary temperature for 1-1.5 h in order to separate more than 90% of the xenon capable of migrating at the given temperature (in the 500-2000°C range).

Separation of Xenon from Chemically Active Gases and Helium. The gases separated from the sample under study are passed through a solid carbon dioxide (−78°C) cold trap 4 (Fig. 2) in which liquid nitrogen or oxygen cannot be used since xenon is retained on the walls of the trap at −183 to −196°C. In 15 min all the residual gases are sorbed at −196°C on activated charcoal in ampul 5. Helium, often contained in samples, cannot be sorbed on activated charcoal under these conditions, and is pumped out through valve 1 for 3 min. Then with sylphon valves 1 and 2 closed the charcoal is heated to 250°C. Simultaneously the temperature of the steel tube 6 with sponge titanium is raised to 900°C. In 15 min the chemically active gases are absorbed by the titanium. Following this the tube is taken from the furance and cooled to room temperature. When valve 2 is opened and valve 3 is closed, the residual gases are sorbed on the activated charcoal in ampul 7 in 15 min. Then, closing valve 2 the xenon purification process is repeated using the titanium getter 8. The xenon separated in this way is discharged into the mass spectrometer through valve 3.

All the equipment except the tube with the samples was made of steel. Before beginning the operating cycle the equipment was pumped out at 300°C for 24 h by two mercury diffusion pumps. During this process the tubes with titanium getter were heated to 950-1000°C and the ampul with activated charcoal to 300°C.

Measurement of Xenon on Mass Spectrometer. It is impossible to measure an ultrasmall amount of fission products such as xenon isotopes on a commercial type mass spectrometer. It was necessary to reconstruct the vacuum part to ensure steady vacuum conditions for the measurements. Two steel pipes filled with SPN-3 getter were attached to the ends of the MI-1201 mass-spectrometer chamber. After heating to 600-700°C (with evacuation by the diffusion pumps) the getter at room temperature ensures maintenance of the operating vacuum conditions in the mass-spectrometer chamber for 3-4 h with the chamber valves closed. Before starting a cycle of measurements the mass-spectrometer chamber had to be outgassed for at least 24 h, 3-5 h of which were at 300°C.

Translated from Atomnaya Énergiya, Vol. 47, No. 6, pp. 389-391, December, 1979. Original article submitted March 27, 1978.

0038-531X/79/4706-1001$07.50

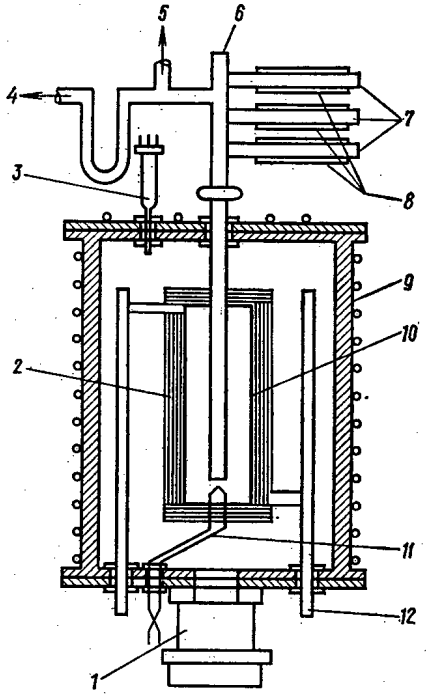

Fig. 1. High-temperature vacuum furnace for extracting xenon from solids: 1) high-vacuum pump; 2) molybdenum screens; 3) thermocouple vacuum gauge; 4, 5) outlets to purification and evacuation systems respectively; 6) window for optical pyrometry; 7) multiply charged structure; 8) heating elements; 9) water cooling; 10) high-temperature heater; 11) tungsten–rhenium thermocouple; 12) cooled current lead-ins.

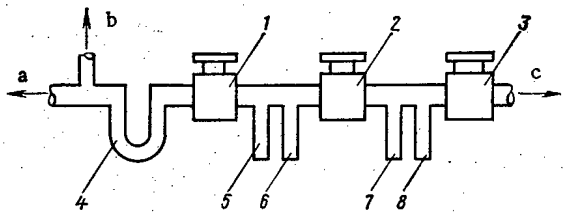

Fig. 2. Schematic diagram of high-vacuum equipment for separating xenon: a) to high-temperature furnace; b) to evacuation system; c) to mass spectrometer.

The cooling systems for the vacuum traps and the electric and water supply systems of the mass spectrometer were reconstructed to ensure automatic around-the-clock vacuum pumping. The flow of liquid nitrogen into the mass spectrometer traps was regulated by a clockwork mechanism, a control system, and a compressor which produced an overpressure in the Dewar flasks as commanded by the clockwork mechanism. The sensitivity of the measurement of ion currents in the receiving end of the mass spectrometer was increased by installing an open louver type electron multiplier which made it possible to measure ion currents from $1.5 \cdot 10^{-13}$ to $1 \cdot 10^{-17}$ A. The background current of the multiplier was no more than $2 \cdot 10^{-18}$ A. The xenon background of a sample of a commercial mass spectrometer was lowered by a factor of 10^5: from approximately 10^{-9} to 10^{-14} cm^3 ($\sim 10^5$ atoms) in the closed chamber.

A metering device – a gas pipet – was attached to the vacuum chamber for continuous monitoring of the sensitivity of the mass spectrometer and to determine the amount of xenon in the samples being studied. By comparing the ion current in the mass spectrometer obtained from xenon from samples containing a known

amount of it with that from the pipet it was possible to calibrate the pipet, i.e., to calculate the amount of xenon of atmospheric isotopic composition in it. In addition, by comparing the xenon ion current of the samples under investigation with that of the pipet it was possible to calculate the amount of xenon in the sample under study. In addition, the xenon in the pipet enables an estimate to be made of the mass discrimination in each experiment: the systematic deviation of the measured isotopic ratios in atmospheric xenon of the pipet from tabulated data – a measure of the isotopic mass discrimination of the instrument. In an MI-1201 mass spectrometer it generally does not exceed 0.3% per amu.

The basic operating regime of the mass spectrometer scan is discrete. At most 11 isotopes are measured. The control automatically switches from one mass to another, stopping at each mass for 2, 4, 8, or 16 sec depending on the program specified. This makes it possible to integrate the ion currents over a specified time of 2 to 16 sec. The integration is performed on a PRM attachment which combines two functions: an analog-to-digital converter and a discrete function integrator. The mass number of the isotope, the intensity, and the running time are recorded on punched tape.

Processing of Experimental Results. In measuring an isotope of mass m in the output current from the dc amplifier is

$$I(m, t) = (N_{\text{i}m_t} + N_{\text{r}m_t} + N_{\text{m}m_t} + N_{\text{l}m_t}) K_{m_t} + I_{0_t},$$

where $N_{\text{i}m_t}$ is the number of ionized atoms of the isotope being measured; $N_{\text{r}m_t}$ is the number of ionized atoms of isotope of mass m remaining in the mass-spectrometer chamber after evacuation stops; $N_{\text{m}m_t}$ is the number of ionized atoms of the isotope of mass m resulting from the "memory" effect; $N_{\text{l}m_t}$ is the number of ionized atoms of mass m resulting from inleakage (quasistatic regime); K_{m_t} is the mass-spectrometer conversion factor which depends on masses and varies with time as a result of instability of the fields of the instrument; I_{0_t} is the initial output current of the dc amplifier.

The value of $N_{\text{r}m}$ depends on the degree of evacuation of the mass-spectrometer chamber; $N_{\text{m}m}$ and $N_{\text{l}m}$ are zero at the instant of admission. Consequently, in order to determine a true isotopic ratio it is necessary to measure all isotopes at $t=0$ (the time of admission). A series of measurements of mass spectra is performed, a correction to I_{0_t} is introduced, and the measured ion currents are extrapolated to the time of admission.

The time dependence of the ion currents can be approximated by an n-th degree polynomial equation. Choosing the degree of the polynomial is a problem. A low-degree polynomial will give a crude description of the physical process, and a high-degree polynomial will not smooth out the "noise" of the experiment. A rule for choosing the optimum degree of the polynomial is given in [1].

The mass spectrometric information was processed by using a universal Nairi computer. Input information was by the punched tape obtained from the output of the mass spectrometer. The program developed includes: taking account of I_{0_t}, choosing the degree of the extrapolating polynomial, extrapolating the ion currents to time $t=0$, calculating the isotopic ratios; introducing a correction for the mass discrimination of the instrument, and calculating the amount of xenon in the sample. The information is processed while the experiment is in progress. The mean square error of the determination of the isotopic ratios of atmospheric xenon (10^{-10} cm^3 for an integration time of 8 sec and the recording of 10 mass spectra) is no worse than 0.3%.

This new variant of the mass spectrometric procedure is already in use in practice and can be employed to solve various physical and engineering problems. From a knowledge of the isotopic composition the shape of the fission fragment mass distribution curve in the range $129 \leq A \leq 136$ can be found for the spontaneous fission of nuclides with very long half-lives. The mass spectrometric procedure described for the isotopic analysis of xenon can be used to search for hypothetical transuranium elements in nature [2]. The method developed is used to search for traces and to investigate the manifestation of a chain process of the fission of ^{235}U in nature [3], and for neutron dosimetry in the study of samples irradiated in a nuclear reactor [4].

By using the procedure developed it is possible from the content of xenon in the monitor and in the samples being investigated to perform an analytic determination of fissile nuclides. For a fission cross section of $\sim 10^2$ b, a fluence of $\sim 10^{19}$ neutrons/cm^2, an amount of fissile nuclides $\sim 10^{-12}$ g can be determined with a relative error of $\sim 15\%$. The error can be decreased to 3-5% if the amount of iodine or barium in the samples and monitor is determined before irradiation. Then, simultaneously with xenon from fission ^{128}Xe or ^{131}Xe is formed, and consequently the concentration of the fissile nuclide in the sample will be determined by the ratio $Xe_f/^{128}Xe$ or $Xe_f/^{131}Xe$ in the sample and the monitor.

LITERATURE CITED

1. D. Hudson, Statistics for Physicists [Russian translation], Mir, Moscow (1967), p. 182.
2. G. Sh. Ashkinadze et al., Geokhimiya, No. 7, 851 (1972).
3. Yu. A. Shukolyukov and Vu Min'Dang, Geokhimiya, No. 12, 1763 (1977).
4. Yu. A. Shukolyukov, Ya. S. Kapusta, and A. B. Verkhovskii, Geokhimiya, No. 4, 572 (1979).

LETTERS TO THE EDITOR

SOME ASPECTS OF THE USE OF LOW-TEMPERATURE RADIATION IN NEUTRON-ACTIVATION ANALYSIS OF BIOLOGICAL MATERIALS

L. M. Mosulishvili and N. E. Kuchava

UDC 543.53

During irradiation in reactor channels, biological specimens are subjected to the radiation effect of neutrons and γ rays. Because of absorption of the energy of nuclear particles and γ rays, there is a rise in the temperature of the specimens and this contributes to the loss of some so-called volatile chemical elements (bromine, iodine, arsenic, mercury, etc.) which constitute part of the biological materials. For this reason, the results of activation analysis of biological specimens in respect of volatile elements can be reliable only with the correct choice of irradiation conditions.

The heating of biological specimens during irradiation in a reactor core with a neutron-flux density of $\sim 2 \cdot 10^{12}$ neutrons/cm$^2 \cdot$ sec was reported for the first time in [1]. It was shown that in the course of irradiation of liquid biological specimens, their temperature may reach about 60°C. The possibility of cooling liquid biological specimens with dry ice was considered in [2]. By irradiating the specimens at a neutron-flux density of $\sim 2 \cdot 10^{12}$ neutrons/cm$^2 \cdot$ sec, it was possible to extend the irradiation time to 13 h. A special system of polyethylene containers, holding biological specimens enclosed in a thick layer of dry ice for neutron irradiation, was proposed in [3]. These technical procedures made it possible to conduct low-temperature irradiation of liquid biological specimens at a comparatively low neutron flux of about 10^{12} neutrons/cm$^2 \cdot$ sec. For a flux density of about 10^{13} neutrons/cm$^2 \cdot$ sec, it was proposed in [4] that biological specimens be irradiated right in a helium cryostat, thus ensuring low-temperature irradiation of biological specimens at a neutron-flux density of $2 \cdot 10^{13}$ neutrons/cm$^2 \cdot$ sec for 5 h. Such technical procedures were used to prevent the loss of volatile elements in the course of neutron irradiation of biological specimens. Clearly, the proposed methods of cooling are insufficient for long low-temperature irradiation of biological specimens by using a comparatively high neutron-flux density [$> 5 \cdot 10^{13}$ neutrons/cm$^2 \cdot$ sec]. In [5] the problem of cooling biological specimens during irradiation with intensive neutron fluxes from a nuclear reactor was solved by using helium gas, cooled to the temperature of liquid nitrogen, circulating in a closed system.

The present paper gives a detailed analysis of the individual stages in low-temperature irradiation of biological specimens which were used in 1970 in a series of investigations on biological materials by the technique of instrumental neutron-activation analysis, conducted in the IRT-M reactor at the Institute of Physics, Academy of Sciences of the Georgian SSR. It would be proper to pose the question: what temperature could be produced by radiation heating in biological specimens during irradiation? As shown by our experiments, this temperature reaches about 300°C at a neutron-flux density of about $5 \cdot 10^{13}$ neutrons/cm$^2 \cdot$ sec. Figure 1 gives the results of temperature measurements in one of the vertical channels of the reactor with a given design of transport container holding the biological specimens (dry blood). The temperature was measured at two points in the transport container, i.e., at the geometrical center and on the outer surface, by means of copper–Constantan thermocouples. As is seen from Fig. 1, there is a temperature gradient from the center to the surface of the transport container holding the specimens. The temperature shift on average is about 35°C at a power of 3 MW.

Figure 2 gives a schematic drawing of systems for cooling biological specimens placed in reactor core. The technical specifications of this system are: working diameter of channel 20 mm, length 8000 mm, cooling zone 600 mm, power 5 MW, helium-gas flow rate 50 m^3/h, and liquid-nitrogen flow rate 60 liters/h. With a given reactor operating cycle, a pressure difference of $(0.2\text{-}0.3) \cdot 10^5$ Pa is maintained continuously. The dependence of the temperature of the biological materials on the irradiation conditions in the cold channel is illustrated in Fig. 3. The container with the specimens was charged into the channel with the reactor at zero power, without helium circulating. During this time there is a slight increase in the temperature of the specimens (time interval I in Fig. 3). Then the circulation of helium gas begins and the temperature begins to drop

Translated from Atomnaya Énergiya, Vol. 47, No. 6, pp. 392-393, December, 1979. Original article submitted March 12, 1979.

0038-531X/79/4706-1005$07.50

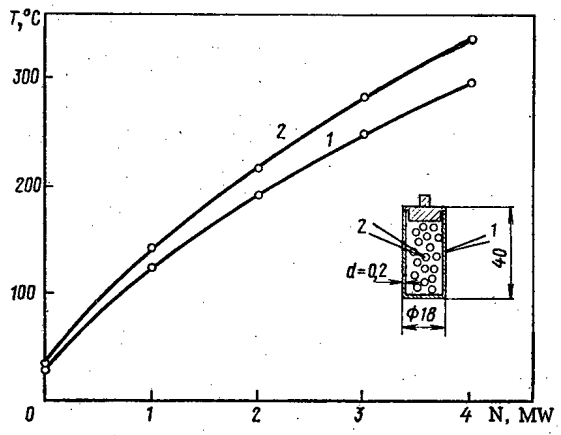

Fig. 1. Temperature of radiation heating of biological specimens vs thermal power of IRT-M nuclear reactor on surface (1) and in center (2) of container: O) experiment.

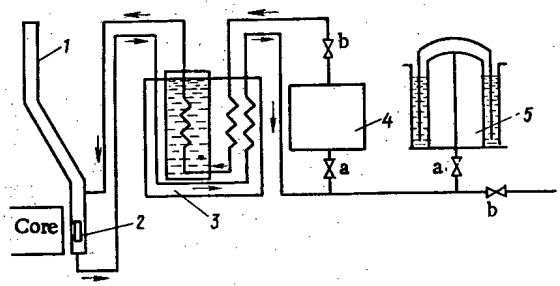

Fig. 2

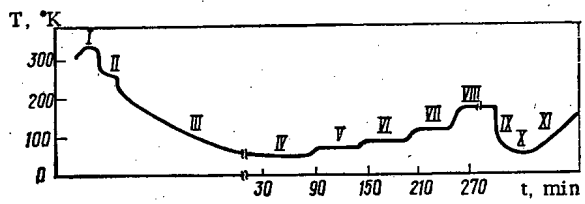

Fig. 3

Fig. 2. Main units of vertical low-temperature system for cooling biological specimens during irradiation: 1) loading channel; 2) specimen; 3) heat exchanger; 4) compressor; 5) gas holder; a, b) low- and high-pressure valves.

Fig. 3. Temperature vs power of nuclear reactor.

sharply (zone II). For 25 to 30 min after the onset of the circulation of cold helium there is a sharp decrease in the temperature of the specimens (zone III). Zone IV corresponds to the equilibrium temperature of the specimens at a power of 1 MW. Zones V-VIII shown in Fig. 3 correspond to a reactor power of 2, 3, 4, and 5 MW, respectively. In zone IX there is an abrupt drop in the temperature of the specimens after the reactor has been put into "zero power." Zone X corresponds to circulation of helium gas without cooling. The irradiation cycle ends with the specimens being removed from the reactor core. As is seen from Fig. 3, with an increase in the reactor power while the helium-gas flow rate remains at a constant given level, there is an increase in the temperature of the irradiated biological specimens, reaching ~170°K at a reactor power of 5 MW. Clearly, when biological specimens are irradiated in the temperature range from 80 to 170°K, the possibility of volatilization of chemical elements is practically eliminated. This low-temperature arrangement makes it possible to maintain a prefixed temperature range of irradiation of biological specimens at various reactor powers by varying the speed at which cooled helium gas is circulated.

LITERATURE CITED

1. D. Brune, K. Samsahl, and P. Webster, Clin. Chim. Acta, 13, No. 3, 285 (1966).
2. D. Brune and K. Jirlow, Radiochim. Acta, 8, 161 (1967).
3. D. Brune, Modern Trends in Activation Analysis, U. S. Govt. Printing Office, Washington, D. C. (1969), p. 203.
4. D. Brune and H. Wenzl, Anal. Chem., 42, No. 4, 511 (1970).
5. É. L. Andronikashvili et al., in: Second Meeting on Use of New Nuclear-Physical Methods for Solving Scientific-Technical and National Economic Problems [in Russian], Izd. OIYaI (Joint Institute for Nuclear Research), Dubna (1976), p. 127.

BORON CONTROL OF WATER-MODERATED WATER-COOLED POWER REACTOR DURING OPERATION UNDER VARIABLE LOADS

E. I. Ignatenko and Yu. N. Pytkin

UDC 621.039.586

A system of boron control has been used in water-moderated water-cooled power reactor (VVÉR) units to compensate for slow variations in the reactivity [1]. The concentration of absorber in the coolant of the main circulation loop (MCL) is changed by makeup with either a highly concentrated boric acid solution or pure water (deionized) with simultaneous drainage of unbalanced water into drainage tanks through a throttling device.

The method of exchanging water to change the concentration of boric acid in the coolant of the MCL results in unbalanced water, containing radioactive products, accumulating in the drainage tanks. Treatment of the drainage water in order to extract boric acid for reuse or storage and purification from radioactive products in special equipment requires expenditures and leads to contamination of the premises and the environment. The liquid radioactive wastes which are obtained during the treatment and whose activity and quantity are determined to a great extent by the operating conditions of the atomic power plant should be stored in special containers.

The VVÉR-440 units in service in the Soviet Union as well as in other countries are operated mainly on a load basis. Under these conditions, the volume of drainage water (including unorganized seepage) in the time between rechargings is about 1500 m^3. Data on the operation of the Kol'sk Atomic Power Plant show that the rates at which containers for storing liquid radioactive wastes are higher than those projected. When the atomic power plant has variable operating conditions [2, 3], the volume of the water drained systematically from the MCL increases more than tenfold. This results in a growth of the total activity of the gaseous-aerosol discharges into the atmosphere and a deterioration of the radiation conditions in the production premises.

The technique of making a reversible change in the boric acid content in the coolant of the MCL on the basis of utilization of the properties of ion-exchange resins, does not fully resolve the problem. Its use is coupled with a considerable quantity of high-activity wastes obtained during the regeneration and replacement of the spent resins. For a reversible change in the boric acid concentration in the MCL coolant in a closed cycle within limits sufficient to prevent transient poisoning with ^{135}Xe during operation of an atomic power plant during the variable-load part of the schedule a more promising technique is that of using a special apparatus (Fig. 1). The principal elements of the apparatus are an evaporator (with electric heaters) and a condenser which at the same time act as volume compensators. In the evaporator, because of the evaporation there is a build-up of a highly concentrated boric acid solution which, when necessary, is fed into the MCL through the adjustable valves. The volume of water in the evaporator is compensated by the inflow of coolant from the MCL through the check valve which protects the electric heaters from overheating when the level in the evaporator drops suddenly. Water without absorber enters the MCL as a result of the condensation of water vapor formed in the evaporator on jets of "cold" water during operation of the spray tower of the condenser. A back-up pump has been provided on the feed line for coolant to the evaporator and condenser in order to increase the rate of change of boric acid in the MCL with part of the MCL cut off.

In order to determine what rating the electric heaters of the condenser must have to prevent transient poisoning of the reactor core with ^{135}Xe when the power unit of the atomic power plant is operating under variable-load conditions, we carried out the necessary calculations. The operating conditions of the atomic power plant with daily unloading from nominal power to 30% and to zero were studied as well as the possibility of restoring the power to the nominal value at any moment of time.

The calculations were carried out for a fixed fuel charge in the VVÉR-440, for 7200 effective hours. The neutron-physical characteristics of the reactor and their variation during the fuel cycle were found by calculation [4, 5] as well as in experiments on the power units of the first department of the Kol'sk Atomic Power Plant. The calculations took account of the presence of a controlling group of assemblies in the reactor core and the change in the coolant temperature with a reduction of power.

Translated from Atomnaya Énergiya, Vol. 47, No. 6, pp. 393-394, December, 1979. Original article submitted April 7, 1978.

0038-531X/79/4706-1007$07.50

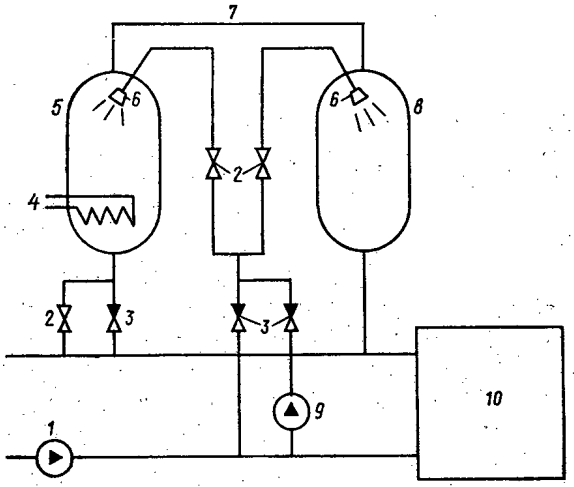

Fig. 1

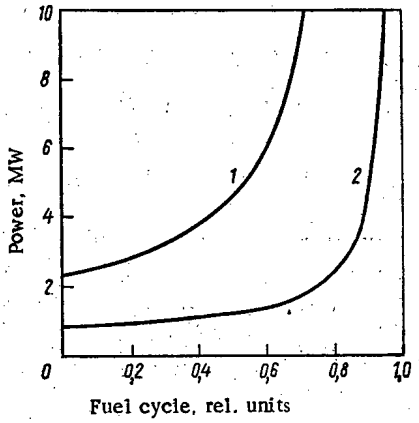

Fig. 2

Fig. 1. Apparatus for reversible change of boric acid content in MCL coolant in a closed cycle: 1) main circulation pump (MCP); 2) adjustable valves; 3) check valve; 4) electric heater; 5) evaporator; 6) spray towers; 7) feed pipe for water vapor from evaporator to condenser; 8) condenser; 9) back-up pump; 10) reactor.

Fig. 2. Calculated power of electric heaters of evaporator at various moments in the fuel cycle.

Figure 2 gives the results of calculation of the necessary power of the electric heaters in the evaporator at various moments in the burn-up cycle with daily power control of the power unit over the ranges from 100% to 0 (1) and from 100 to 30% (2). The character of the curves shows that in the first case the appropriate power of the electric heaters of the evaporator is about 10 MW and in the second case it is 4-5 MW. The calculations were carried out with a margin since no allowance was made for reduction of the reactor power with finite speed and the possibility of the power units being unloaded to the level of intrinsic needs during the daily shutdowns.

The fundamental possibility of the proposed apparatus being employed to vary the boric acid content in the MCL coolant was verified experimentally on the volume-compensation system of a VVÉR-440 unit of the Kol'sk Atomic Power Plant. During the operation of the power unit, a boric acid concentration of 20 g/kg was attained in the volume compensator as a result of the operation of the electric heaters and the discharge of water vapor into a bubbler.

LITERATURE CITED

1. V. A. Sidorenko, Problems of Safe Operation of VVÉR Reactors [in Russian], Atomizdat, Moscow (1977).
2. A. V. Bakanov, At. Tekh. Rubezhom, No. 6, 4 (1975).
3. V. A. Sidorenko, At. Energ., 43, No. 5, 333 (1977).
4. V. N. Semenov, Preprint IÉA-2157, Moscow (1971).
5. D. M. Petrunin, E. D. Belyaeva, and I. L. Kireeva, Preprint IAÉ-2518, Moscow (1975).

OPTIMIZATION OF PROBE DEVICE FOR SELECTIVE $\gamma-\gamma$ BOREHOLE LOGGING

D. K. Galimbekov and B. E. Lukhminskii

UDC 550.835:539.125.52

The probe device proposed in [1] for selective $\gamma-\gamma$ borehole logging (GGBL-S), of a special type with a slit collimator for the source, ensures determination of the effective atomic number Z_e of rocks and permits the interfering effect of their varying density ρ to be eliminated. Tests with this device showed that account must be taken of the interfering effect of microcaverns or of the gap h between the device and the borehole wall over cavern-bearing segments of the shaft.

In the present paper we consider the problem of optimizing a two-probe device (GGBL) consisting of the channel of GGBL-S and a γ-ray profilometer (GP), measuring h (Fig. 1).

The initial system of equations for finding Z_e and h with account for the possible interference between the channels is of the form

$$\begin{aligned} J_1 &= I_1(\rho,\ Z_e,\ h,\ G_1)+\varepsilon_1(\rho,\ Z_e,\ h,\ G);\\ J_2 &= I_2(\rho,\ Z_e,\ h,\ G_2)+\varepsilon_2(\rho,\ Z_e,\ h,\ G), \end{aligned} \tag{1}$$

where J_1 and J_2 are the total readings of the GGBL-S and GP channels, respectively; ε_1 and ε_2 are perturbations caused in the channels by the radiation field of the neighboring channel; I_1 and I_2 are the fluxes of the recorded radiation, bearing the principal information about the measured parameters of the rock; G_1 and G_2 are the sets of variable parameters of the construction of the GGBL-S and GP channels in the space of the parameters G.

Optimization comes down to finding the set of parameters which ensures the maximum of the vector objective function $\eta(G)$, chosen to be the sensitivity to the measured parameter in each channel, i.e.,

$$\eta(G^*)=\max_G\begin{pmatrix}\frac{1}{J_1}\left|\frac{\Delta J_1}{\Delta Z_e}\right|\\ \frac{1}{J_2}\left|\frac{\Delta J_2}{\Delta h}\right|\end{pmatrix}. \tag{2}$$

We prescribe an allowable level of interfering factors

$$\begin{pmatrix}\frac{1}{J_1}\left|\frac{\Delta J_1}{\Delta\rho}\right| & \frac{1}{J_1}\left|\frac{\Delta J_1}{\Delta h}\right|\\ \frac{1}{J_2}\left|\frac{\Delta J_2}{\Delta\rho}\right| & \frac{1}{J_2}\left|\frac{\Delta J_2}{\Delta Z_e}\right|\end{pmatrix}\leqslant\begin{pmatrix}\delta_{11} & \delta_{12}\\ \delta_{21} & \delta_{22}\end{pmatrix}, \tag{3}$$

where δ_{ij} is a small quantity limiting the effect of the j-th interfering factor on the reading of the i-th channel.

It is required that the interference of the channels with each other not exceed a prescribed level g (e.g., 10%)

$$g\begin{pmatrix}J_1\\ J_2\end{pmatrix}\geqslant\begin{pmatrix}\varepsilon_1\\ \varepsilon_2\end{pmatrix}. \tag{4}$$

Constraints (3) and (4) should be complemented with the conditions

$$\rho_1\leqslant\rho\leqslant\rho_2;\ Z_1\leqslant Z_e\leqslant Z_2;\ 0\leqslant h\leqslant h_{\max}, \tag{5}$$

which assign the ranges of ρ, Z_e, and h.

In the range of values of practical interest as far as parameter G is concerned, the perturbation ε_1 is negligible in comparison with J_1. This allows problem (2)-(5) to be solved separately, i.e., this permits the GGBL-S channel to be optimized independently first and then the GP channel to be optimized with allowance for the perturbation of the GGBL-S channel.

Translated from Atomnaya Énergiya, Vol. 47, No. 6, pp. 394-396, December, 1979. Original article submitted May 29, 1978.

0038-531X/79/4706-1009$07.50

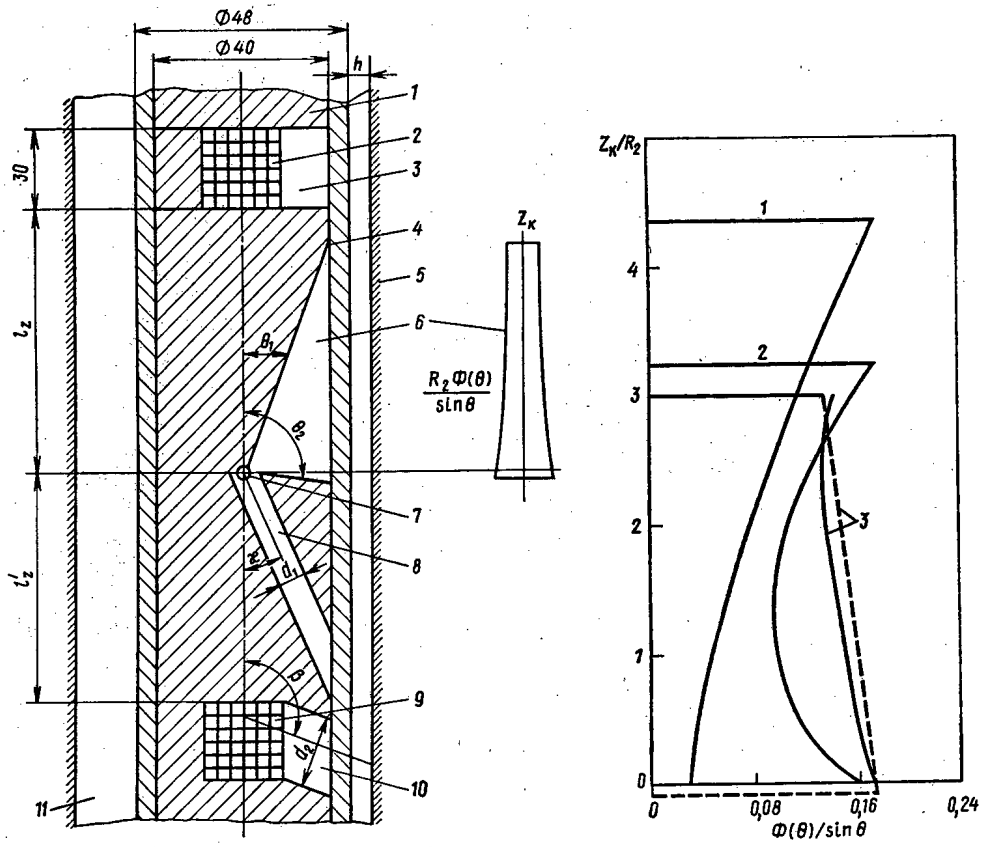

Fig. 1. Geometry of two-probe GGBL-S device: 1) cylindrical lead shield; 2, 3) detector and inlet collimator of GGBL-S channel; 4) aluminum casing of instrument; 5) rock; 6) exit slit collimator of GGWL-S channel; 7) γ-ray source; 8) exit collimator of GP channel; 9, 10) detector and inlet collimator of GP channel; 11) medium filling borehole.

Fig. 2. Diagram for determining the form and dimensions of slit collimator of source and length of optimal GGBL-S probe [l, Z_L, $\Phi(\theta)/\sin\theta$ are given in units of the radius R_2 of the lead shield]: 1, 2) GGBL-S probe with Eu and Se sources ($Z_L/R_2 = 6$ and 3.6, respectively); 3) calculated (——) and experimental (– – –) variants with Se source ($Z_L/R_2 = 3.25$).

In the first stage of optimization of the GGBL-S channel, we solve the firect problem of the GGBL. This is done by using the Monte Carlo method, executed with the aid of the MOK program package [2, 3]. The set of parameters G_1 includes the length l of the probe, the angles θ_1 and θ_2, and the form $\Phi(\theta)$ of the slit collimator of the source. The results of the solution of the direct problem are approximation by smooth functions in all variables [3]. Then, variational methods [4] are used for a number of values of l, θ_1, and θ_2 to choose the form $\Phi(\theta)$ of the slit collimator, ensuring satisfaction of conditions (3). Analysis shows that the increase in J_1 with Z_e is due to the reduction of the range of ρ. It is expedient, therefore, to choose δ_{11} to be equal to the statistical and instrumental errors.

In the optimization of the GP channel use is made of the similarity of the geometry of the channel to the geometry of single scattering. The set of parameters G_2 includes the distance l', the diameters d_1 and d_2 of the collimating apertures, the angles $\varkappa$ and β, and the lower energy threshold E_n of detected γ-ray quanta. In the first stage, an approximate optimization is made by using analytic expressions of single scattering for I_2 and approximation formulas for ε_2. Subsequent refinements, taking account of multiple scattering, are found by direct calculations with the MOK program package.

The scheme was implemented in selecting the optimal design of devices with ^{75}Se and ^{152}Eu–^{154}Eu sources, intended for studying rocks with a density ranging from 2.0 to 4.5 g/cm^3 and with effective atoms numbers of 13 to 22 (ores of nonferrous metals, bauxites, etc.). To assess the reliability of the proposed optimization scheme, calculations were made of one variant of the configuration of an experimental GGBL-S with a slit collimator [1], as shown in Fig. 2. In this case, the sensitivity $(1/\Delta J_1)(\partial J_1/\partial Z_e)$ of the calculated and experimental

channels is equal to 7.5 and 7.8%, respectively. The satisfactory agreement between the parameters of the calculated and experimental probe device permit the proposed algorithm to be recommended for optimization of apparatus of a similar type with other sources and other materials for the casing. For the calculated parameters of the GGBL-S channel we give below the parameters of the GP channel for ^{75}Se and $^{152-154}Eu$ sources, respectively, with a casing thickness of 4 mm and $R_2 = 20$ mm:

	^{75}Se	$^{152-154}Eu$
l_z, cm	7	11
$\varkappa$, deg	27	18
β, deg	90	120
d_1, cm	1.1	1.2
d_2, cm	1.5	1.8
E_n, keV	110	190

Calculations showed that the use of an europium source reduces the sensitivity of the GGBL-S channel by almost half but increases the sensitivity of the GP channel (from 1.5 to 3% in a 1-mm gap).

LITERATURE CITED

1. I. I. Fel'dman, A. M. Blyumentsev, and V. F. Karanikolo, in: Trudy VNIIYaGG "Yadernaya Geofizika," No. 9, Nedra, Moscow (1971), p. 141.
2. B. E. Lukhminskii and D. K. Galimbekov, At. Energ., 39, No. 5, 365 (1975).
3. D. K. Galimbekov, V. F. Karanikolo, and B. E. Lukhminskii, in: Statistical Modeling in Mathematical Physics [in Russian], Izd. VTs SO AN SSSR, Novosibirsk (1976), p. 45.
4. F. L. Chernous'ko and N. V. Banichuk, Variational Problems of Mechanics and Control [in Russian], Nauka, Moscow (1973).

ANGULAR DISTRIBUTION OF GAMMA DOSE RATE AT DEEP PENETRATIONS

N. L. Kuchin, K. K. Popkov, and I. N. Trofimov

UDC 539.121:539.122

We have investigated the angular distribution of the gamma dose rate from a plane isotropic monoenergetic source for penetrations up to 50 mean free paths (mfp) in matter. Calculations were made by the S_n method in the S_6P_6 approximation using the KURAGA-M Program [1]. The source energy E_0 was varied from 0.5 to 10.0 MeV.

Since the angular distribution far from the source is expected to be particularly anisotropic with a pronounced forward peak, we made a special investigation of the possibility of applying the method to describe the angular distributions of the gamma dose rate. The effect of the number of terms l retained in the expansion of the scattering indicatrix in Legendre polynomials on the relative angular distribution of the gamma dose rate $k(\theta, \mu_0 x)$ was studied. The quantity $k(\theta, \mu_0 x) = D(\theta, \mu_0 x) / \int D(\theta, \mu_0 x) \sin\theta \, d\theta$ determines the fractional contribution to the total gamma dose rate from gamma rays traveling at an angle θ with the normal to the source surface. Figure 1 shows $k(\theta = 0, \mu_0 x, l)$ in iron for a plane isotropic gamma source with $E_0 = 8.0$ MeV. Since the curves approach asymptotic values for $\mu_0 x > 30$ and $l \geq 6$, it is concluded that a further increase in l would hardly lead to an increase in the accuracy of the calculations. The quality of the information obtained was checked by using a modified Monte Carlo method which specified a uniform distribution of first collisions over the whole shield thickness with up to 50 splitting boundaries. Figure 2 shows the relative angular distributions of the gamma dose rate from a plane isotropic source with a) $E_0 = 1.0$ MeV and b) $E_0 = 8$ MeV calculated by the Monte Carlo and S_n methods. The results agree within the limits of error of the Monte Carlo method, which does not exceed 30% at a penetration of 30 mfp.

Analysis of the data obtained showed that the character of the angular distribution of the gamma dose rate varies rapidly with the depth of penetration. At a penetration $\mu_0 x < 20$ the anisotropy increases monotonically,

Translated from Atomnaya Énergiya, Vol. 47, No. 6, pp. 396-398, December, 1979. Original article submitted July 4, 1978.

0038-531X/79/4706-1011$07.50

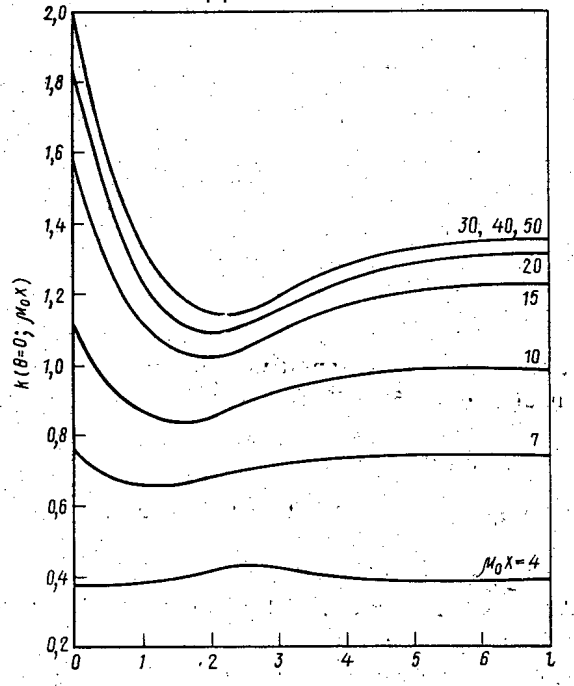

Fig. 1

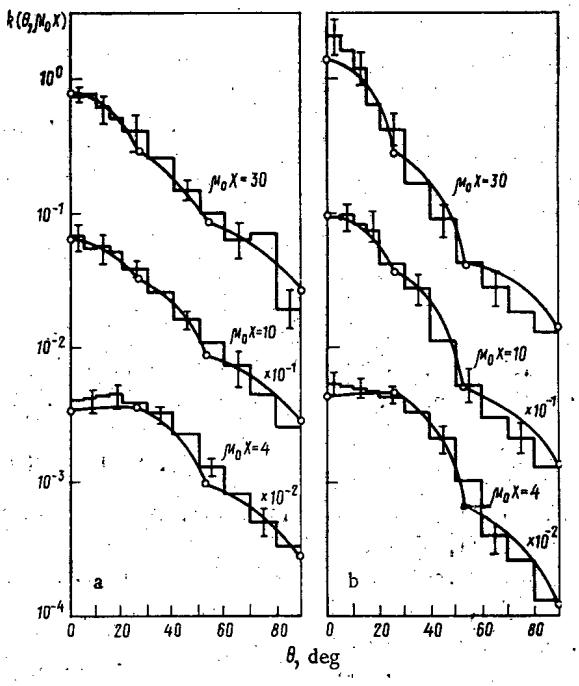

Fig. 2

Fig. 1. $k(\theta = 0; \mu_0 x, l)$ as a function of the order of expansion of the scattering indicatrix in Legendre polynomials.

Fig. 2. Relative angular distribution of gamma dose rate in iron: histograms calculated by Monte Carlo method: ○) calculated by S_n method; ——) linear interpolation in $\cos\theta$ of calculations by S_n method.

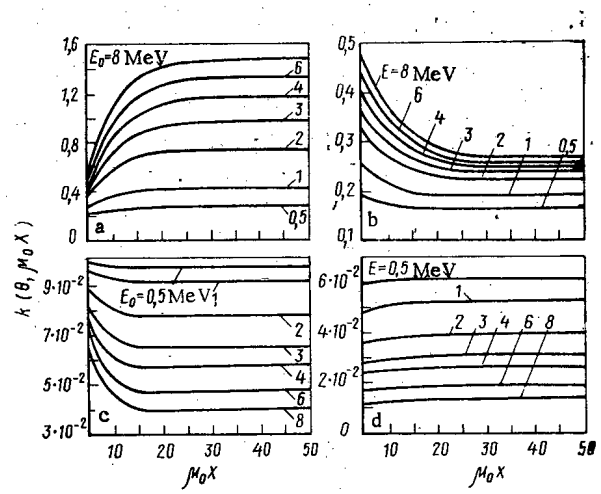

Fig. 3. Relative angular distribution of gamma dose rate $k(\theta, \mu_0 x)$ as a function of depth of penetration for a) $\cos\theta = 1$; b) 0.9; c) 0.6; d) 0.

but at penetrations of more than 20 mfp the angular distribution is stabilized. Similar behavior is observed if the energy E_{min} corresponding to the minimum in the total interaction cross section is greater than E_0. The values of $k(\theta, \mu_0 x)$ for water at fixed values of θ shown in Fig. 3 agree with the discrete reference values assumed in the algorithm.

The asymptotic angular distribution of the gamma dose rate for angles $0° \leq \theta < 90°$ is satisfactorily described by a function of the form $\exp(-\theta/\theta_0)$. The values of the exponential angular coefficients θ_0 are listed in Table 1. The concrete composition is given in [2]. For the materials investigated an increase in the gamma source energy increases the anisotropy of the asymptotic angular distribution of the gamma dose rate. Table 2 lists the coefficients θ_0 for various thicknesses of lead.

TABLE 1. Coefficients θ_0 (in deg) for Asymptotic Form of Angular Distribution of Gamma Dose Rate

Material	E_0, MeV							
	0,5	1,0	2,0	3,0	4,0	6,0	8,0	10,0
Water	51,0	35,0	23,5	20,0	17,5	15,6	14,5	13,7
Concrete	33,0	27,5	20,8	18,5	17,0	15,8	15,4	14,8
Iron	25,6	23,0	19,5	18,0	16,9	16,3	15,9	15,9

TABLE 2. Coefficients θ_0 (in deg)* for Various Thicknesses of Lead

$\mu_0 x$	E_0, MeV							
	0,5	1,0	2,0	3,0	4,0	6,0	8,0	10,0
20	11,5/14,8	15,2/15,2	15,2	14,8	15,3	15,5	15,5	15,5
30	10,7/14,8	14,1/15,2	14,5	14,0	14,2	14,5	14,5	14,5
40	10,2/14,8	13,9/15,2	14,5	14,0	13,9	14,0	14,0	14,0
50	10,0/14,8	13,7/15,2	14,5	14,0	13,8	13,5	13,5	13,5

*In the numerator of the fraction $0° < \theta \leq 26°$; in the denominator $26° < \theta < 90°$.

For $E_0 > E_{min}$ (E_{min} = 3.4 MeV) the angular distribution of the dose rate is practically independent of E_0, but varies as the depth of penetration $\mu_0 x$ is increased. Within the limits of accuracy of the method of calculation the angular distribution of the dose rate after more than 30 mfp of lead can be considered stable for energies E_0 (2, 3, and 4 MeV) which are close to E_{min}. For $E_0 < E_{min}$ (0.5 and 1 MeV) the angular distribution of the dose rate is stabilized only for $\theta > 30°$. At a given energy for $0° < \theta < 30°$ the anisotropy of the angular distribution of the gamma dose rate in lead increases with increasing penetration.

LITERATURE CITED

1. N. L. Kuchin et al., At. Energ., 44, 248 (1978).
2. E. Storm and H. Israel, "Photon cross sections from 1 keV to 100 MeV for elements Z = 1 to Z = 100," Nucl. Data, 7A, 565 (1970).

STRIPPING OF URANIUM IONS OF ENERGY OVER 60 GeV

E. L. Duman and L. I. Men'shikov

UDC 539.17

Unknown superdense or neutron nuclei may arise from phase transitions in the collision of heavy nuclei having energy of some hundreds of MeV/nucleon [1], which has stimulated research on accelerators for heavy ions (up to uranium). This requires quantitative determination of the interactions of such ions with targets, i.e., determination of the charge spectrum after stripping, the angular divergence, and the energy-spectrum broadening. This study formed part of research for heavy-ion accelerator systems [2] to be built at the Joint Nuclear Research Institute, where it is proposed to inject uranium ions of energy 350 MeV/nucleon into a synchrophasotron. Here we consider the material thickness of the target.

Processes Governing the Charge State, Angular Divergence, and Loss. The ultimate target parameters, the energy loss, and the angular divergence of the ion beam are governed by processes occurring in the inner electron shells of the uranium ion. This substantially simplifies the problem and provides simple analytical relationships between the beam parameters at the exit from the stripping target and the thickness and material for kinetic energies above 60 GeV.

The charge state in the ion beam is the result of two opposing processes: ejection of electrons from the uranium by collision with atoms and uptake of target electrons by the multiply-charged ion. If the relative velocity of collision is high, the probability of one-electron ionization can be determined from perturbation theory in the central approximation [3], which is readily extended to the case of relativistic velocities. Then the cross section for one-electron ionization (in atomic units: $\hbar = m_e = e = 1$) is

$$\sigma = 7.2N \frac{Z_a^2}{Z_{ef}^2 v^2} \ln \frac{2{,}2v^2\gamma \exp(-v^2/c^2)}{Z_a Z_{ef}}, \quad (1)$$

where N is the number of electrons in the outer shell of the ion, while $\gamma = (1-v^2/c^2)^{-1/2}$; here we have used a hydrogen-type model for the uranium ion on which there are electrons in the outer shell that move in an effective Coulomb field of a charge Z_{ef} with binding energy $I = Z_{ef}^2/2$. This representation is most fully justified if the charge on the ion is more than 85. However, in our case the stripping of the uranium to charge 85 occurs in the first 10% of the target thickness, and the remaining 90% is characterized by processes in the inner electron shells, for which the hydrogen-type model is most justified. The error does then not exceed 30%.

The following are the main processes that reduce the charge: 1) trapping of 1s electrons from the target atoms by the Coulomb field of the ion, i.e., Brinkman–Kramers trapping; 2) radiative capture, or electron capture with photon emission. In the ultrarelativistic case ($\gamma \gg 1$), the main process that reduces the charge on collision with target atoms is the production of e^+e^- pairs in the Coulomb field of the two nuclei and that of an electron in the K shell of the uranium. However, the contribution of this process to the production of the equilibrium charge can be neglected at the collision speed we envisage.

The following equation [7] gives the cross section for Coulomb capture, with correction for relativistic effects:

$$\sigma_{BK} = \frac{2^7\pi}{5}\left(\frac{\hbar}{m_e c}\right)^2\left(\frac{Z_a e^2}{\hbar c}\right)^5\left(\frac{Z_{эф}e^2}{\hbar c}\right)^5\left(\frac{v}{c}\right)^8 \frac{(\gamma+1)\gamma^8}{(\gamma+\varepsilon)^{10}}, \quad (2)$$

where $\varepsilon = \sqrt{1-Z_{ef}e^4}$ and c is the velocity of light.

If the collision speed is high, the cross section for radiative capture is expressed in terms of the photoionization cross section [7, 8]:

$$\sigma_{rad} = \frac{2K^2}{v^2} Z_a \sigma_p, \quad (3)$$

where Z_a is the number of electrons in the target atom, K is the momentum of the emissive photon, and σ_p is the photoionization cross section, which is given by Stobbe and Zauter equations [4] for the relativistic and non-

Translated from Atomnaya Énergiya, Vol. 47, No. 6, pp. 398-399, December, 1979. Original article submitted December 11, 1978.

0038-531X/79/4706-1014$07.50

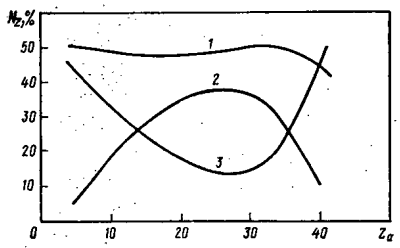

Fig. 1. Charge state N_Z of a uranium ion beam as a function of target atomic number Z_a for an energy of 250 MeV/nucleon and Z of: 1) 91; 2) 92; 3) 90.

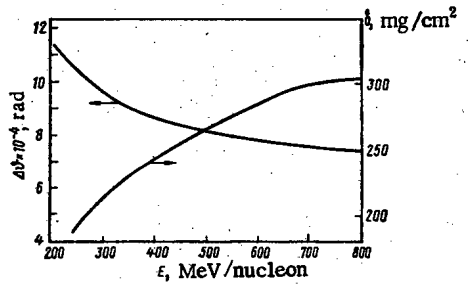

Fig. 2

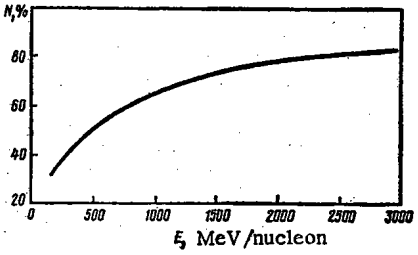

Fig. 3

Fig. 2. Relationship between equilibrium thickness δ of the optimum target, angular divergence $\Delta\vartheta$, and ion energy E.

Fig. 3. Proportion N of uranium nuclei stripped in relation to energy E for the optimum target.

relativistic cases. These equations for σ_p give identical results over a wide intermediate velocity range even for highly charged ions. The frequency of the emitted photon is $\omega = (Z_{ef}^2 + v^2)/2$.

The angular divergence $\Delta\vartheta$ is largely determined by the Coulomb scattering of the colliding particles:

$$\Delta\vartheta = \sqrt{2\left(\int \vartheta^2 d\sigma\right) N_a L}, \tag{4}$$

where $\vartheta = \frac{M_a}{M_i}\sin\theta$ is the scattering angle in the laboratory coordinate system, $d\sigma = \frac{\pi}{2}\left(\frac{ZZ_a}{M_a v^2}\right)^2 \frac{2\sin\theta d\theta}{\sin^4\theta/2}$ is the Rutherford differential scattering cross section, and L is the effective target thickness.

The energy loss and the broadening are due to processes that alter the electronic state and can be calculated from formulas due to Bethe [5] and Pomeranchuk [6].

Target Choice and Relative Content of Nuclei in Beam. The optimum parameters of the target are determined in the main by processes in the K shell of the uranium ion:

$$Z + e \rightleftarrows Y; \quad Y + e \rightleftarrows X.$$

Here Y and X represent uranium ions with 1 and 2 electrons in the K shell, respectively, while Z is a bare nucleus.

We write kinetic equations for these processes:

$$\begin{aligned} \frac{dX}{dl} &= -2\sigma_i X + \frac{\sigma_t}{2} Y; \\ \frac{dY}{dl} &= 2\sigma_i X - \sigma_i Y + \sigma_t Z + \frac{\sigma_t}{2} Y; \\ \frac{dZ}{dl} &= \sigma_i Y - \sigma_t Z, \end{aligned} \tag{5}$$

where $l = N_a x$, x is the target length, $X + Y + Z = 1$, σ_i is the ionization cross section of (1), and $\sigma_t = 2\sigma_{BK} + \sigma_{rt}$, where σ_{BK} and σ_{rt} are the cross sections for Coulomb and radiative capture calculated from (2) and (3), while X, Y, and Z are the proportions of uranium ions and nuclei in the beam.

These equations give us the charge spectrum of the uranium beam in relation to the atomic number of the target material provided at $Z_a/Z_{ef} \ll 1$ for collision energies above 60 GeV. There is a maximum yield of nuclei in the region $Z_a \approx 25$-28 (Fig. 1). The equilibrium thickness δ and the rms scattered angle $\Delta\vartheta$ have been calculated in relation to beam energy (Fig. 2), as has the proportion of nuclei Z in the beam (Fig. 3).

The energy loss and the broadening occurring in the equilibrium thickness under these conditions are almost independent of the energy for collision energies in the range from 0.25 to 2 MeV/nucleon and are correspondingly 700 and 30 MeV.

LITERATURE CITED

1. A. B. Migdal, Zh. Eksp. Teor. Fiz., 61, 2209 (1970).
2. N. I. Venikov et al., in: Proceedings of the Fifth All-Union Accelerator Conference [in Russian], Vol. 1, Nauka, Moscow (1977), p. 88.
3. J. Hansteen and O. Mosebekk, Nucl. Phys., A201, 541 (1973).
4. E. L. Duman and L. I. Men'shikov, Preprint IAE-3053, Moscow (1978).
5. E. L. Duman and L. I. Men'shikov, Dokl. Akad. Nauk SSSR, 244, No. 6 (1979).
6. V. B. Berestetskii, E. M. Lifshits, and A. P. Pitaevskii, Relativistic Quantum Theory, Part 1 [in Russian], Fizmatgiz, Moscow (1968).
7. V. D. Berestetskii, E. M. Lifshits, and A. P. Pitaevskii, ibid., Part 2.
8. I. Ya. Pomeranchuk, Collected Works [in Russian], Vol. 2, Nauka, Moscow (1972), p. 110.

EFFECT OF REACTOR RADIATION ON THERMOELECTRIC THERMOMETERS

A. A. Fraktovnikova, M. I. Redchenko, and A. S. Kruglov

UDC 536.5:621.362

The readings of thermoelectric thermometers (TT) of tungsten–rhenium alloys which are exposed to reactor radiation must be corrected because of the change in thermal emf resulting from radiation defects. The published data are not self-consistent. Thus, readings of a W/W25Re TT were raised 150° at a temperature of 2200°C and a fluence of thermal neutrons of $2.6 \cdot 10^{20}$ neutrons/cm^2 [1], while the readings of a W5Re/W-26Re TT were lowered 90° at a temperature of ~1200°C after irradiation in the MTR reactor for 5500 h [2]. Irradiation of a W5Re/W20Re TT to a fluence of thermal neutrons of $5 \cdot 10^{19}$ neutrons/cm^2 led to an increase in readings by 25° at the freezing point of aluminum [3].

The inconsistency of the published data is evidently a consequence of the great difference in methods and experimental conditions, the chemical compositions and constructions of the TT samples, and the technology of their manufacture and placement in the test section. In view of this we have investigated the behavior of VR5/20 TT made by the same technology and irradiated with neutrons having various spectra (Table 1).

The experiments were performed by two methods.

1. The thermoelectric properties of TT irradiated in a reactor were compared with those of standard samples which had not been irradiated. The results obtained in this way do not depend on transient effects. The effect on them of an induced thermoelectric nonuniformity was taken into account by profiling the temperature gradient along the thermoelectrodes during calibration.

2. The thermoelectric properties of TT during irradiation in a reactor were compared with those of standard Chromel–Alumel TT. The effect of heat release in TT junctions was reduced to a minimum by a closely packed assembly of TT in a sample having a large heat capacity. The effect of heat release on the thermal emf was determined from the difference in readings of samples placed in the test section in the calibration process performed before placing the assembly in the reactor, and the beginning of irradiation. In the present work this difference in readings was 1-3°.

Translated from Atomnaya Énergiya, Vol. 47, No. 6, pp. 399-401, December, 1979. Original article submitted January 8, 1979.

0038-531X/79/4706-1016$07.50

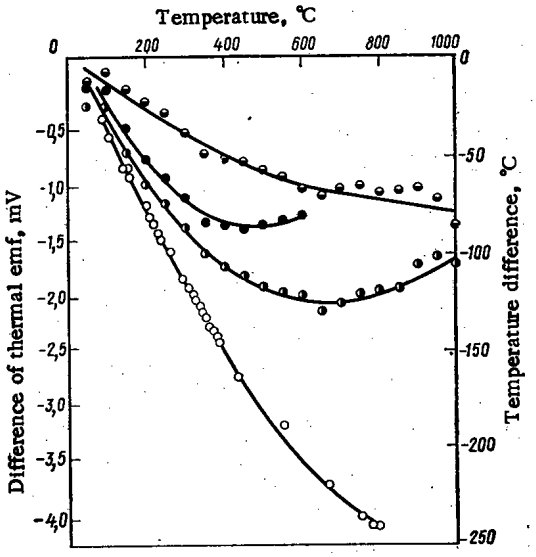

Fig. 1. Change in readings of irradiated VR5/20 tungsten–rhenium thermoelectric thermometers in comparison with readings of standard samples: ●) samples irradiated in the SM-2 reactor up to a fluence of $\sim 2 \cdot 10^{20}$ neutrons/cm^2 in an isochronal annealing process in the 20-650°C range; ◒) after isochronal annealing to 650°C; ◑) during irochronal annealing in the 650-1000°C range; ○) samples irradiated in BR-10 to a fluence of $1.14 \cdot 10^{22}$ neutrons/cm^2 in the calibration process.

TABLE 1. Conditions of Irradiation of TT

Type of reactor	Method of investigation	Maximum irradiation temperature, °C	Maximum neutron flux density,* neutrons/cm^2·sec	Maximum neutron fluence,* neutrons/cm^2
BR-10	In-pile tests	200	$3 \cdot 10^9/10^{14}$	$3{,}4 \cdot 10^{16}/1{,}1 \cdot 10^{21}$
VVR	The same	650	$5{,}7 \cdot 10^{13}/2{,}4 \cdot 10^{13}$	$0{,}7 \cdot 10^{21}/2{,}8 \cdot 10^{20}$
BR-10	Out-of-pile tests	460	—	$4{,}2 \cdot 10^{17}/1{,}14 \cdot 10^{22}$
SM-2	The same	100	$2{,}4 \cdot 10^{14}/4 \cdot 10^{14}$	$1{,}75 \cdot 10^{20}/2{,}9 \cdot 10^{20}$

*Numerator, thermal neutrons; denominator, fast neutrons.

The experiments were performed with miniature VR5/20 TT (microthermocouples) [4] with 0.2-mm-diameter aluminum oxide covered thermoelectrodes. The junctions of the TT were formed by welding the thermoelectrodes together with a cover. No fewer than three TT were irradiated in each experiment. The TT were heated in a reactor by neutron and gamma radiation. The maximum difference in readings of the TT did not exceed 0.5%.

The changes in thermal emf obtained in the calibration of irradiated TT in comparison with the standard samples are shown in Fig. 1. To account for the contribution of structural defects to these changes the samples were annealed. Samples irradiated in the SM-2 reactor were subjected to isochronal annealing in the 20-650 and 650-1000°C temperature ranges. The samples were heated gradually, and held at a constant temperature for 30 min approximately every 50°. The samples were calibrated both during isochronal annealing and after the complete thermal cycle. Figure 1 shows that for temperatures above 900°C annealing has no substantial effect on the thermal emf of irradiated TT. During annealing the thermal emf is partially restored, but its decrease is rather large, amounting to 1.27 mV (80°) at 900°C. The residual changes of the thermal emf are apparently related to both nuclear–chemical transformations of elements, and to structural defects which are not annealed in heating to 1000°C.

TABLE 2. Changes of Readings of TT in BR-10

Irradiation temperature, °C	Reactor power, MW	Fluence of neutrons of all energies, neutrons/cm^2	Deviation of readings, deg
70	1	$6{,}6\cdot10^{18}$	0
80	1	$2\cdot10^{19}$	—1
125	2	$5{,}7\cdot10^{19}$	—8
125	2	$1{,}6\cdot10^{20}$	—15
200	4	$5{,}6\cdot10^{20}$	—31
85	1	$5{,}7\cdot10^{20}$	—8
305 *	0	$6{,}4\cdot10^{20}$	—72
400 *	0	$6{,}4\cdot10^{20}$	—84
480 *	0	$6{,}4\cdot10^{20}$	—87
575 *	0	$6{,}4\cdot10^{20}$	—81
200†	5	$6{,}6\cdot10^{20}$	—22
205	6	$1{,}1\cdot10^{21}$	—37

*Calibration of samples during isochronal annealing.
†After isochronal annealing in the 300-600°C range.

TABLE 3. Change of Readings of TT during Annealing in the VVR Reactor

Fluence of thermal neutrons, neutrons/cm^2	Temperature of samples during measurements, °C	Deviation of readings, deg
$2{,}0\cdot10^{19}$	330	+1
$5{,}2\cdot10^{19}$	370	—7
$1{,}2\cdot10^{20}$	400	—8
$2{,}2\cdot10^{20}$	350	—15
$3{,}5\cdot10^{20}$	625	—20
$3{,}5\cdot10^{20}$	415	—15
$4{,}1\cdot10^{20}$	625	—37
$4{,}3\cdot10^{20}$	520	—24
$6{,}7\cdot10^{20}$	535	—15

Isochronal annealing and repeated calibration could not be performed on samples irradiated in the BR-10 (Table 1) because of severe embrittlement. Data on in-pile tests of changes in the thermal emf of VR5/20 TT performed in the BR-10 are shown in Table 2. The readings of samples at the maximum irradiation temperature (~200°C) were decreased by 33°. After irradiation to a fluence of $6.4\cdot10^{20}$ neutrons/cm^2 the samples were subjected to isochronal annealing in a channel at zero reactor power at the temperature indicated in Table 2. To do this the assembly was equipped with a built-in electric heater. Table 2 shows the changes in readings of TT after a 1-h holding time. Annealing of TT decreased the deviations of the readings to 22°. During further irradiation of annealed TT the changes of their readings continued to increase and reached 37°.

Samples of TT were irradiated in the VVR reactor by thermal neutrons to a fluence of $6.7\cdot10^{20}$ neutrons/cm^2 without special annealing of defects (Table 3). An analysis of the data of Table 3 shows that during irradiation there is partial self-annealing of structural defects, which results in a certain increase in the thermal emf which is particularly noticeable at an irradiation temperature of ~600°C.

The results obtained during isochronal annealing showed that structural defects of materials make a significant contribution to changes in the thermal emf of tungsten–rhenium TT, particularly for irradiation to a fluence of more than 10^{20} neutrons/cm^2. It is known [5] that structural defects of single crystals of tungsten irradiated to a fluence of $1.4\cdot10^{22}$ neutrons/cm^2 at a temperature of ~470°C are annealed at temperature >2000°C. Processes of formation and annealing of defects in tungsten–rhenium thermoelectrodes may differ from those investigated in [5]. However, it is known [6] that the annealing of radiation defects in pure tungsten and in a tungsten–rhenium alloy (W+25% Re) are only slightly different. Therefore, it can be predicted that at a high irradiation temperature (above 1000°C) the role of structural defects in the change of the thermal emf will remain appreciable: the change of thermal emf resulting from irradiation at this temperature cannot be accounted for solely by nuclear–chemical transformations in the thermoelectrode materials.

Thus, when VR5/20 tungsten–rhenium TT of a single standard size made by the same technology were irradiated by neutrons with different spectra, deleterious changes in the calibration relation occurred, reaching 250°C at 800°C and a neutron fluence of $1.14\cdot10^{22}$ neutrons/cm^2. Data on isochronal annealing show that structural defects make a significant contribution to the change of the thermal emf. For TT irradiated with fast neutrons to a fluence of $2.9\cdot10^{20}$ neutrons/cm^2 at 100°C the changes in readings were ~80° after annealing at a temperature of ~1000°C.

LITERATURE CITED

1. W. Kuhlman, "Evaluation of thermal neutron induced errors in the W/W25Re thermocouple," AIAA Paper No. 65-563 (1965).
2. P. Bliss and S. Fanciullo, PWAC-462 (1965).
3. N. V. Markina et al., Fiz. Met. Metalloved., 32, 1316 (1971).
4. V. I. Subbotin et al., Teploenergetika, No. 5, 91 (1965).

5. M. I. Zakharova et al., At. Energ., 38, No. 2, 78 (1975).
6. L. Keys et al., J. Nucl. Mater., 33, 337 (1969).

SOME DISTINCTIVE FEATURES OF THE SPECTRA OF DELAYED NEUTRONS

B. P. Maksyutenko, A. A. Shimanskii,
Yu. F. Balakshev, and S. F. Gritskevich

UDC 539.173.84

Knowledge of the spectra of delayed neutrons is necessary for calculation of reactor kinetics. By far most of the experimental research to date has been devoted to the investigation of steady spectra, which, just as nonsteady spectra, can be calculated from the spectra for the individual precursors. The discrepancy of the spectra calculated in this way and the experimental spectra is presented in Fig. 1 [1]. It is related to inaccuracies in the values of the fragment–precursor yield ratios and the probabilities of their emitting delayed neutrons. This has an appreciable effect even for such a well-studied element as ^{235}U when it comes to its fission by thermal neutrons.

Two-dimensional measurements have begun of the spectra of delayed neutrons, and the counting rate has been recorded as a function of the energy and time. The results in this case do not depend on knowledge of the fragment yields and the neutron emission probabilities; therefore, they can be used directly in calculations of the nonsteady mode of reactors. We note several qualitative characteristics.

The instrumental spectrum of delayed neutrons is shown in Fig. 2 in the sequence of its variation during the time after turning off the neutron source (irradiation time of 5 min). The amplification was chosen so that as much of the high-energy spectrum was captured as possible to the detriment of the resolution (we chose 256 energy channels and 64 time channels). The channel width was 17.2 keV. As is evident, there is a characteristic abrupt softening of the spectrum with increasing time; this conclusion is in agreement with the results of calculations based on spectra from the individual fragment–precursors [1].

A spectrum with an amplification larger by a factor of 2.5 (6.9 keV per channel) is shown in Fig. 3. Here the line structure of the spectrum in the low-energy region is of interest. According to statistical theory [2], the spectrum of the delayed neutrons from individual precursors is a line spectrum with from 200 to 1000 lines at 1 MeV. Under these circumstances it is not possible to count on the resolution of individual lines in the near future. An attempt was made to isolate groups of lines by using the method of least directed divergence [3]. The shape of the peak of epithermal neutrons upon recording the background (it is shown in Fig. 3) served as the resolution function. With such processing the peaks begin to be clearly isolated from groups of levels (on the average from four to 25 lines occur per peak). The instrumental spectrum in the interval 4-12 sec was processed directly without subtracting the background and taking the reaction cross section into account only as a means of checking the possibilities of the method. The effective value of the energy of line groups and

TABLE 1. Effective Energies of Line Groups in the Spectrum of Delayed Neutrons from ^{235}U, keV

This paper	Ref. [1]	This paper	Ref. [1]	This paper	Ref. [1]
21	—	89	—	186	180
34	—	103	—	210	—
48	—	120	110	234	230
62	—	145	130	248	250
76	80	165	160		

Translated from Atomnaya Énergiya, Vol. 47, No. 6, pp. 401-403, December, 1979. Original article submitted January 8, 1979.

0038-531X/79/4706-1019$07.50

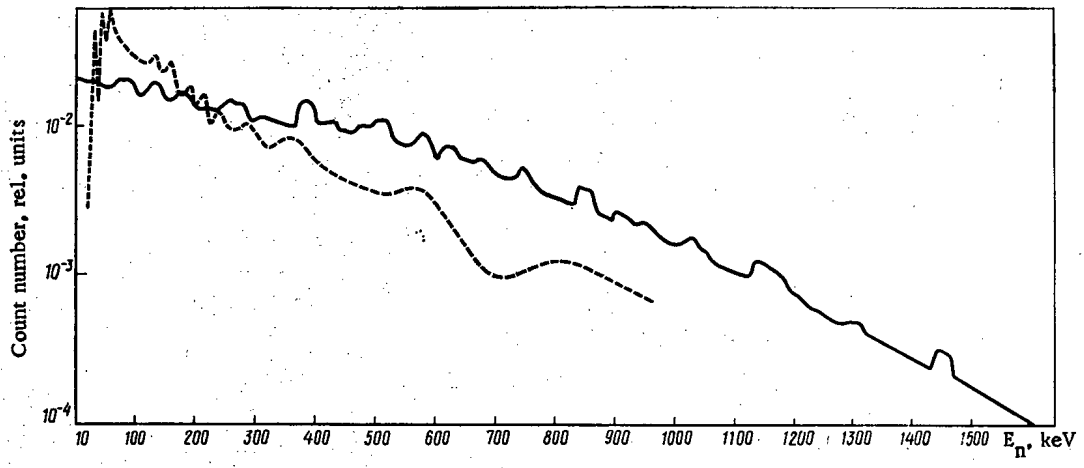

Fig. 1. Spectrum of delayed neutrons upon fission of ^{235}U [1]: ——) calculation based on the spectra of the precursors; ----) experiment (the irradiation, delay, and measurement times are 1.9, 0.2, and 1.8 sec, respectively).

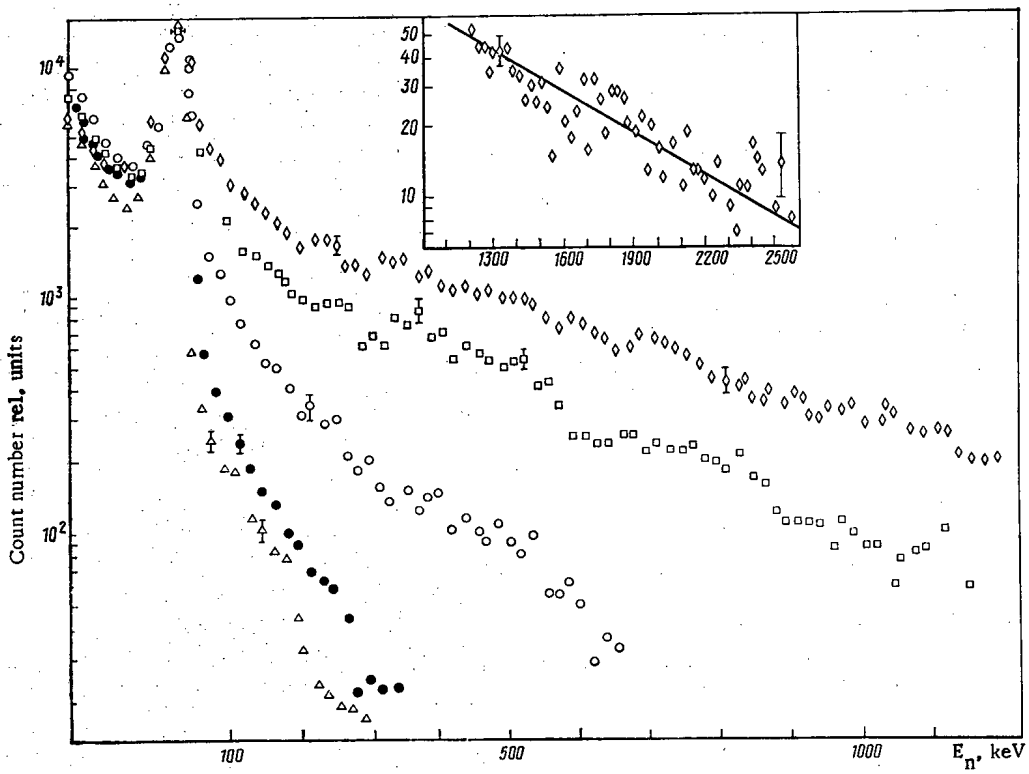

Fig. 2. Instrumental spectra of delayed neutrons of ^{235}U during 4-5 (◇), 26-28 (□), 124-132 (○), 308-324 (●), and 612-644 sec (△) – the background. The spectra are matched to the amplitude of the thermal peak. For orientation the statistical scatter is indicated at some places.

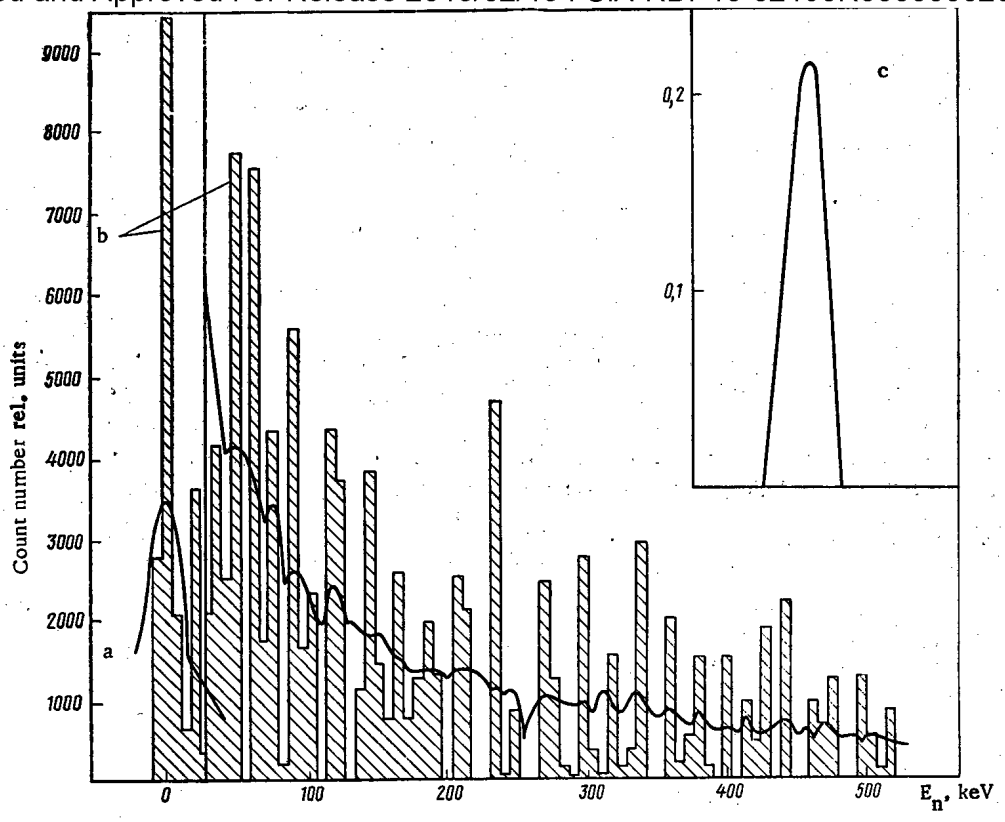

Fig. 3. Instrumental and processed spectra of the delayed neutrons of ^{235}U: a) instrumental; b) restored spectrum (× 5) after 2000 iterations; c) resolution function.

their relative contribution was determined. Depending on the number of energy groups used in the reactor calculation, averaging of the yields can be performed over the corresponding energy ranges. The effective energies of the line groups found in the experiment, which are in good agreement with the data for pure precursors, are given in Table 1. The linear structure of ^{137}I in the 200-600 keV energy range (see Fig. 2, □) is scanned clearly enough in the interval 26-28 sec.

LITERATURE CITED

1. G. Rudstam, INDC(SWD), 9/G+P, Res. Rep. LF-70 (1976).
2. J. Hardy et al., Nucl. Phys., A305, 15 (1978).
3. M. Z. Tarasko, Abstract of Candidate's Dissertation, FÉI (1974).

NEW DATA ON THE ALPHA DECAY OF ^{242m}Am

S. A. Baranov, V. M. Shatinskii, and L. V. Chistyakov

UDC 535.33

The use of transuranium elements that have been enriched with some isotope is preferable in spectroscopic investigations, and in particular, in the study of the alpha decay of these isotopes. An investigation of the alpha decay of ^{242m}Am – which has a relatively long half-life ($T_{1/2\alpha} \approx 3.1 \cdot 10^4$ yr) – using a specimen of americium enriched with this isotope yielded new data on its alpha radiation and made it possible to obtain a more complete scheme of its disintegration. Special attention was paid to the radiochemical removal of impurities from the americium. The results of the investigation are given below.

Apparatus Sources. The study of the alpha decay of ^{242m}Am was carried out on a magnetic alpha spectrograph with spatial focusing of the alpha-particle beam at an angle of $\pi\sqrt{2}$ [1]. The material used for the sources was a specimen of americium enriched with ^{242m}Am. The sources for the alpha-spectroscopic measurements were prepared by the method of vaporization in a vacuum. Glass was used as the backing. The dimensions of the sources were 1×60 and 3×60 mm. In the first case the resolving power of the alpha spectrograph (for a spatial angle of $\Omega = 5 \cdot 10^{-4}$ times 4π) was $\Delta E_\alpha = 2.5$ keV, and in the second, when we were looking for the less intensive alpha lines, it was 7.0 keV ($\Omega = 8 \cdot 10^{-4}$ times 4π). As the energy standards, we used the absolute values of the energy of the most intensive alpha lines ^{240}Pu and ^{241}Am: $E_{\alpha_{45}^{40}} = (5123.43 \pm 0.23)$ keV, $E_{\alpha_0^{40}} = (5168.3 \pm 0.15)$ keV and, $E_{\alpha_{103}^{41}} = (5442.98 \pm 0.13)$ keV, $E_{\alpha_{60}^{41}} = (5485.74 \pm 0.12)$ keV [2]. The accuracy of determination of the most intensive lines of the alpha spectrum of ^{242m}Am was ± 0.5 keV. In most of the remaining cases the error did not exceed ± (1.0-1.5) keV [3].

Alpha Decay of ^{242m}Am. According to recent measurements [3] (see also [4]), the alpha decay branch of ^{242m}Am is $(0.45 \pm 0.01)\%$ of the isomeric transition ^{242}Am, which corresponds to a partial half-life of $T_{1/2\alpha} = (3.11 \pm 0.05) \cdot 10^4$ yr [4]. The source investigated in the alpha-spectroscopic experiments contained admixtures of ^{241}Am and ^{243}Am. Naturally, even a small admixture (by weight) of alpha-radioactive americium isotopes with mass numbers of 241 and 243 in the source may mask some weak alpha lines of the ^{242m}Am spectrum that almost coincide in energy.

TABLE 1. Alpha Decay of ^{242m}Am

Present study			[4]		
E_α, keV	I_α, %	Elev, keV	E_α, keV	I_α, %	Elev, keV
5543,3*	—	0			
5517,3†	0,000†	26,5*			
5458,2	0,14	86,6			
5409,3	1,04	136,3	5411	1,2	136
5367,2	1,17	179,1	5367	1,5	180
5313,5	0,69	233,7	5315	0,8	233
~5273	0,86	~274			
5250,0	0,04	298,3			
5248,2	~ 0,11	300,1	5248	0,6	300
5214,7 ?	0,03	334,3 ?			
5206,8±0,5	89,84	342.15	5207	89	343
5173,7 }	0,04	375,8			
~5173 }		~377			
5153,3	0,02	396,6			
5141,6±0,5	5,82	408,48	5142	6,1	410
5088,4	0,19	462,6	5088	0,3	
5082	0,03	468,6			469
5064,2	0,22	437,2	5067	0,2	486
5027,1	0,02	524,9			
4974,9	~ 0,002	~578			

*Determined from gamma radiation.
†Possible admixture of α_{605} ^{242}Cm.

Translated from Atomnaya Énergiya, Vol. 47, No. 6, pp. 404-405, December, 1979. Original article submitted January 8, 1979.

0038-531X/79/4706-1022$07.50

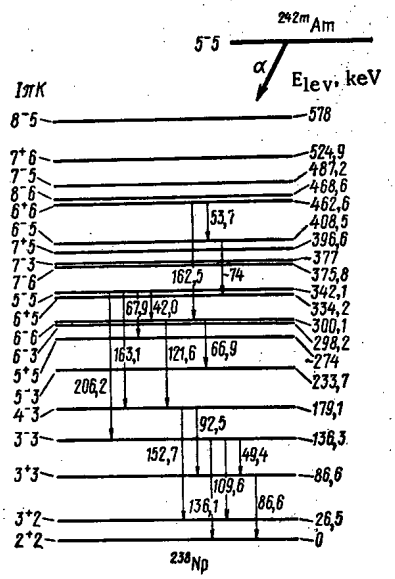

Fig. 1. Scheme of energy levels of the ^{238}Np nucleus.

The investigation of the alpha spectrum of ^{242m}Am was carried out immediately after the preparation of the source in an alpha-particle energy range of 4800-5570 keV. Most of the spectrum was taken at an alpha-spectrograph resolving power of $\Delta E_\alpha = 2.5$ keV. A number of exposures lasting 10-100 h were taken. The alpha particles were recorded with A-2 photoplates. The results of the analysis of the alpha spectra are shown in Table 1. Here we list the energy of the alpha particles (E_α keV), their intensity (I_α, %), and the energy of the levels (E_{lev}, keV) of the odd–odd nucleus ^{238}Np. It appears that the alpha spectrum of ^{242m}Am contains in the high-energy part a few more weak alpha lines masked by the more intensive alpha groups of the spectrum of ^{241}Am. In the first part of the table we summarize the data obtained by F. Asaro et al. and shown in the table of isotopes in [4] (see also [5]). A comparison of the results shows that in these experiments more than 12 new groups were found in of the alpha spectrum of ^{242m}Am.

Energy Levels of the ^{238}Np Nucleus. In the alpha-particle range investigated, we discovered more than 20 alpha groups corresponding to alpha transitions to the excited states of the ^{238}Np nucleus (see Table 1). Thus, the scheme of energy levels of this nucleus, shown in Fig. 1, contains more than 20 levels in a relatively narrow range of excitation (0 ~ 600 keV). Here we show only the experimentally discovered levels from the alpha decay. The energy of the α_0 line was determined from the gamma radiation ($E_\gamma = 86.68 \pm 0.03$ keV). The gamma spectrum was studied by means of Ge(Li) and Si(Li) detectors, with an americium specimen having the same isotope composition. Most of the detected gamma transitions in the ^{238}Np nucleus are shown in the scheme.

As can be seen from Fig. 1, the scheme contains seven bands. The initial levels of these bands have quantum characteristics $I\pi N = 2^+2$ [1] (the ground state of the ^{238}Np nucleus*); 3^-3; 3^-3; 5^+5; 6^-6; 5^-5 [2] (the favorable band); 6^+6. This sequence of bands and their quantum characteristics do not contradict the classification from the standpoint of odd proton and neutron Nilsson orbitals of adjacent odd nuclei of ^{241}Am and ^{243}Cm [5, 6]. According to this classification, it is not impossible that the lower part of the scheme contains bands with initial characteristics 2^-2. The levels with $E_{lev} \approx 216$ and 258 keV, which we found but which are not listed in the table, are apparently members of this band.

The authors are grateful to A. A. Artyunov, Yu. N. Dmitriev, and K. I. Merkulov for their help with the alpha-spectroscopic investigations, and also to V. A. Davidenko for his attention to and interest in this work. We thank V. A. Pchelin and V. M. Shubko for some of the radiochemical work, and Yu. F. Rodionov and Ts. Vylov for their help in the study of the gamma spectrum.

LITERATURE CITED

1. S. A. Baranov et al., Izv. Akad. Nauk SSSR, Ser. Fiz., 23, 1402 (1959).
2. A. Rytz, Atomic Data and Nuclear Data Tables, No. 12, 479 (1973).

*The spin of the ground state of the ^{238}Np nucleus (I = 2) was determined in [7].

3. A. G. Zelenkov et al., At. Energ., this issue, 405.
4. R. Barnes et al., J. Inorg. Nucl. Chem., 9, 105 (1959).
5. C. Lederer, J. Hollander, and I. Perlman, Table of Isotopes, Sixth Ed., Wiley, New York–London–Sydney (1967).
6. F. Asaro, M. Michel, S. Thompson, and I. Perlman, in: Proceedings of the Rutherford Jubilee International Conference, Manchester, UCRL 9566 (1961), p. 32.
7. E. Hyde, I. Perlman, and G. Seaborg, The Nuclear Properties of the Heavy Elements. Vol. II, Prentice-Hall, Inc., Englewood Cliffs, New Jersey (1964), p. 859.
8. R. Albridge, J. Hubbs, and R. Marrus, Phys. Rev., 111, 1137 (1968).

NEW MEASUREMENTS OF THE PARTIAL HALF-LIVES OF AN ISOMERIC STATE OF ^{242m}Am

A. G. Zelenkov, V. A. Pchelin, Yu. F. Rodionov, L. V. Chistyakov, and V. M. Shubko

UDC 539.1.14:539.1.16

In recent years, in connection with the needs of nuclear power generation and various branches of the atomic industry, much attention has been given to the question of the need to obtain more accurate nuclear data on actinides [1], and in particular the half-lives of the transplutonium elements [2, 3]. One of these insufficiently studied nuclides is the long-lived isomer ^{242m}Am, whose lifetime and partial half-life with respect to alpha decay were described 20 years ago in [4]. They were found to be equal to 152 ± 7 and $(3.20 \pm 0.16) \cdot 10^4$ yr, respectively.

We made repeated measurements of these values in order to verify them and make any necessary corrections. A product with high enrichment in the nuclide under investigation was used for the measurements. The simplest problem was to determine the partial half-life with respect to alpha decay. It was calculated from a comparison of the mass ratio of ^{242m}Am and ^{241m}Am in a product with an alpha radiation spectrum measured with semiconductor spectrometers and a magnetic alpha spectrograph and was found to be $(3.12 \pm 0.05) \cdot 10^4$ yr. In the determination a value of 432.6 ± 0.6 yr [3] was used for the half-life of ^{241}Am.

The total lifetime of ^{242m}Am was measured by two methods. In a freshly purified product, using a semiconductor alpha spectrometer, we made four series of measurements of the accumulation of the ^{242}Cm formed as a result of the beta decay of ^{242}Am. The rate of accumulation of the alpha activity of ^{242}Cm with respect to the alpha activity of ^{242m}Am was found to be $(3.22 \pm 0.04) \cdot 10^{-2}$ h^{-1}. This made it possible to find the half-life of ^{242m}Am:

$$T_{1/2} = 141.9 \pm 1.7 \text{ yr}.$$

In the calculations we used the following values for the half-life of ^{242}Cm and the ^{242}Am beta decay branch: 162.8 ± 0.4 days [3] and $83 \pm 0.5\%$ [5, 6].

To determine the half-life of ^{242m}Am, we also made measurements of the ratio between the intensity of the alpha radiation and the total intensity of the conversion radiation and beta radiation of ^{242m}Am and ^{242}Am, using proportional 4π counters. For maximum effectiveness in the recording of the low-energy radiation, the product was mounted on thin gilt films. We took account of the correction for the accumulation of ^{242}Cm, found by parallel measurements using a semiconductor alpha spectrometer. Measurements were made on seven targets made of freshly purified product. The ratio of the total intensity of the conversion radiation and beta radiation of ^{242m}Am and ^{242}Am to the intensity of the alpha radiation of ^{242m}Am was found to be equal to 431 ± 6. From this we obtained a value of $T_{1/2}$ ^{242m}Am $= 139.7 \pm 1.8$ yr. In the calculations it was assumed that the relative intensity of the electron capture of ^{242}Am in the ground state is $6.5 \pm 0.3\%$ [5, 6], and the fluorescence yield is 0.96. On the basis of our measurements, we recommend adopting a value of 141 ± 2 yr for the half-life of ^{242m}Am and $0.45 \pm 0.01\%$ for the probability of alpha decay.

Translated from Atomnaya Énergiya, Vol. 47, No. 6, pp. 405-406, December, 1979. Original article submitted January 8, 1979.

0038-531X/79/4706-1024$07.50

LITERATURE CITED

1. In: Proceedings of an Advisory Group Meeting on Transactinium Isotope Nuclear Data. Karlsruhe, 3-7 Nov. 1975, Report IAEA-186.
2. S. A. Baranov, A. G. Zelenkov, and V. M. Kulakov, At. Energ., 41, No. 5, 342 (1976).
3. Summary Report of the First Coordinated Research Meeting on the Measurement of Transactinium Isotope Nuclear Data. Report IAEA INDC (NDS)-96/N. Vienna (1978).
4. R. Barnes et al., J. Inorg. Nucl. Chem., 9, 105 (1959).
5. F. E. Chukreev, Yu. I. Grigor'yan, and E. N. Shurshikov, in: Theses of the 28th Conference on Nuclear Spectroscopy and the Structure of the Nucleus [in Russian], Nauka, Leningrad (1978), 556.
6. International File of Data on the Structure of the Atomic Nucleus (1974).

DETERMINATION OF REACTIVITY EXCESS FROM RESULTS OF CRITICAL AND SUBCRITICAL EXPERIMENTS

A. Yu. Gagarinskii, O. E. Zhukov,
A. F. Zaitsev, V. V. Petrov,
R. R. Sadykov, and L. S. Tsygankov

UDC 621.039.519:621.039.519.2

The prediction of the behavior of a reactor during operation from calculations of the change in the neutron multiplication factor k_{eff} or the reactivity ρ is based on a determination of the initial reactivity excess which is compensated by control rods. Experiments near the critical state or in the subcritical state of the reactor determine a value which more or less closely approximates the reactivity excess sought.

Suppose for simplicity that the reactivity of the reactor depends on two parameters a and b which can range over values

$$a_1 \leqslant a \leqslant a_0 \text{ and } b_1 \leqslant b \leqslant b_0,$$

such that

$$\rho(a_0, b_1) = \rho(a_1, b_0) = 0. \tag{1}$$

The typical procedure in experiments near the critical state is to measure the derivative of the reactivity with respect to one of the parameters over a range which ensures that the system can be maintained in a critical state by varying the other parameter. The measured value of the derivative, e.g. $(\partial\rho/\partial b)\,[a_{cr}(b), b]$ is used to compute the "integral reactivity"

$$\rho_\Sigma = \int_{b_1}^{b_0} \partial\rho/\partial b\,[a_{cr}(b), b]\,db, \tag{2}$$

which differs from the reactivity excess

$$\rho_0 = \rho(a_0, b_0) = \int_{b_1}^{b_0} \partial\rho/\partial b\,(a_0, b)\,db \tag{2a}$$

by the amount

$$\Delta\rho = \rho_0 - \rho_\Sigma = \int_{b_1}^{b_0} db \int_{a_{cr}(b)}^{a_0} \frac{\partial^2\rho(a, b)}{\partial a\,\partial b}\,da. \tag{3}$$

The difference between the values of the reactivity for two states of the reactor

$$\rho_\alpha = \rho(a_0, b^*) - \rho(a_1, b^*), \tag{4}$$

where $b^* \leq b_1$, is determined from subcritical experiments. It is easy to show that

$$\Delta\rho = \rho_0 - \rho_\alpha = \int_{b^*}^{b_0} db \int_{a_1}^{a_0} \frac{\partial^2\rho(a, b)}{\partial a\,\partial b}\,da. \tag{5}$$

Translated from Atomnaya Énergiya, Vol. 47, No. 6, pp. 406-407, December, 1979. Original article submitted January 8, 1979.

0038-531X/79/4706-1025$07.50

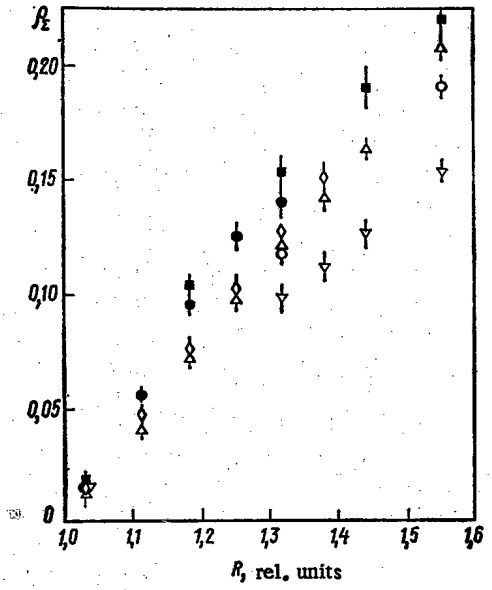

Fig. 1

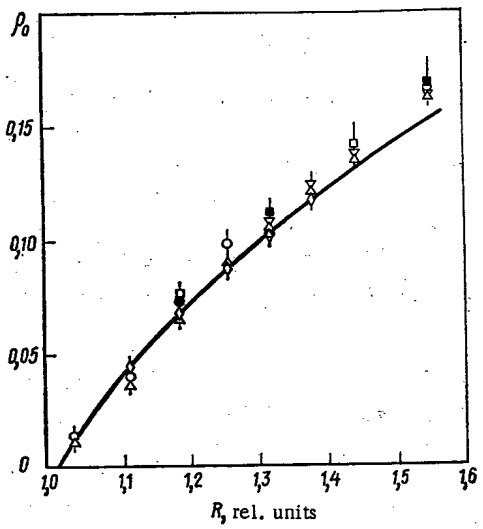

Fig. 2

Fig. 1. Integral reactivity as a function of core radius: ◇) $S_{ma}/S_{core} < (S_{ma}/S_{core})_{opt}$; △) $S_{ma}/S_{core} \approx (S_{ma}/S_{core})_{opt}$; ▽) $S_{ma}/S_{core} > (S_{ma}/S_{core})_{opt}$ (parameters *a*, b): ○) parameters *a*, c; ●, ■) parameters b_2, $C_{1,2}$.

Fig. 2. Reactivity excess as a function of core radius; ——) calculated; notation same as in Fig. 1.

Thus, the difference between the reactivity excess and the measurable quantity is determined by the sign and magnitude of the mixed derivative of the reactivity with respect to the two parameters. In some simple cases, for example for a bare homogeneous reactor, $\Delta\rho$ ((3), (5)) can easily be determined within the framework of the accepted slowing down model, and even turns out to be zero [1]. However, in a typical experiment with a reactor having a reflector ρ_Σ (2) determined by adding moderator and unloading fuel may differ appreciably from the reactivity excess sought, and it is recommended [2] that correction (3) be calculated.

In general, a calculational analysis of corrections (3) and (5) is clearly necessary, although it is a cumbersome addition to experiments to determine reactivity excess. The effectiveness of using few-group calculational methods developed for a wide class of systems [3] was shown by the example of a compact uranium reactor. The high sensitivity of k_{eff} to the core shape as a result of its small size permitted an experiment to be set up in such a way as to ensure the measurement of both the sign and magnitude of the correction $\Delta\rho$ (3) over a wide range.

Experiments were performed with a practically homogeneous core composed of assemblies of closely packed fuel elements and surrounded by an infinite water reflector. The reactivity was changed by moving down several adjacent central assemblies as is done in controlling a water-cooled water-moderated power reactor (their position is parameter *a*), changing the radius of the core by varying the number of assemblies (parameter b), and by poisoning the moderator with boric acid (its concentration is parameter c).

It is easy to see that for a given core there is a certain optimum number of central assemblies whose withdrawal gives a maximum change of reactivity. Then by varying *a* and b and maintaining a critical state of the system, the sign and magnitude of the mixed derivative $(\partial/\partial b)(\partial\rho/\partial a)$ and the corresponding correction $\Delta\rho$ (3) are determined by the sign and magnitude of the difference between the ratio of the cross-sectional area of the mobile assemblies (ma) to that of the whole core S_{ma}/S_{core} and its optimum value $(S_{ma}/S_{core})_{opt}$.

The experimental procedure in critical experiments consisted in measuring the reactivity for small deviations of *a* from the critical value and varying b or c. In the first case the measurements were performed for three variants of the number of displaced assemblies: one close to optimum, one larger, and one smaller. In the second case measurements were made for two values of b. The values of ρ_Σ (2) attributable to a core of a certain radius (Fig. 1) were obtained by integrating the $\partial\rho/\partial a$ curves from the critical value of *a* (for an unpoisoned core of given radius) up to its value corresponding to the two parts of the core being completely together. In subcritical experiments by varying b ($S_{ma} = 0$) for two values of c the reactivity ρ_α was determined by the Simmons–King method [4] with a theoretical–experimental correction for the dependence of the neutron generation time on the core radius.

The values of k_{eff} in the range of variation of *a*, b, and c were calculated in the two-group diffusion approximation. The macroscopic parameters of the medium were obtained by using a lattice homogenization program with a four-group representation of the neutron spectrum with universal constants in the slowing-down region to resonance energy, and treating thermalization in the modified monatomic gas approximation. The range of variation of parameters in the two-dimensional calculations was chosen to be completely adequate for the experimental range, which permitted the determination of the calculated value of ρ_Σ (2) just as in the experiments, i.e., by integrating the differential reactivity with respect to the parameter *a*. The values of ρ_α (4) were calculated similarly for the experimental values of b and c. The calculated corrections $\Delta\rho$ (3, 5) were determined from these results and the calculated values of the reactivity excess of a core of given radius $\rho_0(R)$. The reactivity excesses obtained by summing the experimental values of ρ_Σ, ρ_α and the calculated corrections $\Delta\rho$ are compared with the calculated values of ρ_0 in Fig. 2. Figure 2 shows that the experimental values of the integral reactivity for cores of the same radius vary by as much as 40% depending on the method of measurement (Fig. 1), but when the calculated corrections are introduced the values of the reactivity excess agree within the limits of experimental errors. The difference between the experimental and calculated values of a large reactivity excess is comparable with the characteristic error in calculating k_{eff} of uranium reactors by few-group methods ($\sim 10^{-2}$).

Thus, the calculation of k_{eff} for states of a reactor which can be realized in experiment practically completely removes the difficulties of interpreting the results of measurements of large reactivities and enables one to obtain the correct value of the reactivity excess.

LITERATURE CITED

1. T. S. Dideikin and B. P. Shishin, At. Energ., 29, 215 (1970).
2. V. S. Shulepin and L. P. Matveenko, At. Energ., 28, 355 (1970).
3. G. A. Bat', N. M. Trukhachev, and M. V. Fedulov, in: Physics of Nuclear Reactors. Collection of articles from MIFI, No. 1 [in Russian], Atomizdat, Moscow (1968), p. 129.
4. B. Simmons and J. King, Nucl. Sci. Eng., 3, 595 (1958).

EFFECTS OF THE EXIT CHANNEL ON THE NEUTRON DISTRIBUTION IN BERYLLIUM

V. N. Bogomolov, V. S. Gal'tsov, I. I. Zakharkin, and P. P. Prokudin

UDC 621.039.562.24

It is often necessary to have a cavity to accept specimens or to extract the neutron beam in many neutron-physics experiments such as irradiating specimens.

The exit channel causes anisotropy in the physical parameters of the medium, and it therefore perturbs the neutron distribution. The perturbation is naturally related to the dimensions of the channel, the form of the cross section, and the magnitude and direction of any neutron concentration gradient.

The perturbation can be examined for a particular system by extrapolation to a channel of zero cross section. For this purpose one makes measurements with channels of various areas. Very often, an integral method of measuring the neutron energy spectrum is employed, e.g., an activated indicator is used to record the distribution with and without the channel. It is then necessary to perform an energy-dependent correction for the detailed conditions.

In general, the channel produces a perturbation in the neutron distribution, but the energy spectrum may be only slightly dependent on the spatial coordinates, in which case the perturbation caused by the channel contains no energy dependence and merely amounts to a change in the neutron density near the channel. This type of perturbation is common in systems with crystalline moderators (graphite, beryllium, and beryllium oxide). This occurs because the energy dependence of the transport cross section is only slight for thermal neutrons above the Bragg limit. For the above materials, for example, the region where the irregularity in σ_{tr} becomes inappreciable starts at about 0.03 eV.

Translated from Atomnaya Énergiya, Vol. 47, No. 6, pp. 407-408, December, 1979. Original article submitted January 8, 1979.

0038-531X/79/4706-1027$07.50

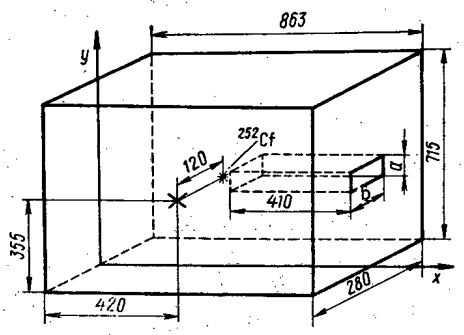

Fig. 1

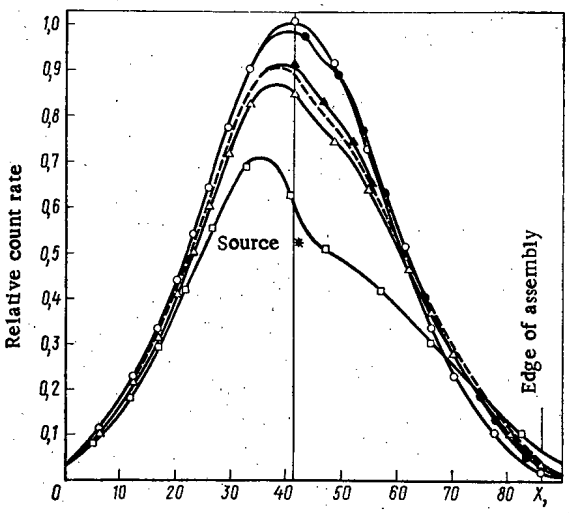

Fig. 2

Fig. 1. Basic dimensions of the beryllium prism containing the channel and geometry of the experiment.

Fig. 2. Distribution of the neutron density along the axis of the beryllium prism for channels of various cross sections (statistical errors in the experiment not more than 1%): ○) diameter 1.2 cm; ●) $a = 4$ cm, $b = 4$ cm; ▲) $a = 8$, $b = 4$; ———) $a = 4$, $b = 12$; Δ) $a = 12$, $b = 4$; □) $a = 12$, $b = 12$.

The fraction of the neutrons for which σ_{tr} differs from a constant makes only a small contribution to the density, which can be neglected to a first approximation, i.e., it is possible to assume that the spectrum is everywhere the same. On this basis it is assumed that the energy spectrum of the neutrons in such a system is more invariant under the perturbation than it is for example in assembly containing a hydrogenous moderator.

There are theoretical discussions [1-3] of the effects of cavities on the flux distribution; the diffusion approximation is commonly used, which is simple and obvious, but it has certain limitations in this field. On the other hand, the use of more rigorous methods is not always justified. Therefore, in certain instances it is desirable or even necessary to perform an experimental check on the perturbation, particularly for systems of small size.

We have examined the effects of the exit channel on the neutron density distribution in beryllium by measuring the neutron density at the axis of a beryllium prism for various cross sections of the exit channel (Fig. 1). The neutron detector was an SNM-13 counter, which moved within an aluminum tube of diameter 12 mm lying along the axis of the channel. The efficiency of this detector is inversely proportional to the neutron speed, so the neutron count rate is proportional to the neutron density. The prism was exposed to a ^{252}Cf neutron source providing about $1.7 \cdot 10^7$ neutrons/sec, which was placed in the prism with the coordinates shown in Fig. 1.

Figure 2 shows the measured distributions along the axis for channels of various sizes; the initial distribution was that obtained with a through channel of diameter 12 mm. This is described satisfactorily by a Gaussian distribution:

$$\Phi(x) = \exp[-(x-d)^2/2\sigma^2],$$

where $\sigma = 16.8$ cm is the standard deviation, $d = 42$ cm being the point representing the peak. Figure 2 shows that a channel of dimensions up to 4×4 cm introduces virtually no perturbation into the neutron distribution whereas a channel of 12×12 cm reduces the neutron density at the bottom of the channel nearly to half and substantially distorts the general distribution.

The main conclusion is that the exit channels commonly used in physics experiments, which are rarely larger than 4×4 cm, introduce virtually no distortion into the neutron density in a beryllium system if the dimensions are larger than those used here. Calculations by the method of [3] agree well with these experiments, although the calculations are based on an infinite block of beryllium.

LITERATURE CITED

1. V. I. Bryzgalov et al., in: Slow-Neutron Spectra [in Russian], Atomizdat, Moscow (1971), p. 315.
2. L. Kaspers and A. Yansen, ibid, p. 332.

3. G. A. Bat', A. S. Kochenov, and L. P. Kabanov, Research in Nuclear Reactors [in Russian], Atomizdat, Moscow (1972).

AN EDDY-CURRENT METHOD OF CHECKING FOR LEAKS OF WATER (STEAM) IN A LIQUID-METAL COOLANT

V. N. Tipikin

UDC 620.179.14(088.8)

Experience with the BN-350 fast-reactor during 1972-5 [1] has shown that fast systems are needed for monitoring leaks of water into the sodium. The method of measuring the electrical conductivity of the sodium by the use of eddy currents is applicable. The excitation coils are fed with ac and induce eddy currents in the pipeline containing the liquid metal, whose strength is dependent on the conductivity, which in turn is affected by the presence of any bubbles, etc. The magnitude of the eddy current and therefore the number of bubbles can be judged from the current in the exciting coil or the emf in special measuring coils.

Published data indicate that this method is widely used abroad in research systems for observing the penetration of gas or steam into liquid metals and can be used on industrial systems [2-7]. The applications of instruments of this type are restricted by the fact that the transducer signal is substantially dependent on the temperature of the metal and on the temperatures of the windings. The signal from the eddy-current transduce due to temperature change may be comparable with the signal produced by the passage of bubbles of gas or vapor. The signal is also affected by the resistance of the working winding, the conductivity of the liquid metal, and details of the working coil, particularly temperature-dependent changes in the geometry. Preliminary experiments have shown that 60% of the overall temperature error is produced by inductance change in the working winding (due to temperature-dependent change in the geometrical dimensions), while 30% is due to change in the resistance and 10% to change in the conductivity of the liquid metal.

Here some test results for eddy-current transducers developed in 1969-72 for monitoring for continuity in liquid-metal coolants are presented [8, 9]. Each transducer consists of working (inductive) and compensation sections. The thermal-compensation section is made with a bifilar winding to have a resistance equal to that of the working section. The two sections are placed in a common body and are geometrically identical and are exposed to identical temperatures: they are connected in adjacent arms of an ac bridge. An oscillator is connected to one diagonal and a measuring instrument to the other. The other circuit components are designed such that the impedance changes in the adjacent arms in response to any change in the temperature are equal to modulus and phase.

The instrument has been tested with liquid-metal testbeds filled with sodium at 300-450°C with injection of argon, water, or water vapor into the loop. The flow rate of the metal was measured with magnetic flowmeters, while the flow rate of the gas or vapor was measured with a throttle. Means were provided for separating the gas or vapor.

The secondary instrument was an ID-21 unit designed for use with inductive pressure transducers of differential-transformer type. The signal was passed to a KSP-4 recording potentiometer.

The sensitivity was found to be high (about 7/mV 1% gas without amplification), while the results were highly reproducible and the detection of artificial leaks was reliable. The lag in response was determined by the time needed for the gas to travel from the leak to the transducer. The time constant of the transducer itself was a few milliseconds. The transducer has worked for 2.5 years to a total of over 4000 h in one system. The instrument has also been used to check for a separation of gas from a liquid-metal loop and for testing various separation devices.

A similar instrument has been used since early 1977 for checking the filling of pipelines with sodium. This was set up on the sampling line in a BR-10 experimental reactor. The secondary instrument in the sodium sampling was an INI-3 induction transducer developed at the Power-Physics Institute and fitted with remote sound and light signals. The output signal was linearly related to the gas content.

Translated from Atomnaya Énergiya, Vol. 47, No. 6, pp. 409-410, December, 1979. Original article submitted January 8, 1979; revision submitted March 16, 1979.

0038-531X/79/4706-1029$07.50

Eddy-current measurement of the conductivity thus serves to define the volume of gas in the liquid metal provided that the temperature is constant: the temperature dependence arising from change in the inductance of the working winding caused by changes in the geometrical parameters was eliminated by a design in which both sections of the winding (working and compensation) were completely identical both geometrically and electrically and were at identical temperatures. The inductive coupling between the compensating winding and the metal was eliminated by additional components.

Tests were done with sodium in cold tubes of diameter 32 mm containing hollow capsules to simulate bubbles of gas; it was found that the bubbles of diameter 2-3 mm could be detected reliably. The signal at the amplifier output from a bubble of diameter 3 mm was about 250 mV as measured with a vacuum-tube voltmeter. It was also possible to observe smaller bubbles, e.g., of diameter 1 mm. A report [6] claims detection of bubbles of diameter 0.38-0.62 mm rising freely in an immobile coolant. It was said that a bubble of diameter 0.1 mm gave an output signal of 10 mV, which agrees with our data. We developed and tested transducers for pipes of diameters 10×1, 32×3, 48×4, 75×5, and 300×12 mm in which the tubes pass through the center, and also surface-mounting ones for pipes of diameters 32×3, 75×5, and 108×7 mm, which had inductances from 2 to 200 mH and which could be fitted with magnetic cores.

Tests on the design for pipes of diameter 300×12 mm were performed with a system consisting of a vertical section of pipe closed at the bottom and passing axially through the coil. The working medium was Wood's alloy. Hollow nonmagnetic capsules were used to simulate bubbles, which were introduced into the molten alloy in the upper part. The simulated gas contents ranged from 0 to 10%. The secondary instrument was a PTDT-L transducer designed for working with differential-transformer pressure transducers.

The tests showed that, in principle, it is possible to use these coils with pipelines of large diameter and wall thickness 10-15 mm; the sensitivity to deep bubbles was reduced because of the exponentially decreasing eddy-current density. The sensitivity over the initial part of the scale (for gas contents of 1-3%) was 60 mV per 1% gas.

One of the secondary instruments developed at the Power-Physics Institute has transformed input and a double phase-sensitive bridge circuit (Graetz circuit) [10]. The instrument contained stabilized oscillator and power amplifier. The output went to a KSP-4 pen recorder. The adjustment was such that the maximum deflection at the built-in microammeter (10 μV) or at the potentiometer (10 mV) corresponded to a volume gas content φ of 10%.

Experiments showed reliable detection of water leaks corresponding to hydrogen contents from 0.15 to 5% by volume with the metal at 300-350°C. The magnitude of the signal fell considerably by 400-450°C, and the fluctuations in the signal arising from passage of hydrogen bubbles (produced by reaction of the water with the sodium) became smaller by an order of magnitude, and in some cases no fluctuations were visible. It seems that the hydrogen dissolves completely in the time required for the sodium to pass along the loop from the site of production to the transducer. However, the instrument still recorded an increase in signal of 2-5 mV due to the conductivity change. In certain experiments with brief injection of water (steam), the reading of the instrument went off scale in a few seconds, with a slow return over several minutes to the initial state as the impurities were removed by the cold traps.

At 300-350°C, the instrument recorded clearly the instant of the leak (as corrected for the transport time) and gave highly reproducible results at identical gas contents. Nevertheless, there was considerable temperature dependence for small leaks (about 10 g/h or 0.01% gas by volume), which requires further improvement of the instrument.

The Power-Physics Institute is currently testing eddy-current transducers with improved thermal compensation of surface-mounting and demountable types, with or without magnetic cores, and is also working on reducing the dimensions and improving the circuits of the secondary instruments. Preliminary test data indicate that it should be possible to device a means of detecting steam leaks into sodium free from any temperature dependence and having a sensitivity such as to detect reliably a leak of 0.01% by volume of hydrogen.

LITERATURE CITED

1. O. D. Kazachkovskii et al., At. Energ., 43, No. 5, 343 (1977).
2. U. S. Patent No. 3529234, Class 324-5 (1970).
3. British Patent No. 1316793, class G1S (1973).
4. French Patent No. 1598425, cl. 21c, 15/00 (1967).
5. French Patent No. 2136712, cl. C21c, 17/00 (1973).

6. N. Ullmann, Kernenergie, 17, No. 1, 5 (1974).
7. West German Patent No. 1228831, cl. 42, 3/53 (1960).
8. V. N. Tipikin and V. V. Leshkov, Preprint FEI-840, Obninsk (1978).
9. V. N. Tipikin, Byull. Izobret., No. 43, 147, No. 46, 116 (1978).
10. Metrological Transducers with Analog Output [in Russian], Izd. Ontipribor (1966).

THE TEMPERATURE DISTRIBUTION IN A FUEL PIN AND SHEATH WITH RADIATIVE HEAT TRANSFER

V. F. Kuznetsov

UDC 621.039.517.5

Measurements have been made [1, 2] of the radial and azimuthal energy distributions in a thick block in a heterogeneous reactor (ρ, φ geometry). The present study is a continuation of [3] that presents an analysis of the fine structure of the temperature pattern in the cross section of a fuel pin arising from nonuniformity in the energy distribution.

We envisage the case where the fuel core V_1 and sheath V_2 are separated by an evacuated gap (with heat transfer in accordance with Stefan's law via the surfaces S_1 and S_2), while the heat transfer from the outside surface S_3 in accordance with a nonlinear law. Then the calculation of the temperature pattern $T(\mathbf{r})$, $\mathbf{r} = \{\rho, \varphi\}$ (with the coordinate system centered on the rod) involves solving the following boundary-value problems:

$$\nabla\lambda(\mathbf{r})\nabla T(\mathbf{r}) = -q_v(\mathbf{r}),\ \mathbf{r}\in V_1;$$
$$-\lambda(\mathbf{r}_s)\frac{\partial T(\mathbf{r}_s)}{\partial n_s} = f[T(\mathbf{r}_s), T(\mathbf{r}'_s)],\ \mathbf{r}_s\in S_1,\ \mathbf{r}'_s\in S_2; \quad (1)$$
$$\nabla\lambda(\mathbf{r})\nabla T(\mathbf{r}) = 0,\quad \mathbf{r}\in V_2;$$
$$-\lambda(\mathbf{r}_s)\frac{\partial T(\mathbf{r}_s)}{\partial n_s} = kf[T(\mathbf{r}'_s), T(\mathbf{r}_s)],\ \mathbf{r}_s\in S_2,\ \mathbf{r}'_s\in S_1;$$
$$-\lambda(\mathbf{r}_s)\frac{\partial T(\mathbf{r}_s)}{\partial n_s} = g[T(\mathbf{r}_s)],\ \mathbf{r}_s\in S_3, \quad (2)$$

where $\partial/\partial n_S$ are the derivatives along the exterior normals to the surfaces S_l ($l = 1, 2, 3$); $f[T(\mathbf{r}_S), T(\mathbf{r}'_S)] = \varkappa[T(\mathbf{r}_S)^4 - T(\mathbf{r}'_S)^4]$; $\varkappa = \sigma\varepsilon_{re}$; σ is Stefan's constant; $\varepsilon_{re} = \varepsilon[T(\mathbf{r}_S), T(\mathbf{r}'_S)]$ is the effective degree of blackness of S_1 and S_2; $g[T(\mathbf{r}_s)] = \sum_{p=0}^{m} F_p T(\mathbf{r}_s)^p$ is a given nonlinear function for ($m \geq 2$); k is the ratio of the radii of the core and sheath, which characterizes the size of the gap.

The problem of (1) and (2) can be solved by iteration with a finite-difference or finite-element method, as for a simpler case [4]. However, such calculations are too laborious for engineering purposes, and also the iteration may not converge because of the nonlinearity of the boundary conditions. It is therefore best to split up the treatment into two stages. In the first, we determine the temperatures of the surfaces S_l ($l = 1, 2, 3$), while the temperature pattern within the core and sheath is calculated in the second stage with the known boundary temperatures, which causes no difficulty and can be performed by any standard method.

We consider the first of these stages, in which (1) and (2) are reduced to certain integral equations for the unknown boundary temperatures. In region V_1 (fuel block) the solution is sought in the form

$$T(\mathbf{r}) = T^v(\mathbf{r}) + T^s(\mathbf{r}),$$

where $T^v(\mathbf{r})$ is determined by

$$\nabla\lambda(\mathbf{r})\nabla T^v(\mathbf{r}) = -q_v(\mathbf{r}),\ \mathbf{r}\in V_1;$$
$$T^v(\mathbf{r}_s) = 0,\ \mathbf{r}_s\in S_1. \quad (3)$$

For $T^s(\mathbf{r})$ we have $\nabla\lambda(\mathbf{r})\nabla T^s(\mathbf{r}) = 0$, $\mathbf{r}\in V_1$;

$$-\lambda(\mathbf{r}_s)\frac{\partial T^s(\mathbf{r}_s)}{\partial n_s} = F\left[\frac{\partial T^v}{\partial n_s}(\mathbf{r}_s), T^s(\mathbf{r}_s), T(\mathbf{r}'_s)\right],\ \mathbf{r}_s\in S_1,\ \mathbf{r}'_s\in S_2.$$

Translated from Atomnaya Énergiya, Vol. 47, No. 6, pp. 410-411, December, 1979. Original article submitted January 8, 1979.

0038-531X/79/4706-1031$07.50

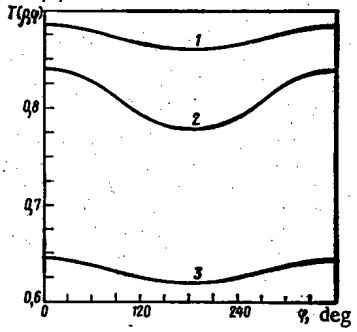

Fig. 1

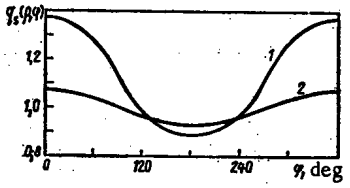

Fig. 2

Fig. 1. Relative temperature distribution $T(\rho, \varphi)$ in a fuel rod in relation to azimuthal angle φ and distance from the center: 1) $\rho = 0.2r_c$; 2) $\rho = r_c$; 3) $\rho = r_0$ (r_c is the radius of the fuel core and r_0 is the outside radius of the sheath).

Fig. 2. Relative azimuthal distribution of the heat flux $q_s(\rho, \varphi)$ at the surface of the fuel core (1) and the outer surface of the sheath (2).

We now consider the auxiliary problem

$$\nabla\lambda(\mathbf{r})\,\nabla G(\mathbf{r}, \mathbf{r}_s) = 0,\ \mathbf{r} \in V_1,\ \mathbf{r}_s \in S_1;$$
$$G(\mathbf{r}_s, \mathbf{r}'_s) = \delta(\mathbf{r}_s, \mathbf{r}'_s),\ \mathbf{r}_s, \mathbf{r}'_s \in S_1. \tag{4}$$

Then

$$-\int_{S_1} \lambda(\mathbf{r}'_s)\frac{\partial G(\mathbf{r}_s, \mathbf{r}'_s)}{\partial n_s}\,T^s(\mathbf{r}'_s)\,d\mathbf{r}'_s = F\left[\frac{\partial T^v}{\partial n_s}(\mathbf{r}_s), T^s(\mathbf{r}_s), T^s_s\right],\ \mathbf{r}_s, \mathbf{r}'_s \in S_1,\ \mathbf{r}''_s \in S_2. \tag{5}$$

This is the integral equation for $T^S(\mathbf{r}_S) = T(\mathbf{r}_S)$ on S_1. We can use any quadratic formula to get a system of nonlinear equations for the temperatures at the nodes of the boundary net. We supplement (5) with analogous equations for the sheath and get a system of three nonlinear vector-matrix equations for the unknown boundary temperatures:

$$\hat{A}_l T_l = F_l,\ l = 1, 2, 3. \tag{6}$$

Here (6) is solved by successive approximation, with each equation within an approximation solved by Newton's method. Although the kernel of (5) is degenerate, the equation can be solved by Newton's method because $(\partial F/\partial T)\ T^S(\mathbf{r}'_S)$ is transferred from F to the left, which gives us a new kernel $\lambda(\mathbf{r}'_s)\frac{\partial G(\mathbf{r}_s, \mathbf{r}'_s)}{\partial n_s} - \frac{\partial F}{\partial T}\,\delta(\mathbf{r}_s, \mathbf{r}'_s)$ that is not degenerate.

The problem of (4) was solved by a grid method with standard algorithms, as was (3); the iteration in each case can be carried through analytically [3] when the form of the distribution has been established and only the amplitude alters (regular mode). The kernel of (5) is derived from the solution of (4) on the basis

$$\lambda(\mathbf{r}'_s)\frac{\partial G(\mathbf{r}_s, \mathbf{r}'_s)}{\partial n_s} \approx \frac{\lambda(\mathbf{r}'_s)}{\Delta n}\{G(\mathbf{r}_s - \Delta\mathbf{n}, \mathbf{r}'_s) - \delta(\mathbf{r}_s, \mathbf{r}'_s)\}$$

and this requires the calculation of $G(\mathbf{r}_S - \Delta\mathbf{n}, \mathbf{r}'_S)$ only for one fixed value of the aximuthal angle, since the problem has rotational symmetry.

Detailed results were obtained by writing the Tempo program in FORTRAN for the BÉSM-6 electronic computer; Figs. 1 and 2 show the azimuthal temperature distribution $T(\rho, \varphi)$ and the radial temperature flux $q_S(\rho, \varphi)$ for the fuel loss at various distances from the center. The energy distribution in the fuel rod was derived from [1, 2].

The distributions for the temperature and radial heat flux of Figs. 1 and 2 are for the case where the properties of the fuel and sheath are dependent only on the coordinate [$\lambda = \lambda(\mathbf{r})$]; the temperature dependence of the thermal conductivity [$\lambda = \lambda(T)$] presents no obstacle to the use of this method in such cases. It is sufficient to use a Kirchhoff transformation for the purpose. Therefore, the method can be used to calculate temperature patterns in fuel rods with uneven energy production and nonlinear boundary conditions.

I am indebted to V. A. Lobyntsev for assistance and Ya. V. Shevelev for valuable criticisms and useful discussions.

LITERATURE CITED

1. N. N. Ponomarev-Stepnoi et al., At. Energ., 34, No. 3, 197 (1973).
2. V. F. Kuznetsov and V. A. Lobyntsev, Preprint: IAE-3029, Moscow (1978).
3. V. F. Kuznetsov and V. A. Lobyntsev, Preprint: IAE-2559, Moscow (1975).
4. J. Donea and S. Giuliani, Nucl. Eng. Design, 30, 205 (1974).

A HOT-NEUTRON GENERATOR WITH A ZIRCONIUM HYDRIDE RETHERMALYZER

B. G. Polosukhin, V. G. Chudinov, B. N. Goshchitskii, V. V. Gusev, and M. G. Mesropov

UDC 621.039.556

A hot-neutron beam of energy 0.1-0.5 eV (wavelength $\lambda \approx 0.9$-0.4 Å) is required in many experiments on the physics of solids and liquids. The proportion of such hot neutrons is small in the thermal-neutron flux from a nuclear reactor. The proportion in a given energy range can be increased by shifting the energy distribution to a higher energy range by means of a rethermalizer operating at a reasonably high temperature.

Current hot-neutron generators (HNG) usually employ graphite as the rethermalizer, or else beryllium or beryllium oxide, in each case as a block of diameter 110-200 mm and length 100-300 mm at T = 800-2000°C [1-4]. When the HNG contains one of these materials, the increase in the hot-neutron flux relative to the value g_0 for the empty channel is by a factor 3-7 at 0.25-0.35 eV, the exact value being dependent on the reactor type, rethermalizer material, dimensions, temperature, and position relative to the core [1-4]. These values are much less than the calculated ones if one considers only the temperature change in the Maxwellian spectrum, which is due to the restricted size of the rethermalizer block and the remoteness of the surface from the core, in addition to the neutron absorption in the material of the rethermalizer and other components.

It has been suggested [2] that an HNG should be based on a zirconium hydride rethermalizer. The large scattering cross section of the hydrogen should result in good rethermalization with small sizes and therefore shorter distances of the HNG from the core. However, it is impossible to heat zirconium hydride above 700-800°C without measures to prevent the hydrogen from escaping. Here we discuss results on an HNG with a $ZrH_{1.7}$ + 1% Nb rethermalizer.

Apparatus. The generator (Fig. 1) is placed in a vertical VÉK-1 channel in the IVV-2 reactor, which is linked to a GÉK-1 horizontal experimental channel directly behind the reflector. The device consists of an outside evacuated aluminum jacket, within which there are two hydride disks of diameter 150 mm and thickness 20 mm each enclosed in sealed jackets of stainless steel of thickness 0.8 mm. Means of temperature control are provided. A gap of about 10 mm between the disks improves the heat transfer if the temperature rises too high on account of radiation heating. The heat shield is installed between the outer and inner jackets. The cavity between the outside body and the jacket can be evacuated to $\sim 1 \cdot 10^{-3}$ Hg or filled with helium gas.

The overall thickness of the rethermalizer is about 40 mm and was chosen on the basis of measurements on a reactor model [5]. The temperatures of the rethermalizer and outside body were monitored with three Chromel–Alumel thermocouples. The outside body was in good thermal contact with the horizontal channel, which provided cooling. Radiation protection was provided by a shielding plug of length about 2 m in the upper part of the HNG. Any possible release of hydrogen from the hydride was monitored from the pressure, which was measured by a standard manometer. Cables suspend the HNG freely at 1-1.5 m above the core.

Test Results and Discussion. The HNG was tested with the reactor operating at 10 MW (the fast-neutron flux at energies above 1 MeV was about $2.5 \cdot 10^{12}$ neutron/cm^2 · sec at the point of installation of the generator, while the thermal-neutron flux was about 10^{13} neutron/cm^2 · sec and the γ-ray dose rate was about $3.2 \cdot 10^4$ R/sec. It was found that the most suitable working temperature for the hydride, T ≈ 700°C, could be attained without evacuating the gap. There was no hydrogen release during the 2-week test period. The temperature of the outside body was about 350°C.

Translated from Atomnaya Énergiya, Vol. 47, No. 6, pp. 412-413, December, 1979. Original article submitted January 13, 1979; revision submitted March 12, 1979.

0038-531X/79/4706-1033$07.50

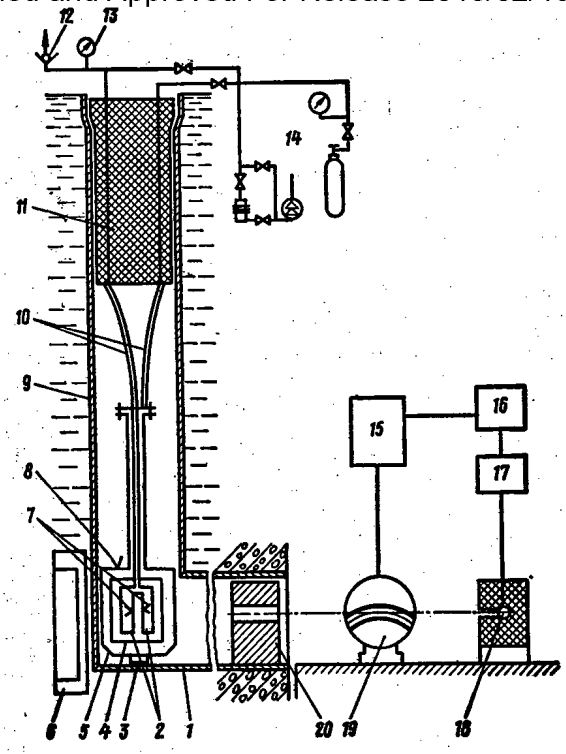

Fig. 1

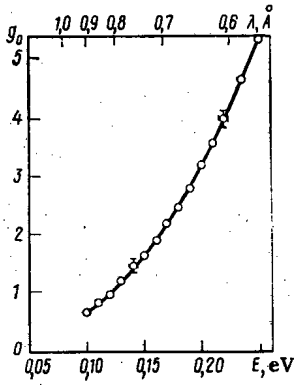

Fig. 2

Fig. 1. General design of the HNG: 1) horizontal reactor channel; 2) zirconium hydride; 3) support; 4) heat shield; 5) outside jacket; 6) reflector; 7) rethermalizer thermocouples; 8) outside-jacket thermocouple; 9) vertical channel; 10) flexible vacuum connections; 11) shielding plug; 12) nonreturn valve; 13) gauge; 14) pumping system; 15) power stabilizer and supplies; 16) time analyzer; 17) counting system; 18) neutron detector; 19) mechanical neutron chopper; 20) collimator.

Fig. 2. Increase in the yield of hot neutrons in relation to energy (the points are from experiment).

The neutron spectrum from the HNG was highly distorted; it was represented by a Maxwellian distribution with a temperature T_n of 860°K for the energy range ~0.25-0.14 eV, as against 625°K for ~0.14-0.0735 eV and 415°K for lower energies, which indicates incomplete rethermalization of the thermal neutrons in the HNG. Figure 2 shows the yield of hot neutrons after the system relative to g_0 for various energies. The result is $g_0 \approx 3.2$ for about 0.2 eV, which agrees satisfactory with the data obtained for the physical model for the IVV-2 reactor [5]. The fraction of fast neutrons at the exit from the channel, as determined from the cadmium ratio, was roughly halved by the HNG, which means that the ratio of the useful neutrons to the background ones at ~0.2-0.25 eV was improved by a factor 6-10.

The results of [1-3] relate to HNG with rethermalizers of graphite and beryllium oxide; the increased yields of hot neutrons in both cases are similar up to an energy of 0.25 eV. The main advantage of the zirconium hydride system by comparison with a HNG using graphite or beryllium oxide at 1000-2000°C is the simplicity of the design, along with reliability and safety in operation and much smaller size. The latter was particularly important on account of the size restriction imposed by the channels. The design is simple because the rethermalizer is at a low temperature ($T \approx 700$°C), which can be obtained by radiation heating without special insulating measures.

We are indebted to V. P. Panyushin and V. I. Savin for collaboration.

LITERATURE CITED

1. O. Abeln et al., in: Proceedings of the IAEA Symposium "Neutron Inelastic Scattering," Copenhagen, 20-25 May 1968, Vol. 2, p. 331.
2. P. Egelstaff, in: Proceedings of the IAEA Panel "Instrumentation for Neutron Inelastic Scattering Research," Vienna, 1-5 December 1969, p. 249.

3. P. Carter, J. Nucl. Energy, 25, No. 1, 11 (1971).
4. G. Bohme, W. Drexel, and F. Wunderlich, Bull. Inf. Sci. Tech. CEA, No. 166, 23 (1972).
5. V. V. Gusev et al., At. Energ., 46, No. 4, 264 (1979).

EFFECTS OF URANIUM-ORE SEGREGATION IN TRANSPORT CONTAINERS IN RAPID GAMMA ANALYSIS

L. N. Posik and I. M. Khaikovich

UDC 550.835

It is usual to employ γ-ray detectors mounted to the side of or above the ore in rapid evaluation of uranium content during extraction and transport in various vessels (tubs, self-tipping trucks, and wagons). The conversion factors (from the measured count rate to the uranium content) are determined by sampling the ores or by the use of monitor radiation sources prepared from averaged ores of the given type. It is important to provide identical physical and geometrical conditions in the γ-ray measurements for the calibration and working analyses. However, most types of cut uranium ore contain fractions up to 300 mm in size, where the uranium is selectively associated with certain grain sizes. This is one of the main reasons for the systematic errors associated with ore segregation during loading and transportation. Usually, the finer grain sizes are the most heavily enriched, for example the 5 mm class is 1.5-8 times richer than the 25 mm class, although in certain cases (magnetite ores and lump-enriched concentrates) one finds the converse relationship. The nonuniformity in the uranium distribution affects the γ-ray results in a way more complicated than that for more usual forms of ore sampling [1].

Ore segregation in γ-ray analysis may result in systematic errors because the larger fractions accumulate at the wall of the container or because the finer fractions accumulate at the bottom, particularly on long transportation routes.

The estimated possible distortion of the γ-ray distribution associated with each factor for a model wagon taken as a parallelepiped of size $l \times h \times a$ [2, 3]. We assume that the cross section of the heap formed by the large fraction during loading is a right-angled trapezium (with its vertex at the surface of the ore). The width of the flanks at the base ξ, which lies at the bottom of the wagon, is defined by

$$\alpha lha = h\xi (a+l) \text{ and } \xi = \alpha al/(a+l), \tag{1}$$

where α is the proportion of large lumps in the ore.

Let β be the portion of the uranium in the large fraction (reckoned for the average for the wagon); the content q in the rest of the ore is defined by

$$\alpha\beta + (1-\alpha)\, q = 1, \quad q = (1-\alpha\beta)/(1-\alpha). \tag{2}$$

If I_0 is the maximum count rate for a uniform distribution of the uranium in the wagon with $\alpha = 0$, then the relative change in the count rate P due to the segregation is

$$P = (\beta I_1 + qI_2)/I_0, \tag{3}$$

where I_1 is the count rate due to the ore in the outer parts of the wagon and I_2 is the count rate from the rest of the ore.

In the ray approximation, the formulas for I_0, I_1, and I_2 with the detector at the side are

$$I_0 = \int_{-l/2}^{l/2} dy \int_{-h/2}^{h/2} dz \int_{H}^{\infty} \varphi(x, y, z)\, dx; \tag{4}$$

$$I_1 = \int_{-l/2}^{l/2} dy \int_{-h_1}^{h_2} dz \int_{H}^{H+f} \varphi(x, y, z)\, dx; \tag{5}$$

Translated from Atomnaya Énergiya, Vol. 47, No. 6, pp. 413-415, December, 1979. Original article submitted January 24, 1979.

0038-531X/79/4706-1035$07.50

TABLE 1. Values of I_2/I_0 and I_1/I_0

α	h_1, cm				
	0	30	60	90	120
	I_2/I_0				
0	0,84	0,96	1,00	0,96	0,84
0,01	0,75	0,86	0,89	0,87	0,77
0,05	0,50	0,57	0,62	0,62	0,55
0,10	0,33	0,40	0,44	0,44	0,40
0,30	0,11	0,14	0,17	0,19	0,18
0,50	0,06	0,08	0,10	0,12	0,12
	I_1/I_0				
0	0	0	0	0	0
0,01	0,09	0,10	0,11	0,09	0,08
0,05	0,35	0,37	0,38	0,34	0,29
0,10	0,52	0,56	0,56	0,51	0,43
0,30	0,74	0,82	0,83	0,77	0,66
0,50	0,78	0,88	0,90	0,84	0,73

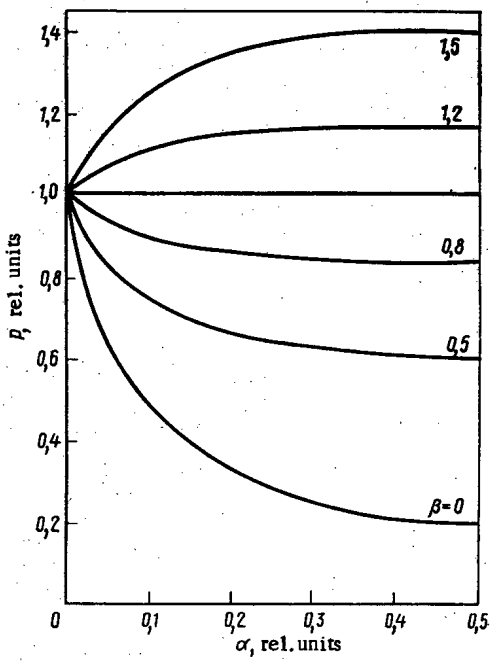

Fig. 1

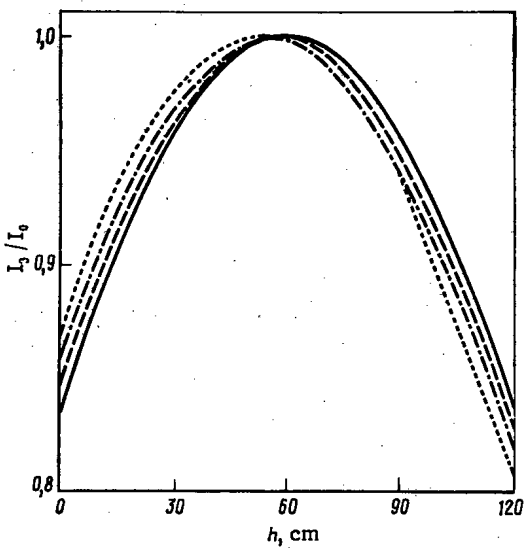

Fig. 2

Fig. 1. Dependence of P on α for various values of β and $h_1 = 60$ cm.

Fig. 2. The h dependence of I_3/I_0 for $a = 1$ (——), 0.9 (– – –), 0.8 (–·–), and 0.7 (·····).

$$I_2 = \int_{-l/2}^{l/2} dy \int_{-h_1}^{h_2} dz \int_{H+f}^{\infty} \varphi(x, y, z)\, dx, \tag{6}$$

where $\varphi(x, y, z) = \frac{\exp[-\mu(1-H/x)\sqrt{x^2+y^2+z^2}]}{x^2+y^2+z^2}$; $f = \xi\left(1 - \frac{h_1 - z}{h}\right)$; μ is the linear attenuation coefficient for γ rays in the ore, and H and h_1 are the distances from the center of the detector to the wall and to the bottom of the wagon, where $h_1 + h_2 = h$, $l_1 + l_2 = l$.

Table 1 gives results for I_1/I_0 and I_2/I_0 for H = 100 cm, h = 120 cm, $l = 12$ m, $a = 3.2$ m for several values of α and h_1; it was assumed in the calculations that the ore density was $\rho = 1.5$ g/cm^3, $\mu/\rho = 0.033$ cm^2/g.

Figure 1 shows P as a function of β, which indicates that the count rate falls from $0.9I_0$ to $0.2I_0$ as α goes from 0.01 to 0.5 for $\beta = 0$ (the large lumps do not contain uranium). At the same time, P falls from 0.95 to 0.6 for the same range in α for $\beta = 0.5$; if the large lumps are enriched in uranium ($\beta > 1$), variation of α within the above limit causes the relative count rate to increase from $1.02I_0$ to $1.16I_0$ for $\beta = 1.2$, as against from $1.05I_0$ to

TABLE 2. Values of I_3/I_0

a	h, cm					$\sum_h \frac{I_3}{I_0}$
	0	30	60	90	120	
1	0,84	0,96	1,00	0,96	0,84	4,6
0,9	0,85	0,96	1,00	0,95	0,83	4,6
0,8	0,86	0,97	1,00	0,94	0,82	4,6
0,7	0,87	0,98	1,00	0,94	0,81	4,6

$1.4I_0$ for $\beta = 1.5$. These cases correspond to loading the wagons with commerical material after radiometric sorting, where the concentrator from the machine classes is enriched by a factor 1.2-1.6 relative to the initial ore [4, 5]. Calculations show that with $0 < \alpha < 0.3$ and $0.8 < \beta < 1.2$ the count rate is affected by amounts ranging from 0 to ± 15% on account of the segregation.

We can estimate the effects from displacement of the fine enriched classes towards the bottom on the assumption that the uranium distribution over the height arising from this process is approximately linear:

$$q(z) = a + b(h - z), \tag{7}$$

where a and b are coefficients and $q(0) = a + bh$ is the mean uranium content at the bottom of the wagon.

Clearly, $q(h/2) = 1$, since this corresponds to the relative mean content of uranium in the wagon, i.e.,

$$a + bh/2 = 1. \tag{8}$$

The relative change in count rate on segregation due to this effect is defined by

$$P = I_3/I_0, \tag{9}$$

where I_0 is defined by (4) and I_3 is defined by modifying (5), in which $\alpha = 0$ and the integrand is replaced by the following expression on the basis of (7) and (8):

$$q(z) = a + 2(1 - a)[(h - z)/h)]. \tag{10}$$

Figure 2 and Table 2 give results for P from (9) for the detector placed laterally, where h is the independent variable and a takes various values.

These results show that the segregation effect results in an increase in the count rate in the lower layers relative to the upper to an extent dependent on the a of (7); the sum of the count rates taken over the height h (Table 2) is constant. Therefore, the effect of segregation of the small classes can be eliminated by averaging the γ-ray measurements over the height of the ore bed. Therefore, rapid analysis of an inhomogeneous ore in a wagon, particularly after prolonged transportation, should be by means of natural detectors whose sensitivity is symmetrically distributed in the vertical plane. If the q(z) is linear, the center of the sensitive zone should coincide with the middle of the ore layer. The results are qualitatively confirmed by γ-ray tests on vertical distributions arising at the walls of the wagons containing ore before and after prolonged transportation.

LITERATURE CITED

1. Handbook on Ore Dressing [in Russian], Vol. 2, Nedra, Moscow (1974).
2. L. N. Posik, At. Energ., 4, No. 5, 470 (1958).
3. L. N. Posik, in: Aspects of Ore Radiometry [in Russian], Nedra, Moscow (1968).
4. V. A. Mokrousov, G. R. Gol'bek, and O. A. Arkhipov, Theoretical Principles of Radiometric Ore Dressing [in Russian], Nedra, Moscow (1968).
5. L. Ch. Pukhal'skii and M. V. Shumilin, Surveying and Sampling of Uranium Deposits [in Russian], Nedra, Moscow (1977).

MINIMUM-DEVIATION REGULATION OF XENON OSCILLATIONS IN A REACTOR

B. Z. Torlin

UDC 621.039.562:621.039.512

Studies have been made [1-3] on the stability of reactors against xenon oscillations for simple control algorithms for the regulators, e.g., ones that maintain the neutron flux constant at the transducers. The same methods are applicable to the analysis of more complex systems and more efficient control techniques, for instance minimum-deviation control by reference to a given distribution Φ. Let the reactor core be fitted with M transducers, and let φ_i be the deviation of the neutron flux from Φ_i recorded by transducer i. Then N fast regulators (with $M \geq N$) require obedience to $\min \sum_{i=1}^{M} \varphi_i^2$*; the reactor responds to a small perturbation x in the material parameter B_0^2 with a deviation φ in the neutron flux, which is described [2] by the equation†

$$\Delta\varphi + B_0^2\varphi + \Phi\left(\sum_{j=1}^{N} \rho_j F_j + x\right) = 0, \tag{1}$$

where ρ_j and F_j are the performance of the regulator j and the spatial location of that regulator, respectively.

We introduce the influence function ψ_j for the control devices:

$$\begin{cases} \Delta\psi_j + B_0^2\psi_j + \Phi\nu_j = -\Phi F_j; \quad j = 1, 2, \ldots, N; \\ (\psi_j, \Phi) = 0; \quad \nu_j = -\dfrac{(\Phi^2, F_j)}{(\Phi, \Phi)} \end{cases} \tag{2}$$

and the function ψ_x

$$\begin{cases} \Delta\psi_x + B_0^2\psi_x + \Phi\nu_x = -\Phi x; \\ (\psi_x, \Phi) = 0; \; \nu_x = -\dfrac{(\Phi^2, x)}{(\Phi, \Phi)}. \end{cases} \tag{3}$$

With these functions we get

$$\varphi = A\Phi + \sum_{j=1}^{N} \rho_j\psi_j + \psi_x, \tag{4}$$

where A is an arbitrary constant.

Clearly, $\sum_{j=1}^{N} \rho_j\nu_j + \nu_x = 0$ and it can be shown that minimum-deviation control is attained if the following conditions are met, which define the algorithm for the fast regulators:

$$\sum_{i=1}^{M} \varphi_i\Phi_i = 0; \tag{5a}$$

$$\sum_{i=1}^{M} \varphi_i\psi_{ij} + \lambda\nu_j = 0; \quad j = 1, 2, \ldots, N, \tag{5b}$$

where λ is a Lagrange multiplier‡ and ψ_{ij} is the value of ψ_j in the zone of transducer i.

This method has been used in a calculation on a homogeneous one-dimensional reactor with two control rods and with the transducers uniformly distributed over the height of the core. Initially it was assumed that the end of one control rod lies at one-third of the height of the core ($z_1 = 1/3$), and the other lies at a height of two-thirds ($z_2 = 2/3$).

*Weighting factors can be used with all the terms in the sum.

†We consider a reactor without fast power feedback to the reactivity, which only simplifies the problem.

‡If the reactor has fast power effects on the reactivity, there is no need for the parameters A and λ in the first term in (4) and in condition (5a).

Translated from Atomnaya Énergiya, Vol. 47, No. 6, pp. 416, December, 1979. Original article submitted January 24, 1979.

0038-531X/79/4706-1038$07.50

If there are two transducers, conditions (5) are identical to the conditions $\varphi_1 = 0$ and $\varphi_2 = 0$.* This is a typical case of local control. The stability of this is characterized by the Randall factor [1, 4] $\mu = 8B_0^2$; change in the disposition of the control rods does not affect the stability.

If there are three transducers, it follows from the (5) that we can provide minimum-deviation control if the regulators maintain $\sum_{i=1}^{3} \varphi_i \Phi_i = 0$ and $\varphi_1 - \varphi_3 = 0$, and in this case also the stability is characterized by $\mu = 8B_0^2$. The stability does not alter if the control rods are placed with their ends at $1/4$ and $3/4$ of the height of the core. In the case of five transducers, it follows from (5) that the control rods must provide $\sum_{i=1}^{5} \varphi_i \Phi_i = 0$ and $(\psi_1 - \psi_5)(\varphi_1 - \varphi_5) + (\psi_2 - \psi_4)(\varphi_2 - \varphi_4) = 0$, and the second of these relations after derivation of the corresponding values $\psi_i = \psi(z_i)$ amounts to $(\varphi_1 - \varphi_5) + (\varphi_2 - \varphi_4) = 0$. The influence function $\psi(z)$ of a control of immersed to a depth z_0 in a homogeneous one-dimensional reactor takes the form

$$\psi(z) = \frac{\sin \pi z_0}{2\pi^2}\left[\sin \pi z \sin \pi z_0 + 2\pi \begin{cases} (1-z_0)\sin \pi z \cos \pi z_0 - z \cos \pi z \sin \pi z_0 & \text{for } 0 \leqslant z \leqslant z_0, \\ (1-z)\sin \pi z_0 \cos \pi z - z \cos \pi z_0 \sin \pi z & \text{for } z_0 \leqslant z \leqslant 1 \end{cases}\right].$$

Further, the value of μ is $8B_0^2$ for five transducers and for an infinite number, from which we conclude that the stability of a reactor with two control rods maintaining minimum-deviation neutron distribution is independent of the number of transducers. One assumes that an increase in the number of transducers should improve the transient response without loss of stability. Other discussions [1, 3] deal with the height stability of a reactor with an automatic regulator and shortened control rod. The end of the rod and the control chamber lie at half the height of the core, while the ends of the shortened control rod and the chambers lie at a point $z_1 = 1/4$ and $z_3 = 3/4$. It can be shown [1] that if the algorithm for the shortened rod is $\varphi_1 - \varphi_3 = 0$, while that for the automatic regulator is $\varphi_2 = 0$, then the stability of the reactor is characterized by $\mu = 3B_0^2$.† From (5) we get that this system provides minimum-deviation neutron control if the algorithm for the shortened control rod is maintained and the automatic regulator is required to produce $\sum_{i=1}^{3} \varphi_i \Phi_i = 0$ then not only will the transient response involve minimum-deviation control but also the stability will be considerably improved: $\mu = 8B_0^2$. The same factor characterizes the stability of this system with four transducers and also in the limiting case of an infinitely large number. As in a reactor with two control rods, or in a reactor with an automatic regulator and shortened control rod, the stability is not dependent on the number of transducers and minimum-deviation control is provided for $\mu = 8B_0^2$.

LITERATURE CITED

1. A. M. Afanas'ev and B. Z. Torlin, At. Energ., 43, No. 4, 243 (1977).
2. A. M. Afanas'ev and D. Z. Torlin, At. Energ., 44, No. 6, 487 (1978).
3. A. M. Afanas'ev and B. Z. Torlin, ibid., p. 530.
4. D. Randall and D. John, Nucleonics, 16, 82 (1958).

*In general, conditions (5) are identical to $\varphi_i = 0$, i = 1, 2, ..., N for $N = \mu$.
†If the automatic regulator is set to control the overall power, then $\mu = 15B_2^0$.

FISSION CROSS SECTIONS OF ^{235}U AND ^{238}U TO NEUTRONS WITH AN ENERGY OF 14.7 MeV

I. D. Alkhazov, V. N. Dushin,
S. S. Kovalenko, O. I. Kostochkin,
K. A. Petrzhak, V. I. Shpakov, R. Arlit, V. Wagner,
F. Weidhaas, V. Grimm,
R. Krause, G. Musiol,
H. Ortlepp, and R. Teichner

UDC 539.17

The majority of the data on fission cross sections has been obtained by measurements relative to some standard – the fission cross section of ^{235}U or the cross section of (n, p)-scattering by hydrogen. It follows from this fact that measurements of cross sections by absolute methods, which permit normalizing the data of relative measurements, are an important and timely problem [1]. This is especially true of ^{235}U, whose fission cross section is an acknowledged international standard.

Our reserach involved making absolute measurements of the fission cross sections of ^{235}U and ^{238}U to neutrons of energy 14.7 MeV as a joint effort by groups at the Dresden Technical University (GDR) and the V. G. Khlopina Radium Institute (Leningrad) with the installations and accelerator of the Technical University. The measurements were made by the method proposed in [2] of recording coincidences of the fission fragments and the α particle comoving with the neutron.

The neutron source was a neutron generator, the T(d, n)^{4}He reaction was used, and the deuteron energy was 130 keV. A target of fissionable material was irradiated with neutrons emitted at an angle of 13° to the direction of the deuteron beam. The neutron energy calculated for the specific conditions of the experiment was 14.71 ± 0.15 MeV. The fission fragments and the α particles comoving with the neutrons (at an angle of 165° to the direction of the deuteron beam), along with coincidences among them, were recorded. On the condition that the cone of neutrons corresponding to the α particles recorded, which is determined by the exit diaphragm of the alpha-detector, falls entirely on the target of fissionable material, the fission cross section is determined by the expression

$$\sigma_f = N_c / N_\alpha n_n,$$

where N_c and N_α are the number of coincidences and α particles recorded and n_n is the number of nuclei of fissionable material per square centimeter of target.

As is evident from this expression, the procedure used has a number of advantages: it is not necessary to measure the neutron flux nor to determine the efficiency of the alpha-detector and the solid angles for the detector and the target, and distortions of the result due to the background of scattered neutrons and neutrons from the D(d, n)^{3}He reaction are excluded. This procedure permits making absolute measurements of cross sections for a number of values of the neutron energy and to place the dependences of fission cross section on neutron energy on an absolute basis. This research is the first of a planned series of measurements for different neutron energies using various reactions, neutron sources, and methods of recording the comoving particles.

In this work a scintillation counter with a thin (0.1 mm) Type NE-102 plastic scintillator served as the detector of the comoving particles. Since the losses in the counting of the α particles do not distort the result and are equivalent only to a decrease in the neutron flux, as is evident from the formula given above, the peak of the amplitude distribution of the α particles was isolated and recorded with the help of a differential amplitude discriminator. The background due to protons from the D(d, p)T reaction, α particles from the (n, α) reaction, and γ-ray photons (determined by means of replacing the tritium target of the neutron generator by a deuterium one, and also by shuttering the α particles with a thin foil) was less than 0.1% [3]. The fission fragments were recorded by an ionization chamber operating in the pulse-current mode. The half-width of the coincidence peak determined with a fast-acting detector and instrumentation did not exceed 2-3 nsec.

Translated from Atomnaya Énergiya, Vol. 47, No. 6, pp. 416-418, December, 1979. Original article submitted January 24, 1979.

0038-531X/79/4706-1040$07.50

TABLE 1. Errors and Corrections in the Determination of Fission Cross Sections, %

Name of correction or error	^{235}U		^{238}U	
	correction	error	correction	error
Weighing of the target		0,75		0,75
Nonuniformity of the target		0,50	5,0	1,50
Statistics of coincidences		0,46		0,48
Random coincidences	−2,81	0,08	−1,92	0,12
Extrapolation to zero energy of the fragments	+0,59	0,04	+0,84	0,09
Frag. losses in layer	0,00	0,20	+0,27	0,20
Scattering and absorption of neutrons	+2,24	0,20	+2,28	0,20
Total error		1,1		1,8

The collection and processing of the data was carried out with CAMAC electronic instrumentation operating on line with a Robotron KRS-4200 computer [4]. The temporal distribution of α particle−fragment coincidences and the energy spectra of the fission fragments and the α particles were continuously recorded in the measurement process, and thus continuous control was exercised over the thresholds and the analog portion of the instrumentation. The program provided for interruption of the measurements and conducting a test of all the digital units of the installation every 100 min.

The topography of the neutron beam was determined with the help of a plastic scintillator 2 mm in diameter in coincidence with an α-particle detector in order that the target of fissionable material be correctly mounted and the condition noted above of a "collimated" (by virtue of the comoving particles) neutron beam striking it be guaranteed. The diameter of the collimated neutron beam containing more than 99% of the intensity was 10 mm in diameter at the surface of the target of fissionable material for a target diameter of 21 mm. Fulfillment of the indicated condition was also confirmed by the constancy of the ratio N_c/N_α over a wide range of distances between the neutron source and the fissionable-material target [3].

The fissionable-material targets were prepared from single isotopes. The contribution of other isotopes did not exceed 0.01% of the principal one. Deposition of the active layers was done by the method of high-frequency sputtering onto rotating thin (0.1 mm) substrates made out of an alloy of iron with nickel. The uniformity of the thickness of the active layer of the ^{235}U target was determined by measuring its α activity with its surface covered by a diaphragm of equal diameter. The departure from uniformity did not exceed 1%. The uniformity of the ^{238}U target was worse. The distribution of active material on the target was measured with an x-ray spectral microanalyzer with an error of 0.1%; it is symmetrical with respect to the center. The correction for the nonuniformity of the target was determined from the measured topography of the neutron beam and the profile of the active layer of the target.

The number of nuclei in the targets was determined by measurement of their α activity on the small scale. The half-life values of $(7.0381 \pm 0.0048) \cdot 10^8$ years for ^{235}U and $(4.4683 \pm 0.0024) \cdot 10^9$ years for ^{238}U obtained in [5] were used in the calculation of the number of nuclei. The mean thickness of the active layer of the targets was 256.7 and 386.3 $\mu g/cm^2$ for ^{235}U and ^{238}U, respectively. Corrections for random coincidences, the extrapolation of the spectrum of fragments to zero energy, the absorption of fragments in the active layer of the target, scattering and absorption of neutrons in the target substrates and other structural materials, and the nonuniformity of the layer of the ^{238}U target were introduced into the measurement results (Table 1).

The correction for random coincidences was determined from the temporal distribution of pulses of fragments and α particles outside the coincidence window. The correction for the absorption of fragments in the active layer of the targets was calculated with the anisotropy of the fission and the translational velocity due to a neutron pulse taken into account according to Carlson's formula and a formula derived by the authors of this paper. The results of the calculations are in good agreement. The correction for scattering and absorption of neutrons was calculated by the Monte Carlo method for the actual geometry of the experiment. The statistical

TABLE 2. Results of Fission Cross Section, Measurements b

Isotope	This paper	Data of other authors
^{235}U	2,073±0,023	2,191±0,040 (14,6 MeV) [7] 1,075±0,040 (14,6 MeV) [8] 2,063±0,039 (14,6 MeV) [9] 2,213±0,022 (14,8 MeV) [10]
^{238}U	1,194±0,022	1,149±0,025 (14,6 MeV) [9] 1,290±0,017 (14,8 MeV) [10] 1,22 (14,6 MeV) [11]

TABLE 3. Ratio of the Fission Cross Sections of ^{238}U and ^{235}U, b

This paper	Data of other authors
0,576±0,012	0,567±0,013 (14,8 MэB) [12] 0,557±0,017 (14,6 MэB) [9] 0,563±0,009 (14,6 MэB) [13] 0,574±0,006 (14,8 MэB) [14] 0,548±0,004 (14,8 MэB) [15]

error of the calculation was no worse than 0.05%. The error of the derived correction was determined mainly by the errors in the cross section values employed in the calculation. Mention was made above of the determination of the correction for target nonuniformity.

As is evident from Table 2, the values of the fission cross sections of ^{235}U are grouped about two values – 2.07 and 2.20 b, which differ with each other by 7%. The published data for ^{238}U also differ by more than 10%. One should note that the higher values for both isotopes are obtained by the method in which measurements are made relative to a standard – the cross section of neutron scattering by hydrogen [7, 10]. Absolute measurements by recording the comoving particles [9] give lower values, which are in agreement with those obtained in this paper. This fact is possibly related to the fact that this method allows effectively excluding the background of scattered neutrons uncorrelated in time, which may play an especially large role for nonthreshold elements. One should also note that the ratio of the cross sections of ^{238}U and ^{235}U obtained in this work from two independent absolute measurements is in good agreement with the value obtained directly by measurement [12, 14] (Table 3).

The authors express their gratitude to P. Reich (Debretsen, Hungarian People's Republic) for calculation of the neutron energy for the conditions of this experiment.

LITERATURE CITED

1. Rev. of Standard Reference Data and Important Cross Section Discrepancies, ANL/ND-77-1; INDC-24/6, Argonne Nat. Lab. (1977), p. 33.
2. I. D. Alkhazov et al., in: Transactions of Neutron Physics Conference [in Russian], Part 4, Izd. FÉI, Obninsk (1974), p. 13.
3. R. Arlt et al., "A fast-acting detector of comoving particles for the measurement of fission cross sections at a neutron energy of 14.8 MeV," Preprint of the Technical University No. 05-3-78, Dresden (1978).
4. V. Grimm et al., in: Transactions of the Ninth Symposium on Nuclear Electronics, Varna, 1977 [in Russian], Izd. OIYaI, Dubna (1978), p. 319.
5. A. Jaffey et al., Phys. Rev., C45, 1889 (1971).
6. G. Carlson, Nucl. Instrum. Methods, 119, 97 (1974).
7. M. Soverby and B. Patrick, Ann. Nucl. Sci. Eng., 1, 409 (1974).
8. I. Czirr and G. Dishu, Nucl. Sci. Eng., 57, 18 (1975).
9. M. Cance and G. Grenier, in: Proceedings of the NEANDC/NEACRP Specialists' Meeting on Fast Neutron Cross Sections of ^{233}U, ^{235}U, ^{238}U, and ^{239}Pu, ANL-76-90, Argonne (1976), p. 237.
10. B. Leugers et al., ibid., p. 246.
11. B. Magurno, ENDF/B IV Cross Section Measurement Standards, BNL-NCS-50464 (1975).
12. S. Cierjacks et al., [9], p. 94.

13. J. Behrens, G. Carlson, and R. Bauer, The Lawrence Livermore Laboratory Evaluated Data Library, Report UCRL-76219 (1975).
14. F. Difilippo et al., [9], p. 114.
15. M. Coates, D. Ganther, and N. Pattenden, in: Proceedings of the Conference "Nuclear Cross Sections and Technology," Vol. 1, Washington, D. C., 3-7 March 1975, p. 262.

EXPERIMENTAL BASIS FOR SIMULATION OF RADIATION ENCOUNTERED IN SPACE FLIGHTS

E. I. Vorob'ev, E. E. Kovalev,
V. A. Sakovich, A. N. Serbinov,
O. D. Brill', B. S. Gribov,
and Yu. I. Zaborovskii

UDC 577.3:539.12.04

A specific problem to be resolved in space flights is that of ensuring radiation safety in connection with the effect of cosmic rays as well as nuclear radiation from on-board installations.

This problem encompasses the following main problems:

establishing standards for the level of radiation with account for the formation of a tissue dose from cosmic rays and the characteristic features of their biological effect;

creation of minimum-mass shielding for a space ship against all forms of radiation, including the use of equipment and the structure;

development of measuring methods and measurement of the dose of cosmic rays on board a space ship;

preparation and execution of additional measures during and after a flight with allowance for the actual and predicted radiation environment, up to and including the use of pharmacological protection if necessary.

The solution of these problems requires a great deal of experimental research which has hitherto been done on γ-ray irradiators, accelerators, and reactors intended for other purposes.

Research on ensuring the radiation safety of space flights is to be extended and deepened considerably by the creation of a special experimental base, a radiation-safety base including an SVV-1 reactor, a B-5 accelerator for protons and multiply charged ions with a beam-separation system, two Almaz γ-ray facilites, and three Topaz γ-ray facilites (Fig. 1). The B-5 proton–ion synchrotron [1], with a capability for stepless energy control, is designed to accelerate protons to 20-200 MeV and a quite wide range of ions to a maximum energy of 50 MeV/nucleon. The intensity of the extracted beam of protons is $2 \cdot 10^{11}$ protons/sec with a current-pulse duration of up to 20 μsec and a pulse-repetition frequency of 50 Hz. The monochromaticity of the extracted beam is $\sim 1\%$.

The accelerator is a weak-focusing synchrotron with four 0-shaped, laminated 90° magnets with a multiturn winding and four rectilinear segments with a length of 56 cm. The radius of the equilibrium orbit is 1.4 m.

The magnets, resonator, and the beam injection and extraction systems are placed inside one common vacuumtight housing, which makes it possible to give up a special vacuum chamber and to obtain an accelerator of small size and low weight (outer diameter 4.2 m, weight 22 tons).

The injector of the synchrotron is an ILU-5 radiofrequency pulsed linear accelerator with drift tubs and two accelerating gaps [2]. The resonator of the injector, with a natural frequency of 30 MHz, consists of a quarter-wavelength line shortened by the capacitance of the drift tube and is excited by a self-excited oscillator mounted directly in it. An accelerator of this kind ensures a regime for the acceleration of both protons and ions, with practically no modifications to the resonator. At the injector outlet the proton energy is 1-1.5 MeV and the ion energy is 0.5-0.7 MeV/nucleon (for $Z/A = 0.5$), the duration of pulse of accelerated particles is 1-2

Translated from Atomnaya Énergiya, Vol. 47, No. 6, pp. 418-420, December, 1979. Original article submitted March 23, 1979.

0038-531X/79/4706-1043$07.50

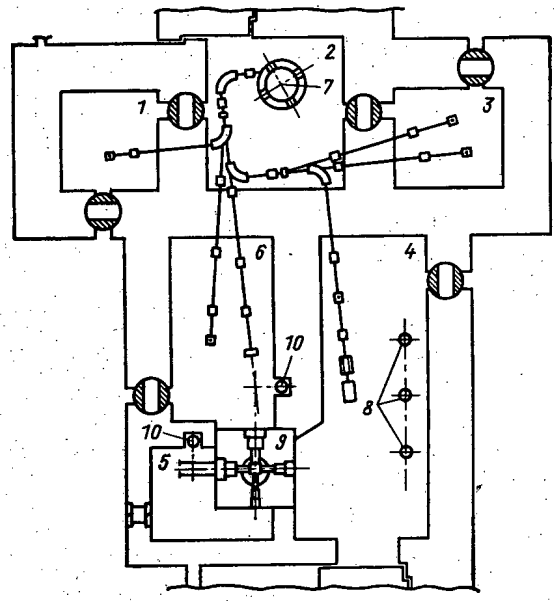

Fig. 1

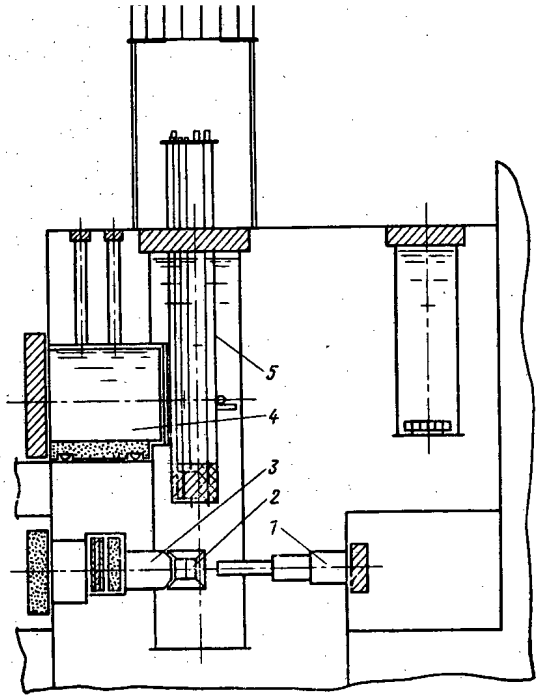

Fig. 2

Fig. 1. Layout of experimental rooms of radiation-safety base: 1-6) experimental rooms; 7) B-5 accelerator; 8) Topaz γ-ray facility; 9) SVV-1 reactor; 10) Almaz γ-ray facility.

Fig. 2. Vertical section of SVV-1 reactor: 1) horizontal three-step channel; 2) niche face; 3, 4) niches; 5) moveable support of core.

μsec, and the mean proton current is several milliamperes. The accelerator proper is housed inside a vacuum tank with a diameter of 800 and a height of about 1800 mm; an oscillator tube and magnetic-discharge pumps are mounted on it.

The proton source is the pulsed source described in [3]. An electron-beam source analogous to that considered in [4] is being developed as a source of multiply charged ions; in the source atoms are ionized by a dense electron beam less than 1 mm in diameter traversing a longitudinal magnetic field of 10 kOe, at a current of several amperes and an energy of 10 keV.

The beam of accelerated particles extracted from the synchrotron is sent by ion guides to four experimental rooms by means of four rotatable 90° magnets and 19 quadrupole lenses. Two pulsed magnets, deflecting the individual current pulses by 6° with a prescribed frequency, direct the beam into the appropriate auxiliary channels.

To monitor the passage and quality of the beam, the accelerator and in various segments of the transport system are provided with a beam-diagnostics system, including pickup stations, current pickups, and TV luminescent pickups. An automated control system based on a controlling computer complex will set the operating conditions of the accelerator and the beam-separation system, measure and monitor the physical and technical parameters of the accelerator, and will read the state of its systems and perform a number of other operations.

The SVV-1 reactor is a special 500-kW water-moderated water-cooled reactor with a vertically moveable core and a hermetically sealed vessel. The reactor core is a 50×50 cm rectangle surrounded by graphite moderator on three sides. The maximum density of the thermal-neutron flux at the center of the core is $1.4 \cdot 10^{13}$ neutrons/cm$^2 \cdot$ sec.

Displacement of the core in the vertical direction made it possible to lead the reactor radiation out into four large experimental rooms and four horizontal channels in two levels, allowing work to be done at one level while experiments are being prepared at the other level (Fig. 2).

In the bottom position (see Figs. 1 and 3) beams of radiation are led out through niche 1 into room 4, niche 2 into room 5, and niche 3 into room 3, as well as into room 3 through a horizontal three-step channel,

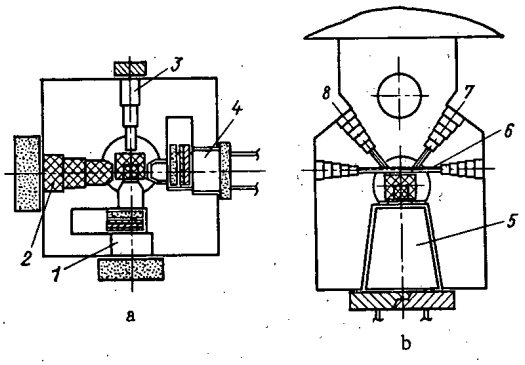

Fig. 3. Experimental equipment of reactor for top (a) and bottom (b) positions of core: 1, 2, 4, 5) niches; 3) horizontal three-step channel; 6) horizontal tangential channel; 7) horizontal channel with diameter of 10 cm; 8) horizontal channel with diameter of 15 cm.

the last step being 60 cm in diameter. The density of the flux of thermal and fast neutrons at the entrance to niche 1 is $9 \cdot 10^{12}$ and $1.3 \cdot 10^{13}$ neutrons/cm$^2 \cdot$ sec, respectively, while at the entrance to niches 2 and 3 and the horizontal channel it is $2.5 \cdot 10^{12}$ and 10^{10} neutrons/cm$^2 \cdot$ sec, respectively.

Niche 1 is intended for radiobiological research. It is a three-step niche, the last step forming a window of 150×150 cm in the reactor shielding. The fast-neutron dose rate at a distance of 50 cm from the niche reaches 1.5 rad/sec. The niche is provided with a valve-filter which enables the contribution of γ rays to the dose to be reduced to 5-10%.

The three-step niche 2 is a thermal column whose last step forms a 120×120 cm window in the reactor shielding. The thermal-neutron flux at the exit from the niches is 10^8 neutrons/cm$^2 \cdot$ sec.

Niche 3 is used to irradiate materials and equipment which are to be placed inside the niche on a special rolling trolley. It is equipped with a valve-filter similar to that set up in niche 1.

With the core in the top position (see Figs. 2 and 3), a wide beam of radiation is led out through niche 4 into room 5. This niche is intended for research on models of shielding and constitutes a trapezoid with 200-cm base on the side of the core and a 300-cm base at the other end; the height of the niche is 300 cm. The niche is equipped with a retractable tank. For carrying out experiments there is a collimated neutron detector which is suspended rigidly from a special bridge crane and by remote control is placed at a given point in room 5 in the horizontal plane passing through the center of the beam of radiation, with this plane rotated through a given angle. At this upper level there is a tangential through channel of diameter 10 cm and two experimental channels of diameter 10 and 15 cm, leading out narrow beams of radiation to the reactor reflectors in room 5.

The Almaz apparatuses set up in rooms 4 and 6 are linear irradiators consisting of 18 ^{137}Cs sources with a total equivalent of 1080 g-eq Ra and which can be brought out from behind the shielding by remote control. These apparatuses make it possible to produce a maximum dose rate of up to 1 rad/sec at a distance of 150 cm from the irradiator, with an inhomogeneity of no more than 20% in the dose rate over a 150×150 cm square cut out in the vertical plane.

The Topaz facility in room 5 consists of pits measuring 12 m in depth and 0.5 m in diameter, reach with a moving carriage holding a ^{137}Cs or a ^{60}Co source with an activity of up to 200 g-eq Ra. This design allows vertical beams of γ rays to be formed with various spreading angles. For experiments on the Topaz facilities there is a collimated γ-ray detector which is suspended from a coordinate system on the wall. The coordinate system permits the detector to be placed by remote control at any point in a vertical plane passing through the axes of the beams of the Topaz facility, with rotation of this plane through a given angle.

Thus, in room 4 biological objects can be irradiated simultaneously with γ rays, neutrons, protons, or multiply charged ions in a desired proportion and in a given time regime. In room 6 materials and equipment can also be irradiated in various regimes and with various ratios of neutron and γ-ray doses. The shielding of all the rooms is such that preparations for experiments can be made in them while beams are fed into other rooms.

As a whole, the experimental base being set up will make it possible to carry out a wide range of investigations on ensuring the radiation safety of space flights, from basic research on radiobiology and physics of shielding to full-scale tests of space ships using time regimes and radiation spectra which simulate space flight conditions.

LITERATURE CITED

1. V. G. Abdul'manov et al., Proceedings of the Tenth International Conference on High-Energy Charged-Particle Accelerators [in Russian], Serpukhov (1977).
2. V. G. Abdul'manov et al., IYaF Preprint, Novosibirsk (1978).
3. V. L. Auslender, V. N. Lazarev, and A. D. Panfilov, IYaF Preprint, Novosibirsk (1978).
4. E. D. Donets and A. I. Pikin, Zh. Tekh. Fiz., 45, No. 11, 2373 (1975).

IRRADIATION DOSE OF THE POPULATION OF THE SOVIET UNION FROM COSMIC RADIATION

R. A. Filov and É. M. Krisyuk

UDC 614.876+612.0.14.482.5

At present the International Commisssion on Radiological Protection takes into account in their recommendations the nonthreshold linear dependence of irradiation aftereffects on dose [1]. In this connection the necessity is emphasized of evaluating the contribution of all sources and all types of human activity to the cumulative radiation dose of a population. Cosmic radiation makes an appreciable contribution (tens of percent) to the radiation dose of the population. The strength of the cosmic radiation dose depends on altitude above sea level and on the geographical latitude of the locality. An estimate of the annual strength of the dose at sea level for the middle latitudes (30.1 mrem/yr) has been given in a lecture of the UN Scientific Committee on the Action of Atomic Radiation (SCAAR) [2]. The radiation dose of the population of individual states and the country as a whole due to cosmic radiation has been calculated in [3] for the USA. Calculations for the population of the USSR have been performed by us.

The dependence of the dose strength on altitude above sea level and on geographical latitude has been taken from [4], whose results have been corrected so that the dose strength at sea level and 45° N. latitude corresponds to the SCAAR estimate. A linear dependence of dose strength on latitude has been assumed. The calculation is performed for all regions, territories, and autonomous republics of the Soviet Union. It was assumed that the radiation rose of all the inhabitants of a region (territory, autonomous republic of the Soviet Union) is equal to the radiation dose of the population of the region center. The altitude above sea level of the region centers was determined with an error of 50-100 m. The population figures of the regions were taken from the data of 1 January 1977 [5]. Below are presented the average radiation doses in mrem/yr of the population of allied republics and the country as a whole due to cosmic radiation calculated with the population distribution over the regions taken into account:

RSFSR	31.7
Ukraine	31.4
Belorussia	32.0
Uzbek	32.4
Kazakh	32.9
Georgia	32.6
Azerbaijan	30.3
Lithuania	31.2
Moldavia	30.8
Latvia	31.2
Kirghiz	40.9
Tajik	34.1
Armenia	38.0
Turkmen	30.6
Estonia	31.4
Average over the USSR	31.9

It is evident that the radiation dose of the population of the allied republics differs little from the average dose for the country. A greater difference is observed for the inhabitants of the individual regions: the

Translated from Atomnaya Énergiya, Vol. 47, No. 6, pp. 420-421, December, 1979. Original article submitted April 23, 1979.

0038-531X/79/4706-1046$07.50

TABLE 1. Interstory Ceilings

Building	Type of ceiling	Thickness of ceilings, g/cm²
Few-story wooden houses	Contemporary construction	13
Old stone houses without remodeling	Sheathed with sheet material	25
after remodeling	Wooden with various dead spaces	25
Reinforced concrete	Wooden or made out of lightened reinforced concrete	40

TABLE 2. Relative Dose of Cosmic Radiation in Buildings of Different Types and Number of Stories*

Number of stories	Wooden houses	Old stone houses	Contemporary houses
1	0,965	0,92	0,86
2	0,94	0,88	0,80
3	0,91	0,84	0,76
4	0,81	0,81	0,72
5		0,78	0,69
6		0,75	0,66
7		0,72	0,64
8			0,625
9			0,61
10			0,595
11			0,58
12			0,565
13			0,555
14			0,54

*The outdoor dose is taken as unity.

population of the Naryn region of the Kirghiz SSR (75.5 mrem/yr) and the Gorno-Badakhshan autonomous region of the Tajik SSR (73.9 mrem/yr) obtain the largest dose, and the population of the Krasnovodsk region of the Turkmen SSR (29.8 mrem/yr) received the smallest. The main error in these estimates is related to equating the radiation dose of the population of a region to the radiation dose of the population of the region center. Taking into account the distribution with altitude above sea level of the population of a region permits refining the estimate of the radiation dose.

One should emphasize that our estimate, just as all the published estimates, has been made without taking account of the shielding of cosmic radiation by the ceilings of buildings. The characteristics of the interstory ceilings of the most widespread types of buildings are given in Table 1 [6]. Taking these characteristics into account and using data on the attenuation of cosmic radiation upon passage through barriers of different thickness and composition [7], the average values of the cosmic radiation screening coefficients by interstory ceilings were calculated; a uniform distribution of inhabitants on the floors of a given building was assumed in the calculation (Table 2). The shielding of cosmic radiaton by interstory ceilings significantly lowers the radiation dose, especially in contemporary multistory buildings. In order to take account of the cosmic radiation shielding effect on the average radiation doses of the population, it is necessary to know how the population is distributed in buildings of different kinds and size. Obtaining this data for the country as a whole offers a definite difficulty.

LITERATURE CITED

1. Radiation Protection [Russian translation], Recommendations of the International Committee on Radiological Protection, Publication No. 26, Atomizdat, Moscow (1978).
2. Sources and Action of Ionizing Radiation, SCAAR Lecture, Vol. 1, UN Press, New York (1977).
3. A. Klement et al., Estimates of Ionizing Radiation Doses in the United States 1960-2000, Report of Special Studies Group, ORP/CGD-72-1, Rockville (1972).
4. H. O'Brien and J. McLoyghlin, Health Phys., 22, 225 (1972).

5. USSR. Administrative-Territorial Division of the Allied Republics [in Russian], Moscow (1977).
6. H. Schindler, Z. Phys., 72, 625 (1931).
7. A. I. Lysova, Reconstruction of Buildings [in Russian], Izd. LISI, Leningrad (1976).

OBITUARY

IN MEMORY OF ALEKSEI PETROVICH ZEFIROV

On September 8, 1979, Professor Aleksei Petrovich Zefirov, Doctor of Engineering Sciences, Corresponding Member of the USSR Academy of Sciences, Laureate of the Lenin and State Prizes of the USSR, large-scale organizer of science and engineering, and prominent Soviet scientist in the area of the metallurgy and technology of nonferrous and rare metals, passed away in his 73rd year.

A. P. Zefirov was one of those who was instrumental in the creation of our domestic industrial technology of radioactive elements. Under his direction a large group of scientists was formed and worked fruitfully, having solves the most important problems of nonferrous and rare-earth metallurgy and the metallurgy of radioactive elements.

Aleksei Petrovich possessed a resourceful scientific and engineering outlook not only in the area of metallurgy but also in neighboring fields of science and engineering: mining, ore enrichment, and economics. He was widely known to the scientific community. A. P. Zefirov was a member of the editorial board of the journal Atomnaya Énergiya, and he participated in the work of many international congresses, conferences, and symposia on the problems of nuclear energy and the technology of radioactive elements. He wrote more than 200 scientific papers during the more-than-50-year period of his activity.

A. P. Zefirov worked hard and fruitfully, combining his organizational and scientific work with his teaching activity. From 1955 to 1958 he was assistant head of the Department of Metallurgy and Metallography of the Moscow Engineering Science Institute, and from 1958 to 1961 he headed the faculty at the Moscow Chemical Engineering Institute. A large number of dissertations was completed and successfully defended under the direction of Aleksei Petrovich. He worked tirelessly for young students and always assumed this to be his duty as a citizen, communist, and scientist.

Aleksei Petrovich performed a lot of public service, and he was selected as a deputy of the Moscow Council and a member of the Proletariat Bureau of the Republic Committee of the Communist Party of the Soviet Union.

Translated from Atomnaya Énergiya, Vol. 47, No. 6, p. 423, December, 1979.

0038-531X/79/4706-1049$07.50

The merits of A. P. Zefirov were highly valued: he was rewarded with two Orders of Lenin, the Orders of the October Revolution, three Orders of the Labor Red Banner, and six medals.

His integrity, sincerity, kindness, and constant readiness to help his comrades and colleagues in their lives and creative activity won the love of all who knew him. The shining memory of this remarkable scientist and person will always be preserved in the hearts of those who had the opportunity of associating and working with him.

AUTOMATIC SYSTEM FOR REACTOR MONITORING, CONTROL, AND SAFETY

P. A. Gavrilov and V. E. Trekhov

The regular branch seminar in the series "Engineering and economic aspects of nuclear power" was held at the NIKIÉT in June, 1979. On the agenda were problems associated with the safe operation of high-power reactors (RBMK-100 and -1500 and VVÉR): improvement of the systems of in-reactor monitoring, local adjustment of the energy-distribution field, functional-group control, ways and means of scram protection, the dynamics of complex unsteady transient processes, the use of computers, and ergonomic problems.

In addition to NIKIÉT workers, the seminar was participated in by representatives of 17 scientific-research, planning, and design organizations.

It was pointed out at the seminar that in the control of present-day large reactors there was a need of auxiliary control and safety loops realizable on present-day commercial controlling machines (e.g., computers of the SM class). In turn, the use of computers in the control loops gives rise to new problems. In comparison with known problems of the automation of power plants to control nuclear installations, that of safety is the most important. And equal attention should be paid to the development of apparatus of the computer control system as well as software. Extensive capabilities for the creation of reliable, efficient reactor-control systems with allowance for the specific safety requirements have been designed into the computer equipment produced by Soviet industry; this equipment constitutes modular systems whose composition can be varied according to the objectives and purposes of the control. The seminar was informed about work done by the NIKIÉT in collaboration with the State All-Union Central Scientific-Research Institute of Comprehensive Automatic Control (TsNIIKA) on the development of multilevel control and safety systems, with redundancy, based on SM computers for atomic power plants with RBMK-1500 reactors. The creation of such systems is inseparable from the development of software. In turn, designing algorithms and programs requires the latest methods for the investigation and optimization of systems, i.e., simulation and graphic analysis. Work done by NIKIÉT in this area was reported.

Of great importance for work on an automated monitoring and control system is the experience on the design and operation of digital systems (information level and "operator counselor" level) gained during creation of the SKALA systems for atomic power plants with RBMK-1000 reactors. These systems have already been tested on six operational power units (Leningrad, Kursk, and Chernobyl'sk atomic power plants).

Great interest was aroused by a communication by specialists from the NIKIÉT on the results of successful testing of a system for local automatic adjustment of the field of energy distribution in the first unit of the Leningrad plant and on the distinctive features of the apparatus of the control and safety system and for monitoring the energy distribution in the RMBK-1000. As for the RBMK-1000 and -1500 reactors, there was a discussion on the use of the "asymmetry principle" in the synthesis of a system for the stabilization of the energy-distribution field of a large reactor and there was also discussion of work done at the NIKIÉT on the construction of zonally asymmetric controllers.

No mean role is played by improvements and experience in the development of in-reactor detectors for the RBMK reactor as well as by the state of the art of reactor thermometry, which were discussed at the seminar.

Ergonomic problems associated with reactor control were taken up in papers on the role of the operator in the control system, on the algorithmization of the functions of the operator, and on improvement of methods and means of presenting information during control of power units.

The seminar considered special problems of monitoring, regulation, functional-group control, metrology, the structure of the apparatus of control and safety systems, materials science, and analysis of transient processes.

The papers aroused lively discussion.

Translated from Atomnaya Énergiya, Vol. 47, No. 6, p. 424, December, 1979.

0038-531X/79/4706-1051$07.50

MEETING OF IAEA TECHNICAL COMMITTEE ON HANDLING OF TRITIUM-CONTAINING WASTES

B. Ya. Galkin and V. V. Tugolukov

The meeting was held in Vienna, Austria, in December, 1978, with the participation of representatives from nine countries as well as Euratom.

The meeting considered sources producing tritium and its content in various flows and products, methods of eliminating it from gas and liquid flows, ways of preparing it for storage and disposal with fixation in various materials, international cooperation, etc.

The communications and discussions served as a basis for a draft of a document which will be published by IAEA as an official document. In the introduction to the document an analysis is made of the state of the art in various countries and recommendations concerning handling are presented. The next section discusses sources of tritium production, presents figures on tritium build-up in Ci/GW(E) per year in reactors of various types, estimates discharge in the form of gas–air and liquid wastes, and shows the distribution of tritium in the flow-sheet of regeneration of spent thermal-reactor fuel.

The technique for removal of tritium is considered as applied to the technology for the regeneration of oxide fuel. Three possible methods are singled out: by driving off from the pulverized fuel before dissolution; isotopic enrichment in water flows; water recycling with final removal of part of the flow and solidification. With oxidation treatment of the fuel (450-650°C) more than 99% of the tritium and the bulk of the ^{85}Kr, ^{140}Xe, ^{14}C, and ^{129}I can be separated and concentrated in a small volume. Tritium in the form of tritiated water can be retained in solid sorbents.

Multistage electrolysis for enrichment of water with tritium is uneconomical because of the energy consumption. A more economical method is based on a combination of electrolysis with catalytic exchange and is recommended for the removal of tritium from H_2O and D_2O, i.e., for fuel-regeneration facilities and for atomic power plants with D_2O moderator. Thus far, however, it has been demonstrated only in pilot plants with a low tritium content. The process is based on the use of hydrophobic catalysts.

In Canada, a small demonstration plant is being planned with a more complex technology, i.e., electrolysis with catalytic exchange and cryogenic distillation. Recycling of water and nitric acid as a means of retaining tritium in the flowsheet of a regeneration plant is attracting considerable attention. Research done in the U.S., France, and Britain on the distribution of tritium in the flows in these plants shows that it is possible to organize the recycling so that tritium present in aqueous solutions will be localized in that part of the flowsheet which includes washing of the extract from the first cycle.

Among other methods of removing tritium from H_2O and D_2O water flows still under study mention should be made of isotopic enrichment with laser excitation, diffusion through metallic membranes, thermodiffusion, and gas chromatography.

Subsequent sections consider the possibility of using process flowsheets of treatment of tritium-contaminated materials in order to convert the tritium into a form suitable for storage or burial with a view to reducing the probability of it being spread. An effective method of fixation is that of producing tritiated metallic (titanium, zirconium, hafnium, and thorium) hydrides which makes it possible to convert the tritium from the gaseous phase into the solid phase. Another method of localization can be that of catalytic hydration of styrene. Nickel in kieselguhr or rhodium in aluminum oxide serves as the catalyst. The tritium leaching rate is insignificant. Thermal decomposition and depolymerization occur at temperatures greater than 280°C. This process is in the early stages of development.

Liquid wastes containing tritium can be prepared for storage by several methods. They include adsorption on dry materials such as cement, and chemical incorporation into organic polymers. Silica gel, zeolites, activated aluminum oxide, and potassium sulfate are recommended as adsorption materials.

Translated from Atomnaya Énergiya, Vol. 47, No. 6, pp. 424-425, December, 1979.

0038-531X/79/4706-1052$07.50

At the present time, cement with a high capacity for water, ranging from 25% (Portland cement) to 50% (high-alumina cement), is most frequently used for fixation of tritiated water. The principal drawback of cements is that of a high leaching rate. To reduce this rate, studies have been made of the possibility of coating cements with bitumens, greases, paraffins, enamels, and various organic polymers. In this case the leaching rate is reduced by decreasing the effective surface area in contact with water. Irrespective of the material used, before burial the wastes should be enclosed in appropriate containers. The section on monitoring points out that considerable experience has been accumulated on tritium detection and appropriate instruments have been built.

In conclusion, the participants in the meeting emphasized that in most countries the practice in handling tritium-containing wastes is inadequate and international cooperation in this field is necessary. As shown by consideration of the economic aspects, the information available at present does not ensure the selection of an economical method of tritium disposal.

The good organization of the meeting and the discussion made it possible in a short time to consider diverse subjects and to map out a program of work for coming years.

SIXTH SESSION OF SOVIET–AMERICAN COORDINATION COMMISSION ON THERMONUCLEAR ENERGY

G. A. Eliseev

The session was held in Washington, D.C., on July 2 and 3, 1979. It considered the results of collaboration in 1978 and the implementation of the controlled fusion program in 1979 and approved the program for 1980. Representatives of both countries reported the successful realization of the 1978 program which had been facilitated in many ways by five years of experience from joint research on the controlled thermonuclear reaction, the strengthened links between the teams of U.S. and Soviet thermonuclear centers, and the atmosphere of mutual confidence and respect. The proceedings of the session noted the nutual benefit flowing from the projects undertaken and the successful implementation of the 1979 program.

Reports on the results of thermonuclear research in the Soviet Union and the United States in 1979 and on plans for further development of this research were presented by the co-chairmen of the coordination commission, E. P. Velikhov and E. Klinter, as well as by the heads of Soviet and U.S. research institutes working on controlled fusion.

The 1980 program approved at the session provides for 25 joint projects in three main areas: experimental and theoretical studies on systems with magnetic confinement of plasma, the design and testing of elements of demonstration thermonuclear reactors, and engineering problems of controlled fusion. Provision was made for the participation of Soviet and American specialists in experiments on the principal thermonuclear facilites and stands of both countries, including the beginning of long-term joint work on the Doublet III tokamak of the General Atomic Co. with the use of the Soviet multichannel fast-atom analyzer. Joint theoretical and design studies on the stability of plasma with reactor parameters as well as calculations on superconducting magnetic systems for thermonuclear machines of the next generation. Studies will continue on the interaction of high-temperature plasma with walls and so will research on the volume and surface radiation damage to materials under conditions imitating reactor conditions. The next, fourth seminar on hybrid reactors (fusion–fission systems) will be held in the Soviet Union.

Under the conditions of the growing energy crisis, the U.S. Department of Energy has recently begun to devote its major attention to "current problems." Appropriations for long-term projects have recently been reviewed and cut. The thermonuclear program has not been changed, a major reason for this being the favorable attitude taken by the U.S. Congress towards thermonuclear power. In the budget for the 1980 fiscal year, appropriations for controlled fusion research run to 513 million dollars (including 364 million for systems with magnetic confinement of plasma). In the 1981 fiscal year these appropriations are to be increased by another 10%. The fusion program has been reinforced considerably by the successes achieved in thermonuclear studies.

Translated from Atomyaya Énergiya, Vol. 47, No. 6, pp. 425-426, December, 1979.

0038-531X/79/4706-1053$07.50

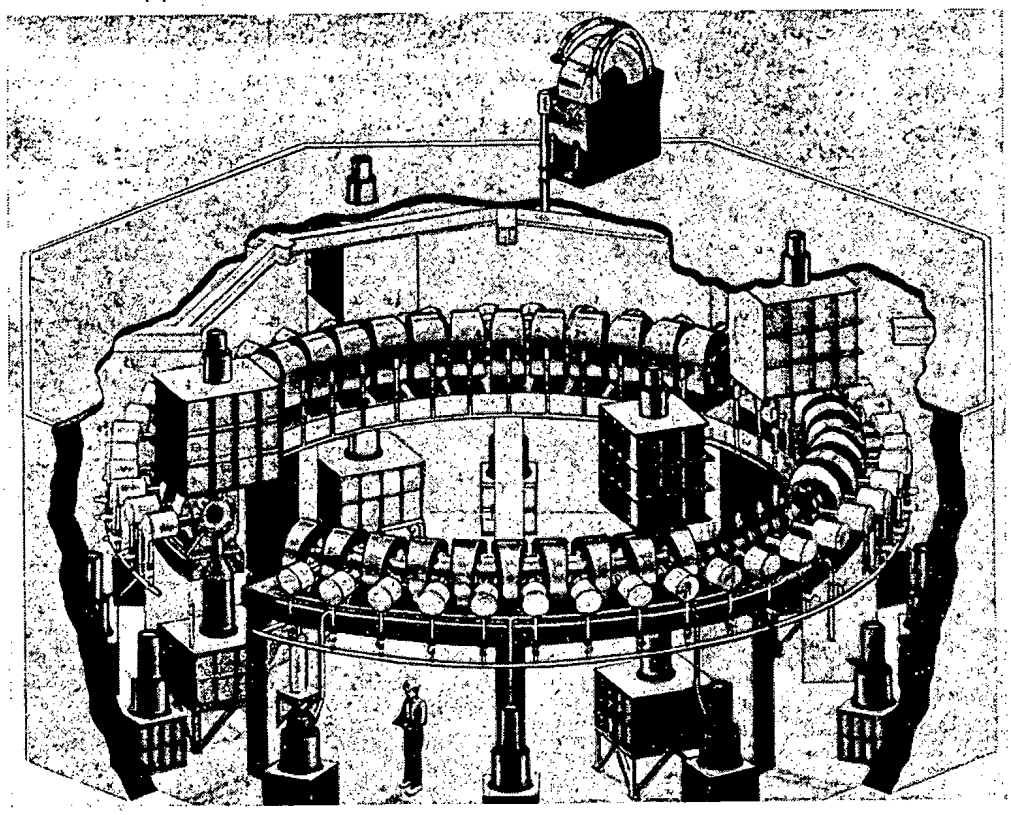

Fig. 1. General view of one variant of an EBT-R thermonuclear installation.

Of these successes, mention should be made primarily of the heating of plasma to 6 keV in the PLT tokamak, the attainment of a stable discharge with $\beta_{max} \sim 10\%$ in the ISX-B tokamak, and attainment of the design parameters in the world's largest tokamak, Doublet III.

In 1979, the U.S. thermonuclear program was analyzed in detail by a Department of Energy commission, headed by J. Foster. On the basis of the recommendations of this commission, significant changes have been made in the program. In particular, it has been decided to expand the basic research on the physics of high-temperature plasma. Work is being extended in some technological areas and, in particular, on the development of special materials and alloys that would be promising for future thermonuclear reactors. Much attention will be paid to the development and experimental testing of alternative thermonuclear systems, among which the EBT (ELMO BAMPY TORUS) system has been advanced to the forefront. This system has been under study for several years now at the Oak Ridge National Laboratory. It constitutes a set of traps with magnetic plugs, connected into a torus. For the purpose of stable plasma confinement, in each of the traps microwaves set up quasirelativistic electron rings, resulting in the formation of a potential well in the paraxial zone for ion confinement. The system functions without a longitudinal current in the plasma, which makes it attractive in the plan for the creation of a steady-state thermonuclear reactor. A stable plasma with a density of $\sim 10^{12}$ cm^{-3} and an electron an ion temperature of 400 and 200 eV, respectively, has been obtained in the small EBT-S device (major radius of torus 1.5 m, minor radius 18.8 cm, longitudinal magnetic field in region of plugs 1.3 T). Notwithstanding the fact that the results do not yet permit a sufficiently reliable estimate to be made of the capabilities of the system in operation with plasma having a substantially higher density and temperature, an EBT experiment on a prereactor scale, i.e., the EBT-R, is being planned in the U.S.A. A competition is being held for designs and Grumman, Ebasco, and McDonnell Douglas are taking part. The deadline for the competition is May 1980.

The next big step envisaged in the long-range U.S. program discussed here is the ETF engineering test thermonuclear reactor. The principal purpose of this facility is to solve general engineering problems of controlled thermonuclear fusion and to create a technological basis for the first thermonuclear power reactors. Concepts of ETF on the basis of a tokamak (Oak Ridge National Laboratory) as well as on the basis of an open magnetic trap (Lawrence Livermore Laboratory) are being worked out at the present time. The decision concerning the construction of the ETF is to be taken in 1984 with account for results which will be obtained on the TFTR tokamak and the MFTF open trap. It should be noted that in respect of the basic parameters the EFT tokamak is extremely close to the INTOR.

SOVIET – AMERICAN MEETING ON ALTERNATIVE THERMONUCLEAR SYSTEMS

E. E. Yushmanov

The meeting, held at the I. V. Kurchatov Institute of Atomic Energy in June 1979, discussed the most promising Soviet and American systems with magnetic confinement of plasma, not like traditional systems. All told, there were 14 papers, 8 Soviet and 6 American. The Soviet delegates presented papers on studies done at the I. V. Kurchatov Institute of Atomic Energy, the Institute of High Temperatures of the Academy of Sciences of the USSR (IVTAN), the Kharkov Physicotechnical Institute of the Academy of Sciences of the Ukrainian SSR (KhFTI), and the Sukhumi Physicotechnical Institute. The American researchers represented the Lawrence Livermore Laboratory, the Plasma Physics Laboratory of Princeton University, the Oak Ridge National Laboratory, the Los Alamos Scientific Laboratory, and the TRW Co.

The principal areas of the present thermonuclear program – tokamaks, open traps, lasers, and high-power corpuscular beams – will, at first glance, undoubtedly resolve the problem of controlled thermonuclear fusion in the near future. First, however, the possibility of any of these programs failing in actual fact is not excluded and, second, even in the event of success work on the search for more successfully solutions can be continued. Alternative programs serve to support the basic programs and further the search for possible other, better solutions, and also ensure healthy competition of ideas, preventing the basic programs from losing creative activity.

One of the main areas of research has been that of experiments with compact toroidal plasma, first performed at the I. V. Kurchatov Institute of Atomic Energy and then repeated at the Los Alamos Laboratory (where this system has been dubbed PFX). In experiments with devices of the theta-pinch type a compact plasma toroid is formed with an embedded poloidal field which ensures thermal insulation. The advantages are unquestionable: small dimensions, high β value, and technical simplicity. The main problem today is that of the stability of the toroid. Theory has thus far not provided a reliable answer and the results of experiments are not unambiguous: in the American experiments the toroid became unstable with time while in the Soviet experiments this did not occur in some cases. But in one way or another experiments employing the principle of a compact toroidal plasma have aroused considerable interest and plans are being made in the United States for research on a considerably larger scale.

Two Soviet papers described a trap with a spatial axis, i.e., a helical torus. In such a system a rotational transformation is produced without the assistance of current or special windings. Among its advantages (in comparison with the tokamak) are better confinement, a higher β value, better stability, steadiness, etc. The complex configuration of the magnetic system, however, makes it difficult to realize from the engineering and technical point of view.

An interesting alternative area is that of the magnetoelectrostatic trap which is being studied at the I. V. Kurchatov Institute of Atomic Energy and the KhFTI. It constitutes an acute-angled system in which the escape of plasma through "gaps" is blocked by electrostatic fields. Advantages of the trap are quite good confinement ($Q \geq 10$), absence of magnetic field in the volume occupied by the plasma, steadiness, and simplicity of heating. At the same time, however, it is necessary that, first, the transitional layer between the plasma and the magnetic field be stable, and, second, electrons trapped in the gaps should leave those gaps continually. Questions as to whether these problems can be solved remain open. The Atoll machine, the most advanced systems of this kind, has now been built at the Kurchatov Institute. Plasma stability will be the object of study in forthcoming experiments.

Other Soviet papers were devoted to the new aspects of the use of an imploding liner, a new configuration of the plasma focus, and a torsatron with a divertor.

In addition to the aforementioned PFX system, the Soviet papers discussed the results of the RFM experiment with field reversal in a mirror trap as well as the RFP experiment with toroidal pinch and field reversal

Translated from Atomnaya Énergiya, Vol. 47, No. 6, pp. 427-428, December, 1979.

0038-531X/79/4706-1055 $07.50

and the EBT bumpy torus. The RFM experiment came into being at the Livermore Laboratory several years ago as a variant of the open-trap program. It would be more correctly looked upon now as a highly promising independent area since the physics of this system is completely different from that of open traps. It is proposed to use this system to produce a plasma toroid with reversed field (similar to compact toroidal plasma) in which the high temperature of the plasma as well as the poloidal field are maintained by a powerful injection of fast atoms. This plasma formation is confined in a steady-state condition in an open trap. Combination of such cells into a long multimodular reactor is being considered. Another variant of reactor is a long solenoid with a continuous sequence of plasma toroids moving along it. Each of the plasma rings lives and "burns" only during the flight while the poloidal field is sustained by self-induction. In this case it is not necessary to have high-power fast-atom injectors, the design of the superconducting windings is simpler, and the reactor becomes a straight tunnel composed of identical modules. The thermal conditions are steady-state. These important technological advantages along with $Q \gg 1$ make the RFM system attractive. Some physical aspects, however, are not yet clear, especially the problem of stability. Livermore Laboratory has hitherto not managed to achieve field reversal by injection since the injected flux of atoms is insufficient given the high losses in the stage when there is still no reversal. The well-known 2XIIB machine has not been rebuilt into the Beta-2 device and fast atoms will be injected into a ready toroid-target with embedded reversed field produced by a specially developed high-power coaxial plasma gun.

An important alternative line of studies is represented by the RFP system, which is under investigation not only in the Los Alamos Laboratory in the United States, but also in Britain, Italy, Japan, and Australia. It constitutes a circular plasma with a strong longitudinal current, located in a toroidal external field, and a stronger field in the opposite direction is embedded in the column. The plasma is confined primarily by the poloidal field of the current. This system is a direct extension of the philosophy of the ZETA and Alpha devices familiar from an earlier period. The advantage of the RFP over the tokamaks consists in the high β value, the high MHD stability, possibility of ohmic heating up to ignition (since there is no limitation on the current), and a high aspect ratio. Experimental results obtained thus far look modest because of the low temperature ($T_e \approx$ 15-20 eV). In the opinion of experimenters, however, this fact is not fundamental and is the result of large radiation losses. As for the general principle of confinement, it is confirmed. Several large facilities, now being built (or being developed) at the present time in various countries, will apparently make it possible to surmount the "radiation barrier." At the Los Alamos Laboratory construction is beginning of the ZT-40 device with a major radius of 114 cm and a minor radius of 20 cm which is expected to yield $n \sim 10^{14}$-10^{16} cm^{-3} at $T \sim 0.1$-1 keV and $\tau \sim 10^{-3}$ sec.

It would seem that the most popular of the American alternative lines of research is apparently that represented by EBT. The idea of this system obtained convincing experimental and theoretical substantiation. The trap constitutes a torus with a large number of bumps ($\gtrsim 20$), forming local traps with a plug ratio ~ 2. It is well known that the bump torus is devoid of toroidal drift because of the "plugotron" drift (replacing the rotational transformation) but is MHD-unstable. In the EBT stability is ensured by the fact that in the central plane of each trap electron-cyclotron resonance produces a peripheral ring of relativistic electrons enveloping the axis. The value of β in the ring is ~ 0.5. These rings so change the conditions that the main toroidal plasma is stable. Only neoclassical transfer is a source of losses. The β value for toroidal plasma may approach 0.4. A reactor based on the EBT would have many advantages in comparison with the tokamak: high β, steady-state operation, absence of alongitudinal field and the troubles associated with it, technological effectiveness of the design (in particular, because of the high aspect ratio and the simple modular design). The Q value would be high since the main toroidal plasma is in a self-sustained burning mode and the energy consumption is associated only with the maintenance of the electron rings. Present-day technology is sufficient for the construction of a reactor, apart from microwave generators but considerable advances are being made in their design.

The principal reason for the attention to the EBT, however, lies not so much in its potential advantages as in proofs obtained in recent years that its physical foundations are correct. Experiments with EBT and EBT-S at the Oak Ridge Laboratory confirmed that the system is an equilibrium system, is stable, has neoclassical transport (in accordance with the theory constructed), is well protected against contamination, and is convenient in respect of heating. Plans are being drawn up in the United States at present for the EBT II machine which will take several years to build (at a cost of about 70 million dollars). In the final stages of experiments, it is believed, this machine will make it possible to get very close to reactor conditions: $n \sim 10^{14}$ cm^{-3}, $T \sim 5$-10 keV, $\beta_{max} \sim 10\%$, $n\tau \sim 10^{14}$. Experts estimate that an experimental reactor could be built by 1990.

The participants in the meeting noted that the exchange of information carried out could be useful and that in future not only should such meetings be continued but that laboratories engaged in work on alternatives should exchange visits. There is a need for meetings with a general discussion of studies on the various alternative programs (similar to the meeting discussed here) as well as more restricted meetings on individual subjects. Such meetings are necessary since no single country is in a position to bear the growing costs in various areas and only exchange and mutual criticism can make up for this. The American researchers came out in favor of convening an international conference in the near future.

SOVIET–AMERICAN MEETING ON "PROBLEMS OF THE INTERFACE BETWEEN HIGH-TEMPERATURE PLASMA AND LIMITER"

V. A. Abramov

The meeting was held at the I. V. Kurchatov Institute of Atomic Energy in June, 1979. The Soviet delegation consisted of workers from Soviet scientific centers engaged in research on controlled thermonuclear fusion. The American researchers represented the major plasma physics laboratories. Physicists from the German Democratic Republic who are taking part in experiments on T-10 also attended.

The meeting considered the experimental results of studies on the interaction of high-temperature plasma with the wall and limiter, the mechanisms by which impurities are formed and enter plasma, theoretical and experimental investigations on divertor layers, and requirements on materials for the first wall, limiter, and inverter plats from the point of view of the tokamak reactor. Most of these topics were dealt with in 23 papers read at the meeting.

A U.S. paper on studies on impurities in the ISX-A device pointed out that there is no problem (of the type of a temperature minimum occurring at the center of the plasma column) associated with heavy impurities. Experimental results obtained with Auger spectroscopy indicate the wide range of masses of the structural materials which can be sputtered by plasma. Since problems with the elimination of hydrogen from titanium sputtered onto the walls were encountered in this device, only gas-discharge purification without gettering of the walls is employed in the ISX-B. The latest experiments on heating the plasma by beams of fast yielded $\bar{\beta}_T = 1.3\%$ and $\beta_T(0) = 4.4\%$ (without the contribution of the beam). With an injection power of 1 MW it was possible to raise $\beta_T(0)$ to 7%.

A joint paper by researchers of the Soviet Union and the German Democratic Republic dealt with Auger-spectroscopic studies on impurities in the T-10 tokamak. As shown by the studies, in a discharge specimens of materials have atoms of the structural materials of the diaphragm and chamber wall, i.e., Fe, Ni, and Cr, as well as O, C, Cl, and Zn. Another U.S. paper on this subject gave values obtained by Auger spectroscopy for the impurity density in the diaphragm in the ALCATOR tokamak: $n_0 + n_N \geqslant 0.1\%$, $n_{Mo} \sim 0.01\%$, $n_{Fe} \sim 0.005\%$. Gas-discharge purification of the walls is now employed in the machine ($p = 8 \cdot 10^{-2}$ Pa hydrogen, $f = 2$ kHz, $W = 1$ kW, discharge duration 10 msec at 2 Hz, longitudinal field 10^3 G). The main conclusion arrived at by the authors of the Soviet paper on various methods of chamber purification was that flow discharge is an extremely convenient and effective method.

One U.S. paper considered the effect that the evolution of the current profile has on the plasma–wall interaction. Although many details of the study remain unclear, the possibility of controlling the entry of impurities into plasma is extremely interesting and useful in the adjustment of new systems.

Some of the papers were devoted to the theoretical and experimental study of diverter systems. In a paper, researchers from the Kurchatov Institute presented results of calculations of the magnetic configuration of the bundle-diverter of a special design making it possible to reduce the current in the diverter windings. At the same time, however, the bumpiness of the toroidal field increases in the vicinity and this may result in additional loss of heat and particles. As shown by estimates, the losses may be small because of the radial electric field. Another paper by researchers from the Kurchatov Institute reported on the results of experi-

Translated from Atomnaya Énergiya, Vol. 47, No. 6, pp. 428-429, December, 1979.

0038-531X/79/4706-1057$07.50

mental studies of the stability of the magnetic configuration by a poloidal divertor with two zero points. The stability region found by the authors apparently is the consequence of the concrete relation between the increment in instability and the duration of the discharge. In a paper, workers of the Institute of High Temperatures of the Academy of Sciences of the USSR (IVTAN) considered the dynamics of particles in a divertor layer in the case of strong circulation. It was found that the temperature of the plasma in the divertor layer could decrease appreciably because of intensification of circulation. A paper from the Kurchatov Institute on the possible use of a stream of incident microshells on the plasma boundary as a diaphragm showed that such a method permits a reduction in the average thermal load on the diaphragm elements by an order of magnitude. Such a diaphragm can perform some of the functions of a divertor. One U.S. paper was devoted to contamination of plasma in INTOR. With the use of silicon carbide coatings on the walls, one might expect insignificant contamination of the plasma for 20-30 sec. A lively discussion was aroused by the opinion that it will be possible to do without a divertor in this device. This subject, however, requires careful theoretical and experimental substantiation.

Several papers presented by Soviet researchers were devoted to the currently intensively studied interaction of fast atoms with various materials, as applied to the problem of the first wall of thermonuclear reactors. A report was given on an experimental investigation of the mechanism of the formation of streams of atoms which could enter the plasma [Moscow Engineering Physics Institute (MIFI)] and on the study of the reflection of light and heavy ions with an energy of 3-30 keV from a stainless-steel surface; the study was carried out on the Iris machine (Kurchatov Institute). The first results were given from the study of gas liberation from zirconium hydride in the course of ion bombardment as a function of the temperature and vacuum conditions (MIFI). A study was made of the influence of the technology of surface treatment on the scattering process. An original technique was presented for determining the diffusion coefficient and the activation energy of deuterium occluded in molybdenum (MIFI).

An interesting U.S. paper gave the latest results from studies on the resistance of various materials to high specific thermal loads. The experiments were conducted with a 10-keV electron beam with a power of 180 MW/m^2. The results permit carbides of materials with a low z (e.g., TiC−C) or various types of graphite to be recommended as a material for the diaphragm. A U.S. paper on the results of studies on the properties of low-z coatings showed that a coating of TiB_2 on a graphite base is satisfactory. As a result, a design was developed for a diaphragm in which a 35-μm TiB_2 layer is deposited on a graphite substrate. A diaphragm of this kind has been installed in the ISX-B machine and one will be built in the PDX machine. Similar topics were discussed in papers by researchers from the I.V. Kurchatov Institute of Atomic Energy and the Institute of Physical Chemistry of the Academy of Sciences of the USSR (IFKh AN SSSR). In their opinion, a solution to the problem of the first wall is to produce a renewable coating of titanium sputtered onto stainless steel and to develop shields to bear the radiation and thermal loads.

The meeting considered unipolar arcs as possible sources of impurities. As shown by the discussion of results, there still some contradictions in experimental results obtained in various tokamaks and the available theory cannot explain certain effects. Further studies on this problem are, therefore, desirable.

On the whole, the work of the meeting showed that a great deal of attention is being devoted in the Soviet Union and the United States to plasma−wall interaction.

SECOND MEETING OF INTERNATIONAL WORKING GROUP ON INTOR

V. I. Pistunovich and G. E. Shatalov

The meeting took place in Vienna, Austria, in June and July, 1979. Its work was organized so that materials on the physicotechnical foundations of INTOR – prepared by the participants of the working group in their own countries – could be compared, the differences on each of the topics discussed could be established, and subjects for further investigations could be designated. Experts from Euratom, the Soviet Union, and the United States were the first to take part in discussions on some of the topics.

In order to achieve a more logical structure in the report on INTOR for the International Council on Thermonuclear Research, the aforementioned topics were grouped into more general sections: plasma, magnets and power, the blanket and tritium, engineering problems, and safety and the environment.

Much attention was devoted to the discussion of the basic parameters of INTOR, with a more detailed discussion of its technical purposes and its place in the controlled fusion program. In the tokamak program, INTOR is intermediate between the devices of the next generation (T-15, TFTR, JT-60, JET) and the demonstration power reactor (DEMO) for the generation of electricity. In view of this, it was recognized that it should be somewhat larger than an engineering–technological reactor. In accordance with the definition of INTOR as the maximum reasonable step beyond the generation of physical devices, the main objectives were formulated.

1. The operating mode should be close to that of a power reactor. This means ignition of the thermonuclear reaction in DT plasma, duration of working pulses no less than 100 sec, neutron load on first wall no less than 1 MW/m^2, and an off-duty factor of no more than 30% between working pulses.

2. The basic technological solutions appropriate for a reactor should be used in INTOR: superconductors in toroidal and poloidal coils, a divertor for ensuring a steady-state burn of the thermonuclear reaction, means of monitoring the power balance in the plasma, auxiliary heating systems, a closed tritium plasma column, a technology for maintenance by remote control, and vacuum technology.

3. INTOR should be provided with blanket modules for engineering tests on: the technology of producing and extracting tritium from the blanket, structural designs of elements, the technology of a blanket for simultaneous production of tritium and electricity, materials for radiation resistance, and solutions concerning plasma control and monitoring.

4. INTRO should demonstrate: the possibility of producing electricity in a thermonuclear reactor and breeding tritium, the capability of the thermonuclear reactor for stable and prolonged operation, and a maximum load coefficient of up to 50%.

These objectives can be carried out in three stages. The first would comprise three years of work with a load coefficient of 10-20%, at first with hydrogen plasma and then with DT plasma, along with the development of operating modes and demonstration of the production of electricity. The second stage would consist of four years of operation with a 25% load, execution of engineering tests on various blanket modules for tritium production, joint production of tritium and electricity, materials testing, as well as alternative solutions for heating and monitoring the plasma. The third stage would cover five years of operation at 50% load for testing the entire facility under conditions close to power conditions, testing the life of materials, and verifying alternative proposals for the production of a considerable quantity of tritium.

Alternative possibilities which could alter the objectives and parameter of INTOR are to be considered by the end of 1979:

increasing the production of tritium to half or all of the quantity required;

increasing the scale of electricity production to 50 MW (E) or reaching a positive electrical balance;

Translated from Atomnaya Énergiya, Vol. 47, No. 6, pp. 429-430, December, 1979.

0038-531X/79/4706-1059$07.50

increasing the specific load of the reactor and the total neutron load to 5 MW·yr/m^2.

The indicated alternative objectives bring the INTOR closer to the DEMO reactor which should produce electricity, produce enough tritium for its operation, and demonstrate the efficiency of the design as a prototype of a commercial reactor.

It is expected that INTOR will go into operation in 1990. The physical problems for DEMO can be expected to be solved by 1993, the testing of the blanket and the solution of the engineering problems of the thermonuclear reactor, which are necessary for its construction, should be completed by 1997, and materials testing, by 2002. It would thus go into operation in 2005 or later.

The meeting drew up the first (working) version of a composite report on INTOR and tables of the recommended parameters. New special questions on each topic were formulated and the answers should be prepared for the third meeting. By that time an estimate should be made of the cost of INTOR and the required human resources and construction schedule should be established.

By decision of the IAEA the work of the international working group has been extended to June 1980. It is envisaged that in 1980 the group will begin drawing up a predraft conceptual project. In the opinion of the members of the Supervisory Committee, this work can be organized through the staffs of the institutes of the participating countries without setting up a special project group.

The third meeting of the International Working Group will be held in October, 1979.

EUROPEAN CONFERENCE ON HIGH-ENERGY PHYSICS

L. I. Lapidus

The conference, which was held in Geneva, Switzerland, in June and July, 1979, was attended by more than 820 researchers. The program comprised five sections: neutrino physics, electron–positron collisions at high energies, charged leptons, hadron interactions, and problems of theory. Review papers were presented at the plenary sessions by 17 rapporteurs and 52 invited speakers.

The PETRA colliding electron–positron beam accelerator at Hamburg, Federal German Republic, reached a particle energy of 27.8 GeV in the c.m. frame of reference. In the near future this will be increased to 32 GeV. This accelerator is being used to look for a new t quark whose mass is estimated at 14-15 GeV as well as to study decays of families of v particles with a mass of ~9.5-10 GeV. Within the framework of quark–gluon concepts, v mesons are a bound state of a b quark and a $\bar{b}$ antiquark in much the same way as the family of J/ψ particles is a bound state of c quark and a $\bar{c}$ antiquark, while a φ meson is a bound state of an s quark and an $\bar{s}$ antiquark. Let us recall that a proton and a neutron are a bound state of three light quarks, u, u, d and d, d, u, respectively. The heavy quarks s, c, b have a nonzero strangeness, charm, and color. Interaction between quarks takes place through an octet of gluons. As a result of an interaction with a large momentum transfer, the presence of quarks and gluons results in the occurrence of a jet of hadrons, strongly interacting particles. The study of the decay of the v particle, possessing a "latent color," revealed decays into three jets. If it is assumed that jets are caused by gluons (nonunique interpretation), then they have a spin of 1, as was expected theoretically. An intensive search is being made for the t quark but at the time of the conference the search has not been successful.

In a pion beam with an energy of 150-176 GeV in CERN reseachers found a narrow resonance in the system $J/\psi - K - \pi$. This points to the existence of particles with a mass of about 5.3 GeV with explicit charm. Such a particle can be formed as the result of the decay of new particles with the quark structure $(\bar{b}u)^-$ and $(\bar{b}d)^0$. At Stanford, California, researchers are studying the spectroscopy of the family of J/ψ particles on the PEP colliding electron–positron beams. In the latest experiments, use has been made of a new, highly effective technique, i.e., a γ-ray detector which consists of a large number of counters incorporating sodium iodate crystals (crystalline sphere). As a result, a new picture of levels of charmonium, a bound system of c and $\bar{c}$ quarks, has been established. The existence of triplet P states has been confirmed while the existence of single states of c and $\bar{c}$ quarks. Investigation of the MARK II facility revealed the existence of rare non-

Translated from Atomnaya Énergiya, Vol. 47, No. 6, pp. 430-431, December, 1979.

0038-531X/79/4706-1060$07.50

leptonic decays of charmed D mesons, which marks the beginning of a new, deeper study of the properties of charmed particles. By the end of 1979 work should be completed at Stanford on the construction of PEP, a new accelerator facility with electron and positron beams with an energy of 36 GeV in the c.m. frame.

In the past two years experimental evidence has been obtained for the existence of a series of bound states ("narrow resonances") of the $p\bar{p}$ system with a mass of 1.94, 2.02, and 2.2 GeV. Some of the new experiments, whose tentative results were discussed at the conference, have not confirmed their existence. The new experiments were conducted in the antiproton beam at Brookhaven and in the pion beam at CERN. The investigations are being continued and the final result will be obtained when the data of all experiments has been analyzed.

A large research program is being conducted with high-energy neutrinos as well as on the physics of weak interactions. Research on neutrino beams is being done by using hybrid facilities: a pellicle stack as a triggering detector, a bubble chamber for target indication, and an electronic part for identification of mesons. Several events of the creation of charmed hyperons have been reliably identified by this technique and measurements have been made of their lifetime, which is about $7 \cdot 10^{-13}$ sec.

A small bubble chamber that has gone into service at CERN has a high repetition rate, 20 expansions per second, with a high spatial rarefaction (~ 15 μm according to the design), allowing it to be used as a triggering detector for interactions.

The overall result of research on neutral currents in weak interactions comes down to the validity of a variant of the unified Weinberg–Salam theory, and the sole parameter of the theory, i.e., the Weinberg angle, is determined very accurately as $\sin^2 \theta_W = 0.23 \pm 0.015$. The next important step, if this theory is valid, is that of detecting the weak-interaction carrier, the Z^0 boson, with a mass of 88.7 GeV/sec^2. The process of neutrino splitting of the deuteron, $\nu_e + D \rightarrow \nu_e + p + n$, has been observed for the first time. The first neutrino experiment for verifying the multiplicative law of lepton conservation has been conducted on the linear proton accelerator as Los Alamos.

Considerable time at the conference was devoted to deep-inelastic processes with the participation of high-energy neutrinos. In the quark-parton picture these processes occur on quarks which are effectively free for the square of the momentum transfer $Q^2 > | 0.3$ GeV/sec $|^2$. The structure functions of nucleons are linear combinations of the quark density in the nucleon with infinite momentum. Experimental data on neutrino processes along with data on inelastic scattering of high-energy electrons make it possible to obtain data about the structure functions of nucleons. An important place was occupied by data obtained by Soviet researchers on the observation of parity nonconsevation effects in heavy atoms in complete agreement with the Weinberg–Salam theory.

The conference discussed hadron collisions at high energies. The data on such processes (both hadronic and leptonic) with a large momentum transfer are interpreted within the framework of the quark–gluon picture (quantum chromodynamics). Processes with the formation of a jet of particles, detailed analysis of the change in the value of the transferred momentum as a function of the incident-particle energy and charge and other correlations in the particle jets, and the "broadening" of one particle jet as the result of gluon bremsstrahlung are in qualitative agreement with quantum chromodynamics. However, the main theoretical problems of the confinement of quarks in hadrons remain unresolved.

Some of the papers were devoted to the polarization (spin) effects at high energies. From the point of view of the quark–parton picture, particular attention is being paid to spin effects at a high momentum transfer. Researchers at the Argonne National Laboratory, U.S.A., studied the scattering of polarized 6-GeV neutrons (12-GeV deuterons) by polarized protons, and measured the polarization correlations. The polarization of hyperons at high energies, when the polarization of the protons in the beam is small, proved to be unexpectedly high. It is proposed not only to continue investigations on spin effects but also to use polarized hyperon beams for exact measurement of the magnetic moments of hyperons, which is of interest from the point of view of the quark structure of hyperons. From this point of view much attention was devoted to processes of hadron collisions with a small momentum transfer, where the main part of the total interaction cross sections is concentrated. In some cases the laws governing the interactions can be comprehended at the quark level.

In their papers, researchers from the Joint Institute of Nuclear Research (JINR) gave the results of experiments performed jointly by the JINR and the Fermilab on jet targets. These results were also the subject of two theoretical papers which considered the processes of the diffraction dissociation of protons. Considerable attention was devoted to the results of studies on the dissociation of pions by nuclei on the basis of JINR–CERN magnetic spark spectrometer.

The 25th anniversary of CERN provided an opportunity at the conference to discuss forthcoming research and plans for the construction of such large new facilities as the LEP large electron and positron accelerator with a center-of-mass energy of ~ 80-200 GeV. The objective of forthcoming studies is to verify attempts to elaborate a unified theory of weak and electromagnetic, weak, and electromagnetic and strong interactions. By 1981 CERN should have completed the construction of an antiproton storage ring, an accelerator facility with protons and antiprotons at a center-of-mass energy of 540 GeV and an emittance of 10^{30} $cm^{-2} \cdot sec^{-1}$. Goals of the first priority are the detection of the Z^0 meson, the study of processes with large transfers, and the search for the formation of new particles.

In theoretical schemes unifying hadrons and leptons into one family, transitions between them are allowed. Thus, the proton also turns out to be an unstable particle. As a result of the weakness of the interaction, the lifetime of the proton is estimated at 10^{30-34} yr. Notwithstanding the great difficulties in carrying out the search for proton decays, two experiments are being prepared for recording scintillation or Cherenkov flashes in 10,000 tons of water.

SECOND INTERNATIONAL SEMINAR ON HIGH-ENERGY PHYSICS AND FIELD THEORY

The seminar, which was held in Protvino in July, 1979, was attended by some 100 Soviet and foreign workers in the field of the theoretical foundations of the microcosm and the mathematics for the description of effects which occur in the interaction of energetic elementary particles.

The participants were representatives of many Soviet scientific centers, in particular the Institute of High-Energy Physics (IVFÉ), the Joint Institute for Nuclear Research (JINR), the P. N. Lebedev Institute of Physics of the Academy of Sciences of the USSR (FIAN), the Institute of Theoretical and Experimental Physics (ITEF), Moscow State University, etc. Foreign scientific laboratories were represented by theoretical physicists from the German Democratic Republic, Czechoslovakia, Bulgaria, Italy, and CERN.

The seminar heard more than 40 review papers and original communications on key problems of the theoretical physics of elementary particles and their interaction. The main topics discussed at the seminar touched on the most topical areas of study in the physics of the microcosm: gauge field theories, including quantum chromodynamics, the exact consequences of the global principles of field theory, the symmetry properties of elementary particles, various models of the field theory, and phenomenology. Much attention was paid to gravitation theory and the supersymmetry approach as well as to the development of the mathematics of present-day theoretical physics. Considerable time was devoted to discussion.

The seminar was fruitful and made it possible for the participants to exchange information about the latest advances in particle physics as well as to broad contacts among various scientific centers.

In view of the fact that high-energy physics is enjoying vigorous development at the present time, holding such seminars is a necessity for successful research and for getting information at an opportune time about current scientific work and about the prospects of investigations. This is why the international seminar at the IFVÉ was conceived as an annual event and the success it has enjoyed in the past two years undoubtedly confirms the desirability of continuing with it.

Translated from Atomnaya Énergiya, Vol. 47, No. 6, p. 431, December, 1979.

0038-531X/79/4706-1062 $07.50

THIRTEENTH EUROPEAN MEETING ON CYCLOTRONS

N. I. Venikov

The meeting was held at the Swiss Institute of Nuclear Research in June, 1979, with the participation of some 100 specialists, including invited delegates from the United States, Canada, and Japan. About one-third of the papers (24) were read while the remainder (43) were presented on posters.

Analyzing the contents of the papers and the discussion, one can make the following conclusions.

1. Enormous interest has been aroused by the start-up of the largest isochronous cyclotron, the U-400, at the Joint Institute for Nuclear Research (JINR) which will yield high-intensity beams of heavy ions.

2. The latest generation of cyclotrons (with separated magnets) have been operating satisfactorily. The most successful has been the complex of cyclotrons at Willigen, Switzerland, where a proton beam has been obtained with an energy of 600 MeV and an intensity of 100 μA with a 99.9% coefficient of extraction from the last cyclotron. With such small losses the intensity can be increased to 1-2 mA and a new circular cyclotron-injector with a higher intensity is being developed at the Swiss institure for this purpose. It is to be put into operation in 1982, raising the power of the beam from the meson factory to 1 MW. Such an accelerator can be used not only as a meson factory but also as a neutron factory. A further increase in the coefficient of beam extraction from the cyclotron (up to 100%) can be achieved by the method of expanding orbits, proposed and studied at the JINR under V. P. Dmitrievskii.

The second accelerator of this generation, the TRIUMF cyclotron at Vancouver, Canada, also produces an external beam of protons with an energy of 500 MeV and an intensity of up to 120 μA for short periods. But the losses at high energy because of the electrical dissociation of negative hydrogen ions in a magnetic field cause a residual induced radioactivity, thus not allowing such beams to be accelerated for a long time. Therefore, in this case it is proposed to bunch ions in order to obtain short but powerful neutron bursts in a lead target surrounded by heavy water. Further plans call for an increase in the energy (but not the intensity) in order to produce a K-meson factory. For this purpose it is proposed to build one more cascade (a circular cyclotron or synchrotron with a high repetition rate).

The VICKSI cyclotron (West Berlin), operating an argon and krypton ions, uses a 6-MW electrostatic accelerator as an injector. The GANIL complex of cyclotrons under construction at Caen, France, will consist of two large cyclotrons with separated magnets and two small cyclotron-injectors.

3. Much attention is being paid to cyclotrons of the new generation, with superconducting magnetic windings. Although some difficulties were encountered with the start-up of the first such cyclotron at the University of Michigan in the United States, primarily because of the necessity to introduce a large number of elements into the cryostat and to lead them out of it (e.g., ion source), there is confidence that the first beam will be obtained early in 1980. At Chalk River, Canada, magnetic measurements are being conducted and research pursued on an rf system for a second such cyclotron. Moreover, new projects are making their appearance, two of them in the Federal German Republic. At Munich, studies are being made on the possibility of constructing a cyclotron with four separate superconducting magnets with a field of 5.5 T in a sector. With the Munich laboratory's 13-MV tandem, which is to be used as an injector, the cyclotron willbe capable of accelerating light ions to 300 MeV/nucleon and uranium ions to 25 MeV/nucleon. Two problems have arisin in the construction of the cyclotron. The first concerns attainment of the required radial dependence of the average field in the injection region. As shown by estimates, the required field profile can be obtained only at double the radius and ways and means of shimming are now being sought. It may be that this problem has no solution; this is the fundamental problem of such cyclotrons with separated magnets. The other problem is that because of the regulation of the finite energy of the ions (from 300 to 25 MeV/nucleon), it is necessary to vary the growth of the average field at the final radius by 1.3 T and powerful correction windings are necessary for this.

At Julich, Federal German Republic, a project has been prepared for a complex consisting of two cyclotrons with continuous superconducting magnets. The complex resembles the one built at the University of

Translated from Atomnaya Énergiya, Vol. 47, No. 6, pp. 432-433, December, 1979.

0038-531X/79/4706-1063$07.50

Michigan but with an important addition: instead of an internal source use will be made of an external microwave source employing electron-cyclotron resonance. Uranium ions are to be accelerated to 100 MeV/nucleon and light ions, to 250 MeV/nucleon.

In the United States, in addition to those cyclotrons already under construction, there are several proposals for the construction of cyclotrons with superconducting magnet windings.

4. The desire to increase the energy of heavy ions in a cyclotron has resulted in intensive studies on new types of sources of ions with high charges. One of them, which is being developed more and more, is a microwave-heated plasma source employing electroncylotron resonance. The best results have been obtained in Grenoble, France, with sources in a stand version. But others of a similar type as applied to the cyclotron are already being developed: at Louvain, Belgium, and Karlsruhe, Federal German Republic.

Penning-type sources are continuing to be optimized and improved. For example, a modified source for obtaining $^{12}C^{4+}$ ions according to the scheme used in the source of the cyclotron at the I. V. Kurchatov Institute of Atomic Energy is being developed at the CERN synchrocyclotron: this will be a source of the straight-channel type, with a collimated plasma-column diameter, high power (30 A, 1000 V) introduced into the plasma in a discharge pulse, and a high density of plasma power ensuring formation of multiply charged ions with a high density. According to plans, 10^{11} $^{12}C^{4+}$ ions per second in the external beam of the synchrocyclotron with an energy of 85 MeV/nucleon would be attained in 1979.

5. Acceleration of intermediate ions (lithium and beryllium), which have properties not possessed by light and heavy ions, is becoming of increasing importance with each year. This is indicated, e.g., by the fact that in 1965 lithium ions were accelerated in only one cyclotron (Kurchatov Institute), in 1970 in one more, at Berkeley (California), and in 1979, in seven at Karlsruhe, Harwell (Britain), the Universities of Texas and Indiana (U.S.A.), and Dresden (German Democratic Republic) and was planned at several others. Multiply charged lithium ions are obtained in various ways. The most efficient is the method employed at the Kurchatov Institute, with an internal straight-channel source of the crucible type. In respect of intensity of the external beam of lithium ions, this cyclotron surpasses others. The only other cyclotrons, besides the one at the Kurchatov Institute, which are used to accelerate beryllium ions are Berkeley (similar in intensity) and at Texas U. (intensity two orders of magnitude lower).

6. The application of cyclotrons is expanding, especially in medicine (cancer therapy, radiography, production of isotopes for medical purposes). Particular attention is being paid to the production of ^{123}I. Large quantities of this isotope are produced even in such unique accelerators as the meson factories at the Swiss Institute (in part of the external beam of the cyclotron-injector with a proton energy of 72 MeV) and in Vancouver. It is also obtained in large quantities in the cyclotrons at Louvain, Julich, and Karlsuhe. In Julich, it is produced in the reaction $^{127}I(d, 6n)^{123}Xe(\beta^+; \varepsilon\text{-capture})^{123}I$ with a deuteron energy of 78 MeV. The $^{124}Te(p, 2n)^{123}I$ reaction is used in more compact cyclotrons. The interest in ^{123}I stems from the fact that the ^{131}I obtained in reactors and also used for medical purposes is more than 50 times worse in respect of dose of radiation for the patients.

7. The meeting discussed various aspects of the technique of designing, constructing, tuning up, and operating cyclotrons. Great interest was taken in the new method of measuring the energy of ions by utilizing their recombination in a beam of electrons of known energy, first proposed at the Kurchatov Institute.

It was decided that the next European meeting on cyclotrons will be held in 1980 at Karlsruhe (Federal German Republic).

BOOK REVIEWS

A. N. Kondratenko

PENETRATION OF A FIELD INTO PLASMA*

Reviewed by S. S. Moiseev

In the past two decades many publications have dealt with the penetration of a varying electromagnetic field into plasma. With each day it becomes more difficult to cope with the flood of information. At the same time, there is little review literature, especially monographs on this area of physics. However, whereas in the case of weakly inhomogeneous plasma these topics have been treated at least in part, there are no such monographs in the case of highly inhomogeneous plasma as well as in the case when the effects at a sharp boundary are taken into account. This gap is filled to a great extent by this book, written by an eminent specialist on wave propagation in highly inhomogeneous media. The monograph covers diverse aspects of field penetration and wave transformation at the boundary of both isotropic and magnetically active plasma in the hydrodynamic and kinetic approximations.

The book expounds a large volume of factual material: wave transformation (transformation of transverse into longitudinal waves) in semibound plasma and plasma layers under the condition of weak and strong spatial dispersion, with and without a constant magnetic field, and in a strongly and weakly inhomogeneous plasma; the penetration, reflection, and absorption of electromagnetic waves with nonresonance frequencies from moving plasma into plasma at rest, under the conditions of normal and anomalous skin effect. In great measure the author has succeeded by reducing the intermediate calculations which he presented in great detail in his earlier book "Plasma Waveguides."

The author devotes considerable attention to the exposition of the physical essence of the effects considered so that the book can be useful to undergraduate and postgraduate students specializing in plasma physics and related fields. The composition of the monograph is felicitous. From simple effects, which are expounded with the aid of hydrodynamic description in plasma without a magnetic field, the author gradually goes on to more complicated effects on spatial dispersion. The last chapter is somewhat separate from the main contents but is not at all extraneous since it provides an essential complementation to earlier review publications with results on the transformation of low-frequency waves in weakly inhomogeneous plasma which differs significantly from the transformation of high-frequency waves.

The following comments should be made: there is a dearth of graphical material, no references are given to experimental papers, and insufficient coverage is given to studies on the interaction of radiation with moving plasma. In the next edition the author should take this into account and expand somewhat on the subjects discussed.

The monograph is useful and necessary both for further development of the theory of plasma and to an even greater extent in connection with the numerous applications of plasma physics. Radiofrequency and laser heating, radio communication, diagnostics of plasma and semiconductors, and diffraction on plasma formations are far from a complete catalog of the areas in which the conclusions of the theory of wave penetration and transformation are used effectively.

*Atomizdat, Moscow (1979).

Translated from Atomnaya Énergiya, Vol. 47, No. 6, p. 433, December, 1979.

0038-531X/79/4706-1065$07.50

T. Cowling

MAGNETIC HYDRODYNAMICS*

B. P. Maksimenko

Magnetohydrodynamics (MHD), conceived in the domains of geophysics and astrophysics, is now developing rapidly and has been finding increasing application in various areas of science and engineering. The object of study are liquid or gaseous conducting media and their behavior in a magnetic field. The range of applications of MHD includes both space and astrophysical problems (the sun, stars, outer space, interstellar plasma) as well as purely "terrestrial" applications in which use is made of hydrodynamic effects (studies on the problem of controlled thermonuclear fusion with magnetic confinement of plasma, MHD generators, MHD pumps, etc.). In connection with this it is timely and opportune that we have a second, substantially revised edition and supplemented edition of a book whose author is one of the leading specialists in this field. The primary objective of the books is to present the foundations of MHD. The choice of material as well the order of presentation have been subordinated to this objective.

In the first chapter, which is devoted to the principles of MHD, Cowling formulates the fundamental concepts, gives the initial electromagnetic and hydrodynamic equations, and presents the electromagnetic consequences stemming from those equations. In the second chapter, which deals with magnetic hydrostatics, he considers problems of magnetostatic equilibrium and instability. The conditions for onset of oscillatory processes with the formation of Alfvén, magnetoacoustic, and hydromagnetic shock waves are analyzed in the third chapter. It gives examples of large-scale oscillations in various astronomical situations. Chapter four concerns the mechanisms responsible for instabilities of the Kelvin–Helmholtz, tearing-mode, and thermal types and conditions for their stabilization. In chapter five, devoted to the passage of magnetic waves through stars and planets, the author presents and discusses the dynamic theory, according to which a magnetic field is sustained by an electric current induced in the interior region as the result of the motion of matter across force lines, just as occurs in a dynamo machine with self-excitation. The application of the MHD approach to low-density plasma is discussed in chapter six.

An undeniable advantage of the book is that in the treatment of quite involved material, the author devotes considerable attention to the physical essence of the effects considered, using the least possible number of mathematical calculations. Wherever possible, theory is compared with the results of experimental research.

Undoubtedly, the book will be useful to all those who are interested in problems of MHD theory and its practical applications.

*Russian translation from the English, Atomizdat, Moscow (1978).

Translated from Atomnaya Énergiya, Vol. 47, No. 6, p. 433, December, 1979.

0038-531X/79/4706-1066$07.50

INDEX

SOVIET ATOMIC ENERGY

Volumes 46-47, 1979

SOVIET ATOMIC ENERGY
Volumes 46-47, 1979
(A translation of Atomnaya Énergiya)

L

M

SOVIET ATOMIC ENERGY

Volumes 46-47, 1979

(A translation of Atomnaya Énergiya)

Volume 46, Number 1 January, 1979

Volume 46, Number 2 February, 1979

Volume 46, Number 3 March, 1979

Volume 46, Number 4 April, 1979

Engl./Russ.

Volume 46, Number 5 May, 1979

Engl./Russ.

Volume 46, Number 6 June, 1979

Volume 47, Number 1 July, 1979

Engl./Russ.

Volume 47, Number 2 August, 1979

ARTICLES

LETTERS

Volume 47, Number 3 September, 1979

Volume 47, Number 4 October, 1979

Volume 47, Number 5 November, 1979

Volume 47, Number 6 December, 1979

NEW RUSSIAN JOURNALS

IN ENGLISH TRANSLATION

BIOLOGY BULLETIN
Izvestiya Akademii Nauk SSSR, Seriya Biologicheskaya

The biological proceedings of the Academy of Sciences of the USSR, this prestigious new bimonthly presents the work of the leading academicians on every aspect of the life sciences—from micro- and molecular biology to zoology, physiology, and space medicine.
Volume 7, 1980 (6 issues) $195.00

SOVIET JOURNAL OF MARINE BIOLOGY
Biologiya Morya

Devoted solely to research on marine organisms and their activity, practical considerations for their preservation, and reproduction of the biological resources of the seas and oceans.
Volume 6, 1980 (6 issues) $115.00

WATER RESOURCES
Vodnye Resursy

Evaluates the water resources of specific geographical areas throughout the world and reviews regularities of water resources formation as well as scientific principles of their optimal use.
Volume 7, 1980 (6 issues) $215.00

HUMAN PHYSIOLOGY
Fiziologiya Cheloveka

A new, innovative journal concerned *exclusively* with theoretical and applied aspects of the expanding field of human physiology.
Volume 6, 1980 (6 issues) $195.00

SOVIET JOURNAL OF BIOORGANIC CHEMISTRY
Bioorganicheskaya Khimiya

Features articles on isolation and purification of naturally occurring, biologically active compounds; the establishment of their structure, methods of synthesis, and determination of the relation between structure and biological function.
Volume 6, 1980 (12 issues) $245.00

SOVIET JOURNAL OF COORDINATION CHEMISTRY
Koordinatsionnaya Khimiya

Describes the achievements of modern theoretical and applied coordination chemistry. Topics include the synthesis and properties of new coordination compounds; reactions involving intraspheral substitution and transformation of ligands; complexes with polyfunctional and macromolecular ligands; complexing in solutions; and kinetics and mechanisms of reactions involving the participation of coordination compounds.
Volume 6, 1980 (12 issues) $255.00

THE SOVIET JOURNAL OF GLASS PHYSICS AND CHEMISTRY
Fizika i Khimiya Stekla

Devoted to current theoretical and applied research on three interlinked problems in glass technology; the nature of the chemical bonds in a vitrifying melt and in glass; the structure-statistical principle; and the macroscopic properties of glass.
Volume 6, 1980 (6 issues) $145.00

LITHUANIAN MATHEMATICAL JOURNAL
Litovskii Matematicheskii Sbornik

An international medium for the rapid publication of the latest developments in mathematics, this quarterly keeps western scientists abreast of both practical and theoretical configurations. Among the many areas reported on in depth are the generalized Green's function, the Monte Carlo method, the "innovation theorem," and the Martingale problem.
Volume 20, 1980 (4 issues) $175.00

PROGRAMMING AND COMPUTER SOFTWARE
Programmirovanie

Reports on current progress in programming and the use of computers. Topics covered include logical problems of programming; applied theory of algorithms; control of computational processes; program organization; programming methods connected with the idiosyncracies of input languages, hardware, and problem classes; parallel programming; operating systems; programming systems; programmer aids; software systems; data-control systems; IO systems; and subroutine libraries.
Volume 6, 1980 (6 issues) $115.00

SOVIET MICROELECTRONICS
Mikroelektronika

Reports on the latest advances in solutions of fundamental problems of microelectronics. Discusses new physical principles, materials, and methods for creating components, especially in large systems.
Volume 9, 1980 (6 issues) $160.00

Send for Your Free Examination Copy

PLENUM PUBLISHING CORPORATION, 227 West 17th Street, New York, N.Y. 10011
In United Kingdom: Black Arrow House, 2 Chandos Road, London NW10 6NR, England
Prices slightly higher outside the U.S. Prices subject to change without notice.